Melt Dynamics in Complex Polymer Systems: Star-shaped Polymers and Polymer Nanocomposite Films

By

Kyle J. Johnson

A dissertation submitted in partial fulfillment
of the requirements for the degree of
Doctor of Philosophy
(Materials Science and Engineering)
in the University of Michigan
2017

Doctoral Committee:

Professor Peter F. Green, Chair
Professor John Kieffer
Professor Nicholas Kotov
Professor Ronald Larson

Kyle J. Johnson
kjjoh@umich.edu
ORCID iD: 0000-0003-1849-0645

To my parents for their unwavering support,

my sister for keeping me grounded, and my friends

for carrying me through difficult times

Acknowledgments

First, I would like to thank my thesis advisor, Professor Peter F. Green. His scientific knowledge and mentorship have been an invaluable resource at times when I have been lost during my research. His encouragement has allowed me to explore challenging scientific research questions and grow as an independent researcher. The skills I have gained during the past 5 years extend far beyond the laboratory, and he has been a large part of my development both inside and outside the laboratory. I would also like to thank the other members of my dissertation committee, Professors John Kieffer, Nicholas Kotov, and Ronald Larson. Whether through teaching graduate courses on topics that exposed me to new ways of thinking or providing insight and critique for my research, each of you has been instrumental to the work in this dissertation.

I have to extend a special thank you to the current and former members of the Green research group who have helped me in immeasurable ways. A special thanks to Dr. Hengxi Yang and Dr. Bradley Frieberg for being outstanding mentors and acting as examples of how to perform research in a professional and effective manner. I owe thanks to Dr. Ban Dong, Dr. Junnan Zhao, Dr. Peter Chung, Dr. Aaron Tan, Jill Wenderott, and Ravi P. Sharma for not only being my colleagues but also my friends throughout my time at the University of Michigan. I

would also like to thank the University of Michigan Materials Science and Engineering department and the many graduate students past and present who have shaped my experience at the University of Michigan.

I must also extend a special thank you to both Emmanouil Glynos and Suresh Narayanan. Both of you have been a part of my growth as a researcher from my first years in graduate school to this point. Your research insight has been instrumental to this work, and I hope that I have done this small part of our long nights together justice.

I would like to acknowledge the NSF funding agency as well as the Alliances for Graduate Education and the Professoriate (AGEP) for supporting my research and providing me with many connections and friendships that will last long after I leave the University of Michigan. I would also like to acknowledge the graduate student communities involved with the Rackham Merit Fellowship (RMF) program which has been a substantial and unwavering source of companionship and support over the years.

Last but not least I would like to express the utmost appreciation to my family. I would like to thank my mother and father, Dr. W. Roy Johnson and Dr. Gloria Jones-Johnson, for seeing me through both my best and worst moments throughout this process. I would like to thank my sister for being my best friend and a better sister than I deserve. Without you all, none of this would have been possible.

Table of Contents

List of Tables

List of Figures

List of Appendices

Abstract

The study of dynamic relaxations in polymer chains has been one of the cornerstones of polymer physics research for over half a century. Increased understanding of polymer chain relaxations has led to the development of macromolecules for packaging, drug delivery and sensor applications. As the challenges for these applications have become more demanding, it is now necessary to tailor polymer relaxation properties in more detailed and specific ways. In this thesis, we investigated two methods for tailoring polymer chain dynamics: (1) manipulation of molecular architecture and (2) introduction of inorganic nanoparticles into a polymer host. First, we demonstrate that the translational dynamics in star-shaped polystyrene can be tailored to behave as either a linear polymer or a soft colloid through the control of the star-shaped polymer molecular parameters such as functionality and arm molecular weight.

We show that this is due to entropic intermolecular interactions caused by a tunable high-density core region close to the star branch point. Second, we show that in thin polymer films, the translational dynamics of the host polymer can be tailored through the introduction of inorganic polymer chain-end grafted particles. When these particles are well-dispersed throughout the polymer host, the relaxations of the host are shown to be strongly dependent on

the confinement of the nanoparticles and the suppression of nanoparticle dynamics – leading to an order of magnitude increase in viscosity. If the particles are not well-dispersed, they are shown to segregate to the film interfaces and cause a region of high viscosity at the film free surface. This work highlights influences of molecular architecture, confinement and interfacial interactions on the dynamic relaxations of polymers and illustrates how these influences can be used to tailor polymer properties.

Chapter 1
Introduction

I.1 Motivation and Objectives

Polymers are used in a number of important technologies ranging from packaging to functional materials in energy and sensor applications.[1–15] Polymers offer flexible, lightweight materials and cheaper manufacturing costs than presented by many inorganic alternatives. The next frontier of advancement in polymeric materials involves tailoring their nano-scale structure in order to further modify their properties. Many strategies are currently used to modify the properties of polymeric materials including copolymerization and blending polymers of different chemistry. [16–23]Two strategies that have always been at the forefront of understanding structure property relationships in polymers are the manipulation of macromolecules topology and the addition of nanoscale fillers to a polymer host.[24–31]

In many polymer applications, confinement of the system to a thin film geometry is required or beneficial. Studies of polymer thin film properties have revealed that a number of properties change upon confinement to a thin film: glass transition temperature, viscosity, and local density.[32–42] There are two aspects of confinement that influence the properties of the

polymer host: interactions between the polymer and a solid or vapor interface and effects caused by geometric confinement of a polymer to film thickness on the order of the polymer radius of gyration. Recent simulations have probed the influences of different interfaces on the dynamics of polymers confined to both supported and free standing films.[37,43] Polymer chains near the free surface are known to gain configurational freedom leading to increased mobility at the free interface due to a reduction in nearest neighbors and longer range confinement effects.[32,42,44,45] Near the substrate, polymer chains are known to have interactions that vary dependent upon the relationship of the polymer with the substrate. For monomers near weakly attractive smooth substrates or non-wetting surfaces, their mobility is increased by comparison to the bulk due to a reduced molecular caging effect.[46–49] When attractive or specific interactions exist between monomers and the substrate, reduced mobility is observed and molecular packing and organization have been measured in some systems. [47,49]As film thickness is decreased, the layers near these interfaces take on a larger fraction of the film and have a more substantial influence on the average film properties. [47,50,51]Polymer chains also exhibit very different behaviors in thin films due to confinement effects, and substantially different behaviors may be observed when film thickness approaches important length scales related to the physical characteristics of the polymer.[52]

Altering the behavior of polymers for both bulk and thin film applications requires control of polymer behavior using a variety of different parameters. One polymer property that allows for unique control of polymer behavior is molecular architecture. Manipulation of polymer architecture allows control of polymer properties while maintaining the same chemical constituents as a linear macromolecule which opens the door for interesting, new behavior. [53,54]The simplest branched architecture is a star-shaped molecule where by a number of linear

chains are connected by a single branch point. Star-shaped polymers have been known to exhibit interfacial behaviors that differ drastically from their linear analogs.[55–58] These changes in interfacial behavior occur because of a reduced enthalpic penalty for star shaped polymers to adsorb to an interface and results in unique properties such as interfacial ordering, wetting, and changes to the glass transition temperature.[59–66]

Another method of modifying polymer behavior is through the addition of nanoscale fillers to a polymer host. The incorporation of these nanoparticles within a polymer host allows for material properties that are unique, and change polymer electrical, optical and mechanical properties.[2,26,28,29] These polymer nanocomposite systems and their associated properties are dependent on dispersion of particles throughout the polymer host. This is particularly challenging since inorganic particles aggregate in the bulk, in order to minimize surface energy, leading to inhomogeneity in their effect on polymer properties. [67–70] This aggregation can be mitigated by grafting linear polymer chains to the surface of the nanoparticle, creating a brush layer which can enhance particle dispersion throughout the polymer host depending upon the interaction between the grafted brush and host chains – as well as particle size/shape. Many studies have been done showing an improvement in particle dispersion using this strategy; however, even these polymer nanocomposite films are subject to interfacial segregation of the particles in supported thin films.[71–73] By manipulating brush and host chain properties, grafting chain density and particle size it is possible to tailor the dispersion of nanoparticles and control interfacial segregation.[74]

Previous work in our group has shown that a number of properties in both star-shaped polymer and polymer nanocomposite systems change upon confinement. Star-shaped polymers have been studied extensively and exhibit a transition from behavior resembling linear chains to

that of a soft colloid as the macromolecular parameters of the polymer are changed.[55,75] This change extends to wetting,[56] aging,[57]and the glass transition temperature of these systems when confined to a thin film.[58] The first part of this thesis will involve an investigation of how the translational dynamics of star-shaped polymers in the bulk influence the transition from polymeric to colloidal behavior in these polymers. The second part of this work will explore the influences of both confinement and interfacial segregation on dynamics in polymer nanocomposite films with grafted particles and linear host polymer chains. These two components will then be used to provide some insight into polymer nanocomposite systems of grafted particles with star-shaped polymer hosts. This research highlights how molecular topology and the addition of inorganic components can substantially influence the dynamics of host polymers when confined to a thin film.

I.2 Background

I.2.1 *Dynamics in Star-shaped Polymers*

A star-shaped macromolecule is composed of a branch point unto which *f* chains, each of molecular weight per arm M_a, are covalently bonded. Due to the entropic restrictions associated with the attachment of molecules to the branch point, the density of chain segments is highest in the central core region and decreases toward the ends of the arms where the chain segments have the largest configurational freedom.[76,77] The radius of the central core region $\boldsymbol{r_c}$ increases with the functionality as $\boldsymbol{r_c \propto f^{1/2}}$. The segments that compose the outer regions of the molecule, the corona, are able to relax freely and intermix with segments from other molecules, filling space.[78] For stars with high functionalities and sufficiently short arms, entropic repulsions are

responsible for the emergence of structural order,[58,79–86] wherein the stars exhibit a tendency to "pack" like soft particles.

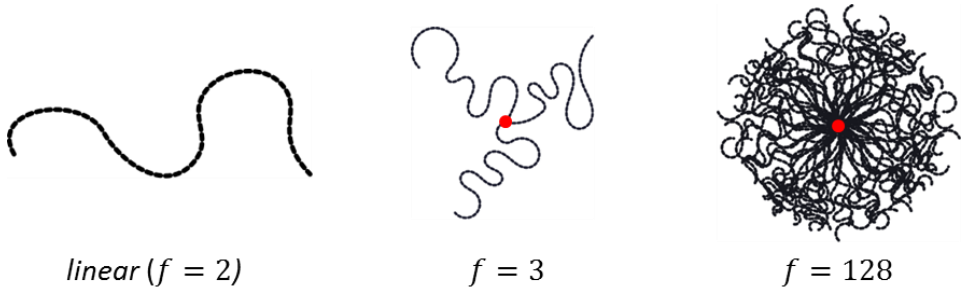

Figure I.1: Schematic representation of star-shaped polymers as functionality is increased

The dynamics of unentangled linear chains are well described by the Rouse model where the diffusion coefficient D is inversely proportional to the molecular weight M of the chain, because the friction coefficient is proportional to the chain length.[87–89] For highly entangled linear polymer melts, the Reptation model, and experiment, describes the translational diffusion of the polymer host chains. In this model, entanglements with neighboring chains restrict the chain to a virtual tube. In order for the chain to move through these obstacles, it must reptate through this virtual tube along its contour length. This model indicates that the translational diffusion coefficient is proportional to M^{-2}.[90,91]

For long-arm, low-functionality, entangled, star-shaped macromolecules, the center of mass motion is facilitated by an arm retraction mechanism, wherein the arm of a star-shaped macromolecule moves along the primitive path within a "tube" toward the branch point.[92–95] Here diffusion is much slower – as the arm retraction process is entropically unfavorable – and depends exponentially on the length of the arm M_a. The segments of the arms near the free ends relax much faster than segments in the core region of the star;[96,97] this behavior and the much

slower center-of-mass dynamics of the chains are responsible for a hierarchy of length-scales and time-scales that characterize the dynamics of star shaped polymers.

Milner and McLeish,[98,99] in a quantitative model describing the dynamics of entangled star-shaped macromolecules, showed that the free end of an arm makes excursions along the primitive path a fractional distance *s*, subject to a potential U_{eff}(s) described by:

$$\boldsymbol{U_{eff}(s) = \frac{15M_a}{4M_e}\frac{1-(1-s)^{1+\alpha}[1+(1+\alpha)s]}{(1+\alpha)(2+\alpha)}} \quad (1)$$

The exponent α is related to the dilution exponent used to account for dynamic dilution effects on the entanglement network. The relaxation time τ(s) used in the Milner-McLeish (MM) model has two components: an activated relaxation time dependent upon U_{eff}(s), $\boldsymbol{\tau_{late}(s)}$, and a relaxation time $\boldsymbol{\tau_{early}(s)}$ related to early time, "Rouse retraction," of the arm free end before it is influenced by the restriction of the branch point. Quantitatively,

$$\boldsymbol{\tau(s) \approx \frac{\tau_{early}(s)\exp[U_{eff}(s)]}{1+\exp[U_{eff}(s)]\frac{\tau_{early}(s)}{\tau_{late}(s)}}} \quad (2)$$

Since U_{eff}(s) is proportional to the ratio of the molecular weight of the arm M_a to the molecular weight between entanglements M_e, then *τ(s)* depends exponentially on M_a/M_e.[92–94,98] The stress relaxation modulus *G(t)* is predicted to depend on *τ(s)* such that:

$$\boldsymbol{G(t) = 2G_N \int_0^1 ds(1-s)^{\alpha} \exp[-\frac{t}{\tau(s)}]} \quad (3)$$

and the frequency dependent complex modulus $G^*(\omega)$ is:

$$G^*(\omega) = 2G_N \int_0^1 ds(1-s)^{\alpha} \frac{-i\omega\tau(s)}{1-i\omega\tau(s)} \quad (4)$$

While the Milner-McLeish model provides a good description of the viscoelastic moduli $G'(\omega)$ and $G''(\omega)$ for low functionality entangled stars,[100,101] it is, or course, not successful at describing the behavior of high functionality star polymers, due to effects associated with the size of the core[79–81,100,102–105] and associated entropic effects, not specifically addressed by the theory.

As functionality is increased to a very large number of arms, $f > 24$, the size of the core becomes large enough that it is possible to observe the emergence of a second relaxation process at time scales longer than that associated with the arm retraction mechanism. As functionality is further increased, this relaxation becomes more distinct and has been related to cooperative rearrangements of the cores of these macromolecules – similar to the behavior of a colloidal system. For short arms, these effects become much more pronounced, and the transition from behavior of low functionality, entangled to high functionality, unetangled stars is currently the subject of great research interest.[55,57,75,81,82]

I.2.2 *Dynamics in Polymer Nanocomposites*

Polymer nanocomposites involve the addition of nanoscale fillers to a polymer host and have been the source of research interests for several decades due to the wide range of improvements provided by adding inorganic particles to a polymer host. The properties of both

components, as well as interactions between them, can yield changes to thermal, mechanical and dynamic properties of the system. Controlling dispersion of these nanoparticles within the polymer host is thereby paramount to control of properties throughout the system. One strategy commonly employed to achieve NP dispersion throughout a PNC is to graft polymer chains onto the NP surfaces.[74,106–114] A number of parameters contribute to the overall morphology of the PNCs: the surface chemistry of the NPs, grafted chains and polymer host chains, the degree of polymerization of grafted and host chains, the NP surface grafting densities $\boldsymbol{\sigma}$, the thermodynamic interactions between the grafted and host chains,[115] as well as the size and shape of the nanoparticles . Intermixing between the grafted and free host chains may be controlled through changes in key physical parameters. In the simple case where, chains of degree of polymerization N grafted on a flat surface, mixed with free chains of identical chemistry (**Flory − Huggins interaction parameter $\boldsymbol{\chi = 0}$**), but of degree of polymerization P, transitions between the situation in which strong mixing occurs between the grafted and free chains (the so-called wet to dry brush condition) and that where limited mixing (dry-brush) occurs is dictated by the condition:[109]

$$\boldsymbol{\sigma\sqrt{N} = (N/P)^2} \quad (5)$$

In bulk PNCs with low NP concentrations, the dynamics of the NPs are strongly impacted by their size with respect to the host polymer chains and by interactions between the grafted polymer chains and host polymer chains. In cases where the particle radius is much larger than the equilibrium polymer coil size or the characteristic entanglement mesh, the dynamics of the particles have been shown to be dictated by the classical Stokes-Einstein (SE) equation.[36,116–121] When the particle size is less than the characteristic entanglement mesh, faster particle

dynamics than predicted by the SE prediction have been observed both experimentally and computationally.[116–118,122]

In the non-continuum regime, particles have been shown to exhibit anomalous behavior which can generally be categorized as either subdiffusive (related to restricted or hindered translational dynamics) or hyperdiffusive (related to a response to internal stress relaxation).[123,124] The diffusion of a particle in a Newtonian fluid as described by Stokes-Einstein equation can be described by a mean squared displacement of which increases with time as $\langle x^2(t)\rangle \propto t^{\alpha}; \alpha = 1$. When the particles are substantially constrained, the particles exhibit subdiffusive behavior due to crowding where $0 < \alpha < 1$. Hyperdiffusive behavior is observed when $\alpha > 1$ and is observed in colloidal gels, entangled polymer systems close to the glass transition temperature, and some entangled polymer systems when the particles are close to the size of the entanglement mesh.

With regard to the dynamics of the host chains of a PNC, the situation depends on whether the host chains are entangled or unentangled. For the simplest case, where $\boldsymbol{\chi = 0}$ and the grafted particles are dispersed throughout an unentangled host, the translational dynamics of the host chains are fast compared to the neat polymer host, whereas the dynamics decrease compared to the neat host when the grafted chain lengths are long compared to the entanglement molecular weight. [125,126] Regarding the segmental dynamics of the host chains in the bulk, the grafted-host chain interactions can lead to increases or decreases in relaxation time by several orders of magnitude at low concentrations. In the case of a brush layer where the host chains strongly interpenetrate the grafted layer, the segmental relaxation time of the host increases by almost an order of magnitude over the behavior of the neat homopolymer chains.[127] When the host chains do not interpenetrate the grafted chain layer as well, the particles have been observed

to decrease the segmental relaxation time by several orders of magnitude. This effect is mitigated at higher concentrations, as the particle aggregate in order to minimize surface energy.

These parameters provide several mechanisms through which the dynamics of the polymer host can be tailored through control of concentration, particle size, particle shape and brush layer interactions.

I.2.3 *Dynamics in Polymer Thin Films*

Polymer thin films have been shown to exhibit very different properties from their bulk analogs, and this allows them to have many applications ranging from coating to drug delivery technologies. A major source of difference between polymer properties in thin films versus the bulk is the increased importance of interfacial interactions. Interfaces have a strong influence on which are both directly adjacent to them as well as monomers 10s of nanometers into the film due to specific substrate-monomer interactions and molecular packing/organization respectively.[128] It should be noted that monomer dynamics and density are heterogeneous as a function of depth throughout the film, and as a consequence monomer density does not directly correlate with local monomer dynamics.[47,129,130] These effects are particularly evident when considering the influences of free volume and local organization on the dynamic behavior of polymer chains.

The influence of interfacial interactions on polymer dynamics becomes more substantial as film thickness is decreased. For very thin films, the film is mostly composed of interfacial layers which force a cut-off of bulk relaxation modes.[57,131] The influence of interfacial behaviors on the glassy dynamics ($T < T_g$) of polymer films becomes more substantial as temperature is

decreased.[57,131] Regarding behavior near the free surface, the dynamics in this region becomes similar to the bulk once the temperature is increased substantially above the glass transition.[48]

The dynamics of polymer chains near the substrate are also strongly dependent upon the smoothness of the substrate and thermodynamic interactions between the polymer chains and the substrate. For smooth films, the dynamics of the polymer chains are shown to become faster as film thickness is increased, while these effects are mitigated for rough films.[129,130] If there are strong, specific interactions between the polymer and the substrate, the dynamics of the polymer host chains can be slowed substantially by comparison to polymers which have non-specific interactions. The local behavior of polymers near interfaces is a primary influence when considering the changes to polymer structure and properties upon confinement to a thin film and opens the doors for their use in many new applications.

In this thesis, we explore two different methods of altering polymer dynamics: the manipulation of molecular architecture to control translational dynamics in star-shaped polystyrene and the different influences of polymer chain-end grafted gold nanoparticles on the dynamics of poly (2-vinyl pyridine) confined to a supported film. Our study of star-shaped polymers explores the influence of star-shaped polymer molecular parameters (functionality and arm molecular weight) on the transition from translational dynamics associated with an arm retraction mechanism to a more cooperative relaxation process associated with colloidal behavior. In our exploration of polymer nanocomposite films, we examine the role of grafted brush layer-host chain dynamics on the dynamics of the host chain upon confinement to polymer films. We explore the role that confinement to relevant length scales in miscible polymer nanocomposites has on polymer host chain dynamics as well as the influence of interfacial interactions and surface segregation on dynamics observed in these films.

References:

(1) Paul, D. R.; Yampol'skii, Y. P. *Polymeric Gas Separation Membranes*; CRC Press, 1993.
(2) Hussain, F.; Hojjati, M.; Okamoto, M.; Gorga, R. E. Review Article: Polymer-Matrix Nanocomposites, Processing, Manufacturing, and Application: An Overview. *J. Compos. Mater.* 2006, *40*, 1511–1575.
(3) Sill, T. J.; von Recum, H. A. Electrospinning: Applications in Drug Delivery and Tissue Engineering. *Biomaterials* 2008, *29*, 1989–2006.
(4) Wang, Y.; Chen, K. S.; Mishler, J.; Cho, S. C.; Adroher, X. C. A Review of Polymer Electrolyte Membrane Fuel Cells: Technology, Applications, and Needs on Fundamental Research. *Appl. Energy* 2011, *88*, 981–1007.
(5) Pillai, O.; Panchagnula, R. Polymers in Drug Delivery. *Curr. Opin. Chem. Biol.* 2001, *5*, 447–451.
(6) Patri, A. K.; Majoros, I. J.; Baker Jr, J. R. Dendritic Polymer Macromolecular Carriers for Drug Delivery. *Curr. Opin. Chem. Biol.* 2002, *6*, 466–471.
(7) Hou, J.; Chen, H.-Y.; Zhang, S.; Chen, R. I.; Yang, Y.; Wu, Y.; Li, G. Synthesis of a Low Band Gap Polymer and Its Application in Highly Efficient Polymer Solar Cells. *J. Am. Chem. Soc.* 2009, *131*, 15586–+.
(8) Williams, M.; Landel, R.; Ferry, J. Mechanical Properties of Substances of High Molecular Weight .19. the Temperature Dependence of Relaxation Mechanisms in Amorphous Polymers and Other Glass-Forming Liquids. *J. Am. Chem. Soc.* 1955, *77*, 3701–3707.
(9) Lendlein, A.; Kelch, S. Shape-Memory Polymers. *Angew. Chem.-Int. Ed.* 2002, *41*, 2034–2057.
(10) Stuart, M. A. C.; Huck, W. T. S.; Genzer, J.; Mueller, M.; Ober, C.; Stamm, M.; Sukhorukov, G. B.; Szleifer, I.; Tsukruk, V. V.; Urban, M.; *et al.* Emerging Applications of Stimuli-Responsive Polymer Materials. *Nat. Mater.* 2010, *9*, 101–113.
(11) Auras, R.; Harte, B.; Selke, S. An Overview of Polylactides as Packaging Materials. *Macromol. Biosci.* 2004, *4*, 835–864.
(12) Balazs, A. C.; Emrick, T.; Russell, T. P. Nanoparticle Polymer Composites: Where Two Small Worlds Meet. *Science* 2006, *314*, 1107–1110.
(13) Coakley, K. M.; McGehee, M. D. Conjugated Polymer Photovoltaic Cells. *Chem. Mater.* 2004, *16*, 4533–4542.
(14) Discher, D. E.; Eisenberg, A. Polymer Vesicles. *Science* 2002, *297*, 967–973.
(15) Adam, G.; Gibbs, J. On Temperature Dependence of Cooperative Relaxation Properties in Glass-Forming Liquids. *J. Chem. Phys.* 1965, *43*, 139-.
(16) Riess, G. Micellization of Block Copolymers. *Prog. Polym. Sci.* 2003, *28*, 1107–1170.
(17) Fasolka, M. J.; Mayes, A. M. Block Copolymer Thin Films: Physics and Applications. *Annu. Rev. Mater. Res.* 2001, *31*, 323–355.
(18) Fasolka, M. J.; Banerjee, P.; Mayes, A. M.; Pickett, G.; Balazs, A. C. Morphology of Ultrathin Supported Diblock Copolymer Films: Theory and Experiment. *Macromolecules* 2000, *33*, 5702–5712.
(19) Roland, C.; Ngai, K. Dynamic Heterogeneity in a Miscible Polymer Blend. *Macromolecules* 1991, *24*, 2261–2265.
(20) Colmenero, J.; Arbe, A. Segmental Dynamics in Miscible Polymer Blends: Recent Results and Open Questions. *Soft Matter* 2007, *3*, 1474–1485.
(21) Alegria, A.; Colmenero, J.; Ngai, K.; Roland, C. Observation of the Component Dynamics in a Miscible Polymer Blend by Dielectric and Mechanical Spectroscopies. *Macromolecules* 1994, *27*, 4486–4492.
(22) Green, P.; Adolf, D.; Gilliom, L. Dynamics of Polystyrene Poly(vinyl Methyl-Ether) Blends. *Macromolecules* 1991, *24*, 3377–3382.
(23) Pham, J. Q.; Green, P. F. The Glass Transition of Thin Film Polymer/Polymer Blends: Interfacial Interactions and Confinement. *J. Chem. Phys.* 2002, *116*, 5801–5806.

(24) Biswas, P.; Kant, R.; Blumen, A. Polymer Dynamics and Topology: Extension of Stars and Dendrimers in External Fields. *Macromol. Theory Simul.* 2000, *9*, 56–67.
(25) Ramakrishna, S.; Mayer, J.; Wintermantel, E.; Leong, K. W. Biomedical Applications of Polymer-Composite Materials: A Review. *Compos. Sci. Technol.* 2001, *61*, 1189–1224.
(26) Godovsky, D. Y. Device Applications of Polymer-Nanocomposites. In *Biopolymers/Pva Hydrogels/Anionic Polymerisation Nanocomposites*; Abe, A., Ed.; Springer-Verlag Berlin: Berlin, 2000; Vol. 153, pp. 163–205.
(27) Winey, K. I.; Vaia, R. A. Polymer Nanocomposites. *Mrs Bull.* 2007, *32*, 314–319.
(28) Gangopadhyay, R.; De, A. Conducting Polymer Nanocomposites: A Brief Overview. *Chem. Mater.* 2000, *12*, 608–622.
(29) Zou, H.; Wu, S.; Shen, J. Polymer/Silica Nanocomposites: Preparation, Characterization, Properties, and Applications. *Chem. Rev.* 2008, *108*, 3893–3957.
(30) Qiu, L. Y.; Bae, Y. H. Polymer Architecture and Drug Delivery. *Pharm. Res.* 2006, *23*, 1–30.
(31) Gao, C.; Yan, D. Hyperbranched Polymers: From Synthesis to Applications. *Prog. Polym. Sci.* 2004, *29*, 183–275.
(32) Keddie, J. L.; Jones, R. A. L.; Cory, R. A. Size-Dependent Depression of the Glass Transition Temperature in Polymer Films. *EPL Europhys. Lett.* 1994, *27*, 59.
(33) de Gennes, P. G. Glass Transitions in Thin Polymer Films. *Eur. Phys. J. E* 2000, *2*, 201–203.
(34) Tress, M.; Erber, M.; Mapesa, E. U.; Huth, H.; Mueller, J.; Serghei, A.; Schick, C.; Eichhorn, K.-J.; Volt, B.; Kremer, F. Glassy Dynamics and Glass Transition in Nanometric Thin Layers of Polystyrene. *Macromolecules* 2010, *43*, 9937–9944.
(35) Serghei, A.; Tress, M.; Kremer, F. Confinement Effects on the Relaxation Time Distribution of the Dynamic Glass Transition in Ultrathin Polymer Films. *Macromolecules* 2006, *39*, 9385–9387.
(36) Kalathi, J. T.; Yamamoto, U.; Schweizer, K. S.; Grest, G. S.; Kumar, S. K. Nanoparticle Diffusion in Polymer Nanocomposites. *Phys. Rev. Lett.* 2014, *112*, 108301.
(37) Mirigian, S.; Schweizer, K. S. Theory of Activated Glassy Relaxation, Mobility Gradients, Surface Diffusion, and Vitrification in Free Standing Thin Films. *J. Chem. Phys.* 2015, *143*, 244705.
(38) Oyerokun, F. T.; Schweizer, K. S. Theory of Glassy Dynamics in Conformationally Anisotropic Polymer Systems. *J. Chem. Phys.* 2005, *123*, 224901.
(39) Kim, H.; Ruhm, A.; Lurio, L. B.; Basu, J. K.; Lal, J.; Lumma, D.; Mochrie, S. G. J.; Sinha, S. K. Surface Dynamics of Polymer Films. *Phys. Rev. Lett.* 2003, *90*, 068302.
(40) Jiang, Z.; Kim, H.; Mochrie, S. G. J.; Lurio, L. B.; Sinha, S. K. Surface and Interfacial Dynamics of Polymeric Bilayer Films. *Phys. Rev. E* 2006, *74*, 011603.
(41) Chremos, A.; Glynos, E.; Koutsos, V.; Camp, P. J. Adsorption and Self-Assembly of Linear Polymers on Surfaces: A Computer Simulation Study. *Soft Matter* 2009, *5*, 637–645.
(42) Yang, Z.; Fujii, Y.; Lee, F. K.; Lam, C.-H.; Tsui, O. K. C. Glass Transition Dynamics and Surface Layer Mobility in Unentangled Polystyrene Films. *Science* 2010, *328*, 1676–1679.
(43) Mirigian, S.; Schweizer, K. S. Communication: Slow Relaxation, Spatial Mobility Gradients, and Vitrification in Confined Films. *J. Chem. Phys.* 2014, *141*, 161103.
(44) Yang, Z.; Clough, A.; Lam, C.-H.; Tsui, O. K. C. Glass Transition Dynamics and Surface Mobility of Entangled Polystyrene Films at Equilibrium. *Macromolecules* 2011, *44*, 8294–8300.
(45) Tsui, O. K. C.; Wang, X. P.; Ho, J. Y. L.; Ng, T. K.; Xiao, X. D. Studying Surface Glass-to-Rubber Transition Using Atomic Force Microscopic Adhesion Measurements. *Macromolecules* 2000, *33*, 4198–4204.
(46) Tsui, O. K. C.; Russell, T. P.; Hawker, C. J. Effect of Interfacial Interactions on the Glass Transition of Polymer Thin Films. *Macromolecules* 2001, *34*, 5535–5539.
(47) Napolitano, S.; Wubbenhorst, M. The Lifetime of the Deviations from Bulk Behaviour in Polymers Confined at the Nanoscale. *Nat. Commun.* 2011, *2*, 260.
(48) Paeng, K.; Richert, R.; Ediger, M. D. Molecular Mobility in Supported Thin Films of Polystyrene, Poly(methyl Methacrylate), and poly(2-Vinyl Pyridine) Probed by Dye Reorientation. *Soft Matter* 2012, *8*, 819–826.

(49) Barrat, J.-L.; Baschnagel, J.; Lyulin, A. Molecular Dynamics Simulations of Glassy Polymers. *Soft Matter* 2010, *6*, 3430–3446.
(50) Tsui, O. K. C.; Zhang, H. F. Effects of Chain Ends and Chain Entanglement on the Glass Transition Temperature of Polymer Thin Films. *Macromolecules* 2001, *34*, 9139–9142.
(51) Napolitano, S.; Pilleri, A.; Rolla, P.; Wuebbenhorst, M. Unusual Deviations from Bulk Behavior in Ultrathin Films of Poly(tert-Butylstyrene): Can Dead Layers Induce a Reduction of T-G? *Acs Nano* 2010, *4*, 841–848.
(52) Napolitano, S.; Capponi, S.; Vanroy, B. Glassy Dynamics of Soft Matter under 1D Confinement: How Irreversible Adsorption Affects Molecular Packing, Mobility Gradients and Orientational Polarization in Thin Films. *Eur. Phys. J. E* 2013, *36*, 61.
(53) Wang, S.; Yang, S.; Lee, J.; Akgun, B.; Wu, D. T.; Foster, M. D. Anomalous Surface Relaxations of Branched-Polymer Melts. *Phys. Rev. Lett.* 2013, *111*, 068303.
(54) Wang, S.-F.; Jiang, Z.; Narayanan, S.; Foster, M. D. Dynamics of Surface Fluctuations on Macrocyclic Melts. *Macromolecules* 2012, *45*, 6210–6219.
(55) Glynos, E.; Chremos, A.; Frieberg, B.; Sakellariou, G.; Green, P. F. Wetting of Macromolecules: From Linear Chain to Soft Colloid-Like Behavior. *Macromolecules* 2014, *47*, 1137–1143.
(56) Glynos, E.; Frieberg, B.; Green, P. F. Wetting of a Multiarm Star-Shaped Molecule. *Phys. Rev. Lett.* 2011, *107*, 118303.
(57) Frieberg, B.; Glynos, E.; Sakellariou, G.; Green, P. F. Physical Aging of Star-Shaped Macromolecules. *ACS Macro Lett.* 2012, *1*, 636–640.
(58) Chremos, A.; Glynos, E.; Green, P. F. Structure and Dynamical Intra-Molecular Heterogeneity of Star Polymer Melts above Glass Transition Temperature. *J. Chem. Phys.* 2015, *142*, 044901.
(59) Sikorski, A. Computer Simulation of Adsorbed Polymer Chains with a Different Molecular Architecture. *Macromol. Theory Simul.* 2001, *10*, 38–45.
(60) Sikorski, A. Dynamics of Adsorbed Star-Branched Polymer Chains: A Computer Simulation Study. *Macromol. Theory Simul.* 2003, *12*, 325–331.
(61) Adamczyk, P.; Sikorski, A. The Influence of the Macromolecular Architecture on Adsorption of Polymer Chains on a Solid Surface. *Polimery* 2010, *55*, 512–517.
(62) Jaworski, S.; Sikorski, A. Properties of Branched Polymer Chains Adsorbed on a Patterned Surface. *Polymer* 2012, *53*, 1741–1746.
(63) Chremos, A.; Douglas, J. F. Communication: When Does a Branched Polymer Become a Particle? *J. Chem. Phys.* 2015, *143*, 111104.
(64) Chremos, A.; Glynos, E.; Green, P. F. Structure and Dynamical Intra-Molecular Heterogeneity of Star Polymer Melts above Glass Transition Temperature. *J. Chem. Phys.* 2015, *142*, 044901.
(65) Chremos, A.; Camp, P. J.; Glynos, E.; Koutsos, V. Adsorption of Star Polymers: Computer Simulations. *Soft Matter* 2010, *6*, 1483–1493.
(66) Egorov, S. A.; Paturej, J.; Likos, C. N.; Milchev, A. Controlling the Interactions between Soft Colloids via Surface Adsorption. *Macromolecules* 2013, *46*, 3648–3653.
(67) Jancar, J.; Douglas, J. F.; Starr, F. W.; Kumar, S. K.; Cassagnau, P.; Lesser, A. J.; Sternstein, S. S.; Buehler, M. J. Current Issues in Research on Structure-Property Relationships in Polymer Nanocomposites. *Polymer* 2010, *51*, 3321–3343.
(68) Mackay, M. E.; Tuteja, A.; Duxbury, P. M.; Hawker, C. J.; Van Horn, B.; Guan, Z. B.; Chen, G. H.; Krishnan, R. S. General Strategies for Nanoparticle Dispersion. *Science* 2006, *311*, 1740–1743.
(69) Rittigstein, P.; Priestley, R. D.; Broadbelt, L. J.; Torkelson, J. M. Model Polymer Nanocomposites Provide an Understanding of Confinement Effects in Real Nanocomposites. *Nat. Mater.* 2007, *6*, 278–282.
(70) Kim, T.; Lee, C.-H.; Joo, S.-W.; Lee, K. Kinetics of Gold Nanoparticle Aggregation: Experiments and Modeling. *J. Colloid Interface Sci.* 2008, *318*, 238–243.
(71) Green, P. F.; Oh, H.; Akcora, P.; Kumar, S. K. *Structure and Dynamics of Polymer Nanocomposites Involving Chain-Grafted Spherical Nanoparticles*; GarciaSakai, V.; AlbaSimionesco, C.; Chen, S. H., Eds.; Springer: New York, 2012.

(72) Kim, J.; Green, P. F. Phase Behavior of Thin Film Brush-Coated Nanoparticles/Homopolymer Mixtures. *Macromolecules* 2010, *43*, 1524–1529.
(73) Arceo, A.; Meli, L.; Green, P. F. Glass Transition of Polymer-Nanocrystal Thin Film Mixtures: Role of Entropically Directed Forces on Nanocrystal Distribution. *Nano Lett.* 2008, *8*, 2271–2276.
(74) Green, P. F. The Structure of Chain End-Grafted Nanoparticle/Homopolymer Nanocomposites. *Soft Matter* 2011, *7*, 7914–7926.
(75) Johnson, K. J.; Glynos, E.; Sakellariou, G.; Green, P. Dynamics of Star-Shaped Polystyrene Molecules: From Arm Retraction to Cooperativity. *Macromolecules* 2016, *49*, 5669–5676.
(76) Daoud, M.; Cotton, J. Star Shaped Polymers - a Model for the Conformation and Its Concentration-Dependence. *J. Phys.* 1982, *43*, 531–538.
(77) Grest, G. S.; Fetters, L. J.; Huang, J. S.; Richter, D. Star Polymers: Experiment, Theory, and Simulation. *Adv. Chem. Phys. Vol Xciv* 1996, *94*, 67–163.
(78) Yu, H.-Y.; Koch, D. L. Structure of Solvent-Free Nanoparticle−Organic Hybrid Materials. *Langmuir* 2010, *26*, 16801–16811.
(79) Pakula, T. Static and Dynamic Properties of Computer Simulated Melts of Multiarm Polymer Stars. *Comput. Theor. Polym. Sci.* 1998, *8*, 21–30.
(80) Pakula, T.; Vlassopoulos, D.; Fytas, G.; Roovers, J. Structure and Dynamics of Melts of Multiarm Polymer Stars. *Macromolecules* 1998, *31*, 8931–8940.
(81) Vlassopoulos, D.; Pakula, T.; Fytas, G.; Roovers, J.; Karatasos, K.; Hadjichristidis, N. Ordering and Viscoelastic Relaxation in Multiarm Star Polymer Melts. *Europhys. Lett.* 1997, *39*, 617–622.
(82) Green, P. F.; Glynos, E.; Frieberg, B. Polymer Films of Nanoscale Thickness: Linear Chain and Star-Shaped Macromolecular Architectures. *Mrs Commun.* 2015, *5*, 423–434.
(83) Glynos, E.; Frieberg, B.; Chremos, A.; Sakellariou, G.; Gidley, D. W.; Green, P. F. Vitrification of Thin Polymer Films: From Linear Chain to Soft Colloid-like Behavior. *Macromolecules* 2015, *48*, 2305–2312.
(84) Willner, L.; Jucknischke, O.; Richter, D.; Roovers, J.; Zhou, L.; Toporowski, P.; Fetters, L.; Huang, J.; Lin, M.; Hadjichristidis, N. Structural Investigation of Star Polymers in Solution by Small-Angle Neutron-Scattering. *Macromolecules* 1994, *27*, 3821–3829.
(85) Rubinstein, M.; Colby, R. *Polymer Physics*; 1 edition.; Oxford University Press: Oxford ; New York, 2003.
(86) Likos, C. N.; Lowen, H.; Watzlawek, M.; Abbas, B.; Jucknischke, O.; Allgaier, J.; Richter, D. Star Polymers Viewed as Ultrasoft Colloidal Particles. *Phys. Rev. Lett.* 1998, *80*, 4450–4453.
(87) Rouse, P. A Theory of the Linear Viscoelastic Properties of Dilute Solutions of Coiling Polymers. *J. Chem. Phys.* 1953, *21*, 1272–1280.
(88) Rouse, P.; Sittel, K. Viscoelastic Properties of Dilute Polymer Solutions. *J. Appl. Phys.* 1953, *24*, 690–696.
(89) Gennes, P.-G. *Scaling Concepts in Polymer Physics*; Cornell University Press: Ithaca, NY, 1979.
(90) Gennes, P. G. de. Reptation of a Polymer Chain in the Presence of Fixed Obstacles. *J. Chem. Phys.* 1971, *55*, 572–579.
(91) Doi, M.; Edwards, S. F. *The Theory of Polymer Dynamics*; Clarendon Press: Oxford, 1988.
(92) Fetters, L.; Kiss, A.; Pearson, D.; Quack, G.; Vitus, F. Rheological Behavior of Star-Shaped Polymers. *Macromolecules* 1993, *26*, 647–654.
(93) Ball, R.; Mcleish, T. Dynamic Dilution and the Viscosity of Star Polymer Melts. *Macromolecules* 1989, *22*, 1911–1913.
(94) Pearson, D.; Helfand, E. Viscoelastic Properties of Star-Shaped Polymers. *Macromolecules* 1984, *17*, 888–895.
(95) Doi, M.; Kuzuu, N. Rheology of Star Polymers in Concentrated-Solutions and Melts. *J. Polym. Sci. Part C-Polym. Lett.* 1980, *18*, 775–780.
(96) Adams, C. H.; Brereton, M. G.; Hutchings, L. R.; Klein, P. G.; McLeish, T. C. B.; Richards, R. W.; Ries, M. E. A Deuterium NMR Study of Selectively Labeled Polybutadiene Star Polymers. *Macromolecules* 2000, *33*, 7101–7106.

(97) Adams, C. H.; Hutchings, L. R.; Klein, P. G.; McLeish, T. C. B.; Richards, R. W. Synthesis and Dynamic Rheological Behavior of Polybutadiene Star Polymers. *Macromolecules* 1996, *29*, 5717–5722.
(98) Milner, S. T.; McLeish, T. C. B. Arm-Length Dependence of Stress Relaxation in Star Polymer Melts. *Macromolecules* 1998, *31*, 7479–7482.
(99) Milner, S. T.; McLeish, T. C. B. Parameter-Free Theory for Stress Relaxation in Star Polymer Melts. *Macromolecules* 1997, *30*, 2159–2166.
(100) Vlassopoulos, D.; Fytas, G.; Pakula, T.; Roovers, J. Multiarm Star Polymers Dynamics. *J. Phys.-Condens. Matter* 2001, *13*, R855–R876.
(101) Watanabe, H.; Matsumiya, Y.; Inoue, T. Dielectric and Viscoelastic Relaxation of Highly Entangled Star Polyisoprene: Quantitative Test of Tube Dilation Model. *Macromolecules* 2002, *35*, 2339–2357.
(102) Semenov, A. N.; Vlassopoulos, D.; Fytas, G.; Vlachos, G.; Fleischer, G.; Roovers, J. Dynamic Structure of Interacting Spherical Polymer Brushes. *Langmuir* 1999, *15*, 358–368.
(103) Kapnistos, M.; Semenov, A. N.; Vlassopoulos, D.; Roovers, J. Viscoelastic Response of Hyperstar Polymers in the Linear Regime. *J. Chem. Phys.* 1999, *111*, 1753–1759.
(104) Roovers, J.; Zhou, L.; Toporowski, P.; Vanderzwan, M.; Iatrou, H.; Hadjichristidis, N. Regular Star Polymers with 64 and 128 Arms - Models for Polymeric Micelles. *Macromolecules* 1993, *26*, 4324–4331.
(105) Vlassopoulos, D.; Fytas, G.; Roovers, J.; Pakula, T.; Fleischer, G. Ordering and Dynamics of Soft Spheres in Melt and Solution. *Faraday Discuss.* 1999, *112*, 225–235.
(106) Akcora, P.; Liu, H.; Kumar, S. K.; Moll, J.; Li, Y.; Benicewicz, B. C.; Schadler, L. S.; Acehan, D.; Panagiotopoulos, A. Z.; Pryamitsyn, V.; *et al.* Anisotropic Self-Assembly of Spherical Polymer-Grafted Nanoparticles. *Nat. Mater.* 2009, *8*, 354-U121.
(107) Kango, S.; Kalia, S.; Celli, A.; Njuguna, J.; Habibi, Y.; Kumar, R. Surface Modification of Inorganic Nanoparticles for Development of Organic-Inorganic Nanocomposites-A Review. *Prog. Polym. Sci.* 2013, *38*, 1232–1261.
(108) Hasegawa, R.; Aoki, Y.; Doi, M. Optimum Graft Density for Dispersing Particles in Polymer Melts. *Macromolecules* 1996, *29*, 6656–6662.
(109) Ferreira, P. G.; Ajdari, A.; Leibler, L. Scaling Law for Entropic Effects at Interfaces between Grafted Layers and Polymer Melts. *Macromolecules* 1998, *31*, 3994–4003.
(110) Gast, A.; Leibler, L. Interactions of Sterically Stabilized Particles Suspended in a Polymer-Solution. *Macromolecules* 1986, *19*, 686–691.
(111) Gast, A.; Leibler, L. Effect of Polymer-Solutions on Sterically Stabilized Suspensions. *J. Phys. Chem.* 1985, *89*, 3947–3949.
(112) Wijmans, C.; Zhulina, E.; Fleer, G. Effect of Free Polymer on the Structure of a Polymer Brush and Interaction Between 2 Polymer Brushes. *Macromolecules* 1994, *27*, 3238–3248.
(113) Chandran, S.; Begam, N.; Padmanabhan, V.; Basu, J. K. Confinement Enhances Dispersion in Nanoparticle-Polymer Blend Films. *Nat. Commun.* 2014, *5*, 3697.
(114) Chandran, S.; Begam, N.; Basu, J. K. Dispersion of Polymer Grafted Nanoparticles in Polymer Nanocomposite Films: Insights from Surface X-Ray Scattering and Microscopy. *J. Appl. Phys.* 2014, *116*, 222203.
(115) Matsen, M. W.; Gardiner, J. M. Autophobic Dewetting of Homopolymer on a Brush and Entropic Attraction between Opposing Brushes in a Homopolymer Matrix. *J. Chem. Phys.* 2001, *115*, 2794–2804.
(116) Tuteja, A.; Mackay, M. E.; Narayanan, S.; Asokan, S.; Wong, M. S. Breakdown of the Continuum Stokes-Einstein Relation for Nanoparticle Diffusion. *Nano Lett.* 2007, *7*, 1276–1281.
(117) Cai, L.-H.; Panyukov, S.; Rubinstein, M. Mobility of Nonsticky Nanoparticles in Polymer Liquids. *Macromolecules* 2011, *44*, 7853–7863.

(118) Yamamoto, U.; Schweizer, K. S. Microscopic Theory of the Long-Time Diffusivity and Intermediate-Time Anomalous Transport of a Nanoparticle in Polymer Melts. *Macromolecules* 2015, *48*, 152–163.
(119) Guo, H.; Bourret, G.; Corbierre, M. K.; Rucareanu, S.; Lennox, R. B.; Laaziri, K.; Piche, L.; Sutton, M.; Harden, J. L.; Leheny, R. L. Nanoparticle Motion within Glassy Polymer Melts. *Phys. Rev. Lett.* 2009, *102*, 075702.
(120) Ganesan, V.; Pryamitsyn, V.; Surve, M.; Narayanan, B. Noncontinuum Effects in Nanoparticle Dynamics in Polymers. *J. Chem. Phys.* 2006, *124*, 221102.
(121) Jang, W.-S.; Koo, P.; Bryson, K.; Narayanan, S.; Sandy, A.; Russell, T. P.; Mochrie, S. G. Dynamics of Cadmium Sulfide Nanoparticles within Polystyrene Melts. *Macromolecules* 2014, *47*, 6483–6490.
(122) Grabowski, C. A.; Mukhopadhyay, A. Size Effect of Nanoparticle Diffusion in a Polymer Melt. *Macromolecules* 2014, *47*, 7238–7242.
(123) Hoshino, T.; Murakami, D.; Tanaka, Y.; Takata, M.; Jinnai, H.; Takahara, A. Dynamical Crossover between Hyperdiffusion and Subdiffusion of Polymer-Grafted Nanoparticles in a Polymer Matrix. *Phys. Rev. E* 2013, *88*, 032602.
(124) Srivastava, S.; Agarwal, P.; Mangal, R.; Koch, D. L.; Narayanan, S.; Archer, L. A. Hyperdiffusive Dynamics in Newtonian Nanoparticle Fluids. *Acs Macro Lett.* 2015, *4*, 1149–1153.
(125) Yamamoto, U.; Schweizer, K. S. Theory of Nanoparticle Diffusion in Unentangled and Entangled Polymer Melts. *J. Chem. Phys.* 2011, *135*, 224902.
(126) Egorov, S. A. Anomalous Nanoparticle Diffusion in Polymer Solutions and Melts: A Mode-Coupling Theory Study. *J. Chem. Phys.* 2011, *134*, 084903.
(127) Oh, H.; Green, P. F. Polymer Chain Dynamics and Glass Transition in Athermal Polymer/Nanoparticle Mixtures. *Nat. Mater.* 2009, *8*, 139–143.
(128) Napolitano, S.; Glynos, E.; Tito, N. B. Glass Transition of Polymers in Bulk, Confined Geometries, and near Interfaces. *Rep. Prog. Phys.* 2017, *80*, 036602.
(129) Hanakata, P. Z.; Douglas, J. F.; Starr, F. W. Interfacial Mobility Scale Determines the Scale of Collective Motion and Relaxation Rate in Polymer Films. *Nat. Commun.* 2014, *5*, 4163.
(130) Hanakata, P. Z.; Douglas, J. F.; Starr, F. W. Local Variation of Fragility and Glass Transition Temperature of Ultra-Thin Supported Polymer Films. *J. Chem. Phys.* 2012, *137*, 244901.
(131) Ediger, M. D.; Forrest, J. A. Dynamics near Free Surfaces and the Glass Transition in Thin Polymer Films: A View to the Future. *Macromolecules* 2014, *47*, 471–478.

Chapter II
Dynamic Transitions in Star-shaped Polystyrene

II.1. Introduction:

Molecular topology can strongly influence the physical properties of polymers. Examples of physical properties include surface tension,[1,2] the preferential segregation of branched macromolecules to surfaces,[3,4] glass transition temperatures of both bulk and thin films,[5–7] wetting phenomena,[8,9] physical aging,[10–12] dynamics,[13–19] and bulk rheological behavior.[20–22] Recent molecular simulations,[23,24] together with new molecular design principles and synthetic strategies[25–28] that enable molecules with tailored chemistries, controlled molecular weight distributions and specific molecular weights to be synthesized, have enabled a deeper understanding of the influence of molecular topology on the physical properties of polymers. Of specific interest in this paper is the rheological behavior of star-shaped macromolecules of varying functionalities f (number of arms) and molecular weights per arm M_a. A star-shaped macromolecule is composed of a branch point unto which f chains, each of molecular weight per arm M_a, are covalently bonded. Due to the entropic restrictions associated with the attachment of

molecules to the branch point, the density of chain segments is highest in the central core region and decreases toward the ends of the arms where the chain segments have the largest configurational freedom.[29,30] The radius of the central core region r_c increases with the functionality as $r_c \propto f^{1/2}$. The segments that compose the outer regions of the molecule, the corona, are able to relax freely and intermix with segments from other molecules, filling space.[31] For stars with high functionalities and sufficiently short arms, entropic repulsions are responsible for the emergence of structural order,[7,12,21,22,32–36] wherein the stars exhibit a tendency to "pack" like soft particles. These structural effects are manifested in the physical properties of stars-wetting, thin film glass transition temperatures and the glass transition – particularly with functionalities, greater than approximately 4 – 6.

The translational diffusion of macromolecules is strongly dependent on molecular topology. The dynamics of unentangled linear chains are well described by the Rouse model where the diffusion coefficient *D* is inversely proportional to the molecular weight *M* of the chain, because the friction coefficient is proportional to the chain length.[37–39] For highly entangled linear polymer melts the Reptation model, and experiment, indicates that the translational diffusion coefficient is proportional to M^{-2}.[40,41] For long-arm, low-functionality, entangled, star-shaped macromolecules, the center of mass motion is enabled by an arm retraction mechanism, wherein the arm of a star-shaped macromolecule moves along the primitive path within a "tube" toward the branch point.[42–45] Here diffusion is much slower – as the arm retraction process is entropically unfavorable – and depends exponentially on the length of the arm M_a. The segments of the arms near the free ends relax much faster than segments in the core region of the star;[46,47] this behavior and the much slower center-of-mass dynamics of the

chains are responsible for a hierarchy of length-scales and time-scales that characterize the dynamics of star shaped polymers.

Milner and McLeish,[48,49] in a quantitative model describing the dynamics of entangled star-shaped macromolecules, showed that the free end of an arm makes excursions along the primitive path a fractional distance *s*, subject to a potential U_{eff}(s) described by:

$$U_{eff}(s) = \frac{15M_a}{4M_e}\frac{1-(1-s)^{1+\alpha}[1+(1+\alpha)s]}{(1+\alpha)(2+\alpha)} \quad (1)$$

The exponent α is related to the dilution exponent used to account for dynamic dilution effects on the entanglement network. The relaxation time τ(s) used in the Milner-McLeish (MM) model has two components: an activated relaxation time dependent upon U_{eff}(s), $\tau_{late}(s)$, and a relaxation time $\tau_{early}(s)$ related to early time, "Rouse retraction," of the arm free end before it is influenced by the restriction of the branch point. Quantitatively,

$$\tau(s) \approx \frac{\tau_{early}(s)\exp[U_{eff}(s)]}{1+\exp[U_{eff}(s)]\frac{\tau_{early}(s)}{\tau_{late}(s)}} \quad (2)$$

Since U_{eff}(s) is proportional to the ratio of the molecular weight of the arm M_a to the molecular weight between entanglements M_e, then $\tau(s)$ depends exponentially on M_a/M_e.[42–44,48] The stress relaxation modulus $G(t)$ is predicted to depend on $\tau(s)$ such that:

$$G(t) = 2G_N \int_0^1 ds(1-s)^{\alpha} \exp[-\frac{t}{\tau(s)}] \quad (3)$$

and the frequency dependent complex modulus $G^*(\omega)$ is:

$$G^*(\omega) = 2G_N \int_0^1 ds(1-s)^\alpha \frac{-i\omega\tau(s)}{1-i\omega\tau(s)} \quad (4)$$

While the Milner-McLeish model provides a good description of the viscoelastic moduli $G'(\omega)$ and $G''(\omega)$ for low functionality entangled stars,[16,20] it is, or course, not successful at describing the behavior of high functionality star polymers, due to effects associated with the size of the core[20–22,32,50–53] and associated entropic effects, not specifically addressed by the theory.

The majority of experimental work on star polymers has been dedicated to entangled, low functionality molecules, where the Milner-McLeish model provides an adequate description of the dynamics. Relatively little emphasis has been placed on the study of short-arm, high functionality star polymers[23,32,33], whose dynamics are not described by the Milner-McLeish model. Recent simulations[23,33] and experiments[7,12] suggest evidence of a transition from chain-like to colloid-like behavior for star polymers with functionalities as low as f=6 with sufficiently short arms. To further explore this transition we performed oscillatory shear measurements to develop deeper insight into the behavior of star polymers possessing a wide range of functionalities - $2 \leq f \leq 64$- and molecular weights per arm- 7 kg./mol. $\leq M_a \leq$ 80kg./mol. (See Table 1). Combinations of f and M_a that delineate boundaries where the mechanisms of arm-retraction and cooperative dynamics, associated with spatial ordering of the molecules, occur are identified and discussed.

II.2. Experimental Section:

The star-shaped polymers (Table 1) were synthesized via anionic polymerization under high vacuum[52,54,55] conditions; star polymers identified with an asterisk (*) were purchased from Polymer Source Inc. (Canada). The glass transition temperatures T_g of the molecules were measured using modulated differential scanning calorimetry. The oscillatory shear rheometry measurements were performed using an ARES 2K FRTN1 strain-controlled rheometer (TA Instruments, USA) with parallel plates 8 mm in diameter. Temperature control was achieved using an air/nitrogen convection oven to create an inert atmosphere during measurements at all temperatures. Samples were pressed into disks using a Carver Press and a custom built mold. These samples were then placed on a bottom plate, and temperature was increased until melt conditions were achieved, after which the samples were compressed. After an equilibration time, the samples were trimmed and further compressed to a thickness of 0.5 to 1.0 mm. Before measurements were performed at each temperature, the samples were held for 20 to 30 min in order to allow relaxation of residual stresses. The thermal expansion of the plates was taken into account by making appropriate changes to the gap spacing as temperature was varied. Measurements were taken over a temperature range of $120℃\ to\ 180℃$ depending on the sample. Frequency sweeps varied from 200 to 0.1 rad./sec. in order to maintain stability of the samples at higher temperatures; the strain amplitude was kept in the linear viscoelastic regime, which was determined by a strain sweep at 200 rad/s for every temperature. Multiple runs were performed at every temperature in order to ensure the reproducibility, equilibration, and thermal stability of the samples for the given experimental parameters.

Table II.1: Star-shaped polymer molecular parameters

Name	Functionality	Ma (kg/mol)	Tg (˚C)	$Z=M_a/M_e$	PDI

LPS-50K*	**2**	**25,000**	**102.5**	**1.88**	**1.02**
SPS 4-7K	**4**	**7,000**	**99.8**	**0.53**	**1.03**
SPS 4-55K	**4**	**55,000**	**105.6**	**4.14**	**1.03**
SPS 4-85K	**4**	**85,000**	**105.9**	**6.39**	**1.03**
SPS 8-10K*	**8**	**10,000**	**82.2**	**0.75**	**1.03**
SPS 8-29K	**8**	**29,000**	**90**	**2.18**	**1.02**
SPS 8-57K	**8**	**57,000**	**91.9**	**4.29**	**1.02**
SPS 16-14K	**16**	**14,000**	**71.3**	**1.05**	**1.02**
SPS 16-29K	**16**	**29,000**	**91.1**	**2.18**	**1.02**
SPS 16-57K	**16**	**57,000**	**92.8**	**4.29**	**1.01**
SPS 32-8K	**32**	**9,000**	**79.9**	**0.68**	**1.03**
SPS 32-36K	**32**	**36,000**	**86.3**	**2.71**	**1.03**
SPS 32-52K	**32**	**52,000**	**87.7**	**3.91**	**1.01**
SPS 32-80K	**32**	**80,000**	**105.4**	**6.02**	**1.01**
SPS 64-8K	**64**	**9,000**	**76.8**	**0.68**	**1.02**
SPS 64-36K	**64**	**36,000**	**85.7**	**2.71**	**1.01**
SPS 64-52K	**64**	**52,000**	**86.6**	**3.91**	**1.01**
SPS 64-80K	**64**	**80,000**	**105.2**	**6.02**	**1.01**

The number of entanglements per arm to $Z_a = \frac{M_a}{{M_e}^0}$, where ${M_e}^0$ is the entanglement molecular weight of an equilibrated linear chain (=13,300 g/mol),[56] ranged from 0.5 to 6.

In order to provide a perspective on how the size of core region with respect to the size of the total star we applied the scaling argument from the Daoud-Cotton model, which indicates that the radius of the core region scales as:

$$r_c \sim f^{1/2} l_p \tag{5}$$

with the persistence length, l_p, corresponding to the size of statistical unit. The number of statistical units that are a part of the core region¸ *N*, is related to the functionality as:

$$f \sim N^2 \tag{6}$$

Through equations 5 and 6 the size of the core region can be rewritten as:

$$r_c \sim N l_p \quad (7)$$

Suggesting that, the volume fraction of the core region may change substantially for polymers of different l_p, for the same M_a and f. For this scaling argument, we assume that the behavior of the star-shaped polymer core in the melt is similar to its behavior in a theta solvent. The radius of gyration of the star, R_g, while not applicable in the melt, does help provide some perspective on the size of the core. The radius of gyration of the star was calculated using the equation presented by Likos[9,57]:

$$\langle {R_g}^2 \rangle_{star} \sim \frac{3f-2}{f^2} \langle {R_g}^2 \rangle_{linear} \quad (8)$$

which generates a star radius of gyration dependent on both functionality and total star molecular weight (since the linear R_g of polystyrene in a theta solvent depends on molecular weight as $R_g \propto \sqrt{M_w}$).The radius of gyration of linear polystyrenes was taken from literature[58] and used to determine the radius of gyration of the star with equation 8.

The data in Table 2 shows the radius of the core with respect to the star radius of gyration for the star-shaped polymers used in this study. The persistence length of polystyrene used was $l_p = 0.73\ nm$.

Table II.2: Star-shaped polymer core radius and radius of gyration

Name	r_c (nm)	R_g (nm)
SPS 4-7K	1.46	3.69

SPS 8-10K	2.065	4.63
SPS 16-14K	2.92	5.60
SPS 32-9K	4.13	4.54
SPS 64-9K*	5.84	4.56
SPS 8-29K	2.065	7.88
SPS 16-29K	2.92	8.06
SPS 32-36K	4.13	9.07
SPS 64-36K	5.84	9.12
SPS 4-55K	1.46	10.35
SPS 8-57K	2.065	11.05
SPS 16-57K	2.92	11.29
SPS 32-52K	4.13	10.90
SPS 64-52K	5.84	10.96
SPS 4-85K	1.46	12.86
SPS 32-80K	4.13	13.53
SPS 64-80K	5.84	13.60

It is evident from table 2 that the core region occupies a comparatively large volume fraction of molecules with short arm stars, for a fixed functionality. Note that this scaling behavior is not reliable when the number of entanglements per arm $Z < 1$. The asterisk in the table denotes where the scaling argument fails to accurately model the core size. For these polymers, we assume that the core occupies nearly the entire size of the star-shaped polymer.

II.3. Results & Discussion:

We observed a transition from the linear viscoelastic behavior for linear-chain and for low functionality star polymers, to behavior that manifests the influence of the core size - $r_c \propto f^{1/2}$- for molecules with functionalities $f \geq 8$. In order to understand this transition, the dynamics of an entangled linear chain polystyrene is first summarized in Figure 1, where G' and G'' are plotted as a function of frequency, and at low frequencies $G' \sim \omega^2$ and $G'' \sim \omega$. The relaxation rate $1/\tau_e$, or frequencies $\omega_e = 1/\tau_e$, associated with the onset of entanglement effects,

and ω_R ($\omega_R = 1/\tau_R$) associated with Reptation where are depicted. These parameters will serve as a basis of comparison with those of the star polymers. In order to fit our data to the Milner-McLeish model, we relied on a hierarchical algorithm, developed by Larson and coworkers.[59–61]

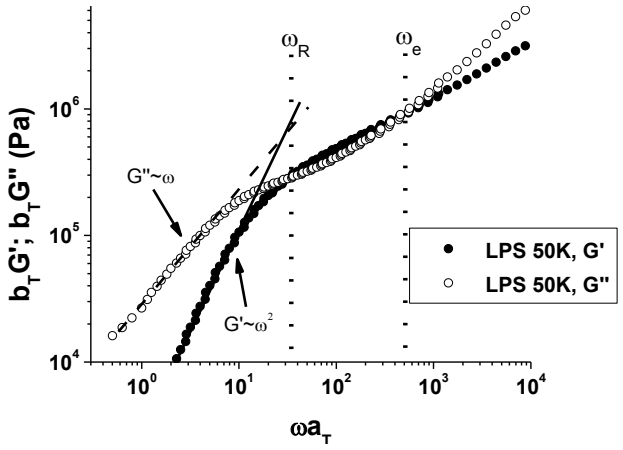

Figure II.1: Storage and loss modulus master curves for linear polystyrene, M_w= 50 kg/mol. Solid and dashed lines represent linear viscoelastic predictions of the frequency dependent storage and loss moduli, respectively. The dotted vertical lines correspond to the relaxation frequencies ω_e associated with the entanglement effects and ω_R, associated with Reptation. The reference temperature is T_{REF}=150°C.

In this algorithm, the plateau modulus, $G_{N,}$ and entanglement time, τ_e, used to achieve the fits were taken directly from the experimental data; the entanglement spacing, M_e, and monomer size were assumed to be the same as linear polystyrene. Vlassopoulos and co-workers used a similar method to fit the Milner-McLeish model to viscoelastic data for star-shaped polybutadiene and polyisoprene molecules.[51]

It is confirmed in Figure 2 that for low functionality stars (f=4), the Milner-McLeish model does a good job of describing $G'(\omega)$ and $G''(\omega)$, as expected.[48] The plateau modulus is, nevertheless, slightly underestimated for the for the longest arm star polymer (M_a=85 kg/mol).

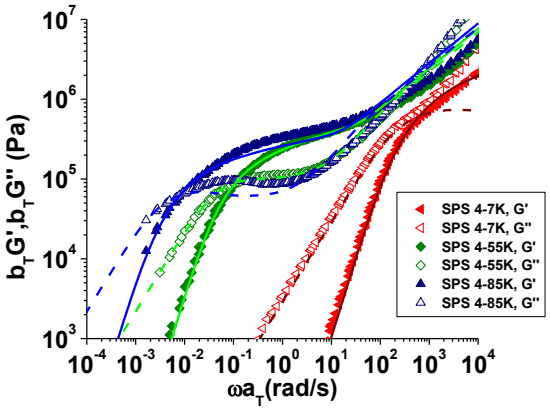

Figure II.2: Storage and loss modulus master curves for 4 arm stars. Closed symbols for experimental data of storage modulus; open symbols for experimental data of loss modulus. Red left triangles (SPS4-7K); green diamonds (SPS4-55K); blue triangles (SPS4-85K). Dashed curves correspond to MM fits for the loss modulus; solid curves correspond to MM fits for the storage modulus. Colors of fits correspond to the respective experimental data. Reference temperature is $T=T_g+50°C$.

As expected, the behaviors of the higher functionality stars are not appropriately described by the Milner-McLeish predictions. This is illustrated in Figure 3 where the storage and loss moduli for the high functionality stars (f=64, 9 kg/mol < M_a < 80 kg/mol) are shown to exhibit an additional relaxation processes in the low frequency regime. The relaxation denoted by ω_R* is associated with the arm relaxations; it is necessarily molecular weight dependent. The second relaxation ω_c is identified by the intersection of the lines extrapolated from the low frequency values of G' and G'' -in the terminal regime – and are associated with the emergence of a new mechanism that facilitates center of mass motion. The effect of this second process on

the viscoelastic response is especially apparent in the plot of *tan δ =G''/G'* versus ω/ω_{min} (Figure 3b), where the shoulder in *tan δ* is prominent. The deviation from the linear viscoelastic predictions increase as the arm length decreases and the functionality increases. Vlassopoulos and coworkers determined that the emergence of ω_c, is associated with a cooperative relaxation process .[20–22,51] Experiments and simulations show evidence of structural ordering of the macromolecules with high *f* and low M_a; [7,23,30,50,52] this is consistent with the assessment that a cooperative process would play an increasingly important role in the dynamics as *f* increases and the arm lengths decrease. This would be one reason the Milner-McLeish model is not applicable to high functionality stars.

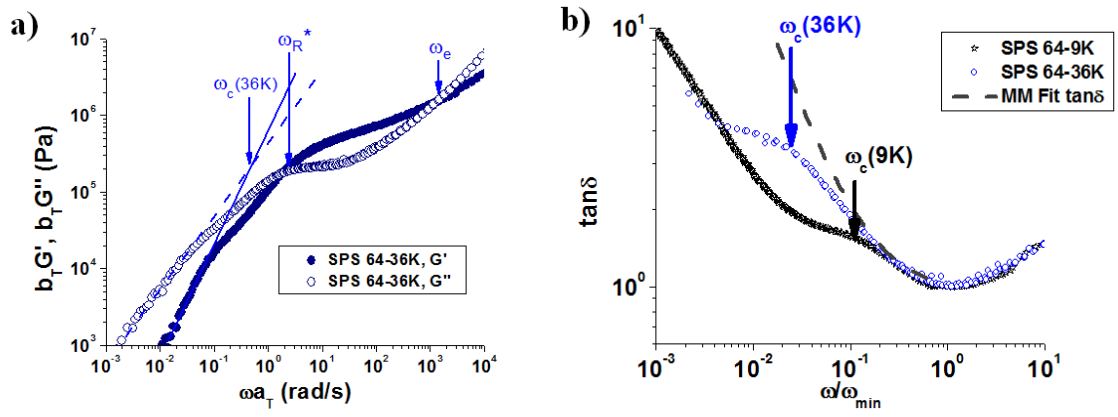

Figure II.3: a) Storage and loss modulus master curves for SPS 64-36K star shaped polymer. Closed symbols for experimental data of storage modulus; open symbols for experimental data of loss modulus. The terminal regime scaling of the storage and loss moduli are described by blue solid and dashed lines respectively. Reference temperature is $T=T_g+50$ ˚C. **b)** Normalized *tanδ* plotted as a function of normalized frequency. Black stars SPS 64-9K. Blue circles SPS 64-36K. Dashed line represents normalized MM fit for tanδ. MM fit parameters: G_N*=4.5e5 Pa*, τ_e*=0.05s*, M_e*=13.3 kg/mol*.

The transition from a purely arm relaxation process to a purely cooperative relaxation process is due to the increasing core fraction - r_c/R_g – and the associated tendency of the molecules toward structural ordering. Note further that because the core occupies a larger

volume fraction of the star with increasing f ($r_c \propto f^{1/2}$), the star becomes less compliant -the segments in this region are increasingly stretched and have a higher packing density. This is responsible for the weaker frequency dependence of G' in the low frequency range. This chain-like to colloidal-like transition is also evident in the behavior of thin films, wetting, and dynamics in this range of functionalities and molecular weights.[6-12]

The influence of changes in "packing" of the molecules with functionality is evident in both the shift parameters and the glass transition temperatures of these stars. The master curves (time-temperature superposition, TTS) of the storage and loss moduli used in this study were achieved through horizontal shifts. Figure 4 shows the horizontal (a_T) shift factors used to generate the master curves in this study. The vertical shift factors of the systems were independent of both functionality and arm length ($b_T = 1$). For the stars of higher molecular weight, the horizontal shift factors are very similar to those of a linear polystyrene chain (WLF parameters of $C_1^g = 14.41$ and $C_2^g = 53.60K$ (dark line), which are in good agreement with values of linear polystyrene in the literature, $C_1^g = 13.7$ and $C_2^g = 50K$).[62] The shift factors of these long arm stars appear to be largely independent of functionality (4a). However, as the arm length is decreased and the functionality is increased, the WLF parameters begin to differ from the behavior of the longer arm stars (4b). For the high functionality, short arm stars the WLF parameters deviate substantially from linear behavior. The value of C_2^g increases substantially for these high *f*, low M_a stars (4c), which is indicative of a significant decrease in fragility as these star-shaped polymers begin to order and the intermolecular interactions have a more pronounced impact. As these star-shaped polymers approach the behavior of a hard colloid, it is to be expected that time temperature superposition would no longer be relevant as interactions in hard colloid systems are temperature independent.

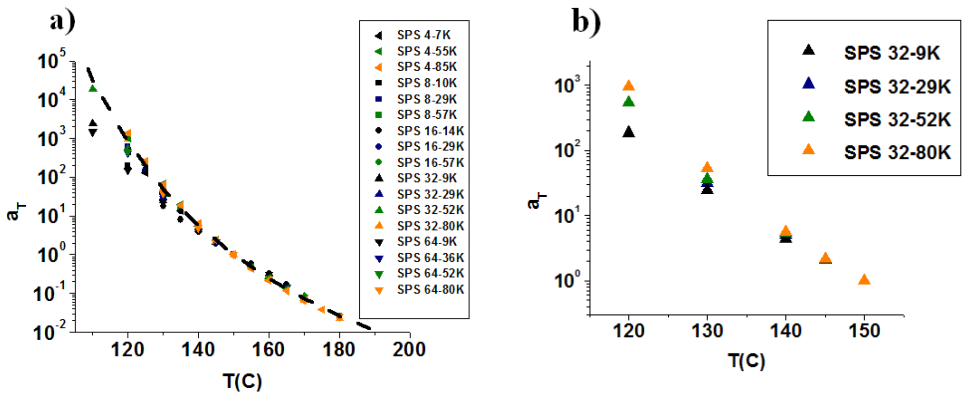

c)

	C_1^g	C_2^g
SPS 32-9K	16.86	71.83
SPS 32-36K	16.24	60.89
SPS 32-80K	12.33	57.06

Figure II.4: a) Horizontal shift factors of all stars at T=150˚C. Solid line is WLF Fit to data. **b)** Horizontal shift factors of 32 arm stars at T=150˚C. **c)** WLF parameters for 32 arm stars.

The glass transition temperatures of these star-shaped molecules exhibit distinct changes with *f* and M_a regime, as shown in Figure 5, where the glass transition temperature is plotted as a function of the number of chain ends/total star M_n. For very long arms, regardless of functionality, the behavior is similar to that of linear-chain polystyrene, as described some time ago by Fox and Flory.[63] It might be anticipated that the number of chain ends per molecule would increase the fractional free volume, leading to a decrease in T_g. This effect would not be apparent for long chains, as confirmed by these data. However, it becomes significant when the arm lengths of the molecules are shorter; the effect is much larger for the star-shaped polymers, as anticipated. Surprisingly, the decrease is not a strong function of *f*; in fact there is a saturation in the behavior with increasing *f* for arms of moderate lengths, $M_a \sim M_c$ or greater. Moreover the T_gs of the shortest arms ($M_a < M_e$) are higher than some of the molecules of intermediate arm

lengths, (see Table 1, SPS 16-14K). These behaviors are associated with the structure and packing of the star-shaped molecules with increasing *f* and decreasing M_a. The viscosity-temperature behavior of these molecules is less "fragile" than their high molecular weight analogs. Overall, this is consistent with the existence of intermolecular interactions (ordering) between the stars, mentioned earlier, as *f* increases and M_a decreases.

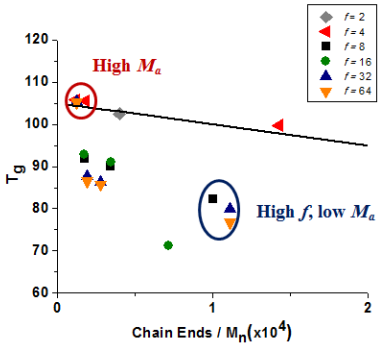

Figure II.5: Glass transition temperature (T_g) plotted as a function of the number of chain ends/ total molecule M_w. Dark line represents expected behavior for linear chains based on Fox-Flory equation.

As indicated earlier, the influence of the effects of ordering in high *f* star polymer melts has been suggested to begin for short arms at functionalities of $f \geq 6$.[23,33] to get further insight into this issue with regard to the dynamics of PS, we investigated the behavior of stars of *f=8* and varying values of M_a (*10 kg/mol<M_a<57 kg/mol)*. The data in Figure 6 reveal that while the arm-retraction mechanism primarily determines the dynamics for the SPS 8-57K and SPS 8-29K molecules, the behavior of the SPS 8-10K sample is different. The storage modulus of this molecule, with the unentangled arms, exhibits a slightly weaker frequency dependence. While the core region for these moderate functionality stars is not particularly large,[21,29] the influence of the core coupled with the short arms would be responsible for the increased storage modulus (more elastic behavior) at low frequency.

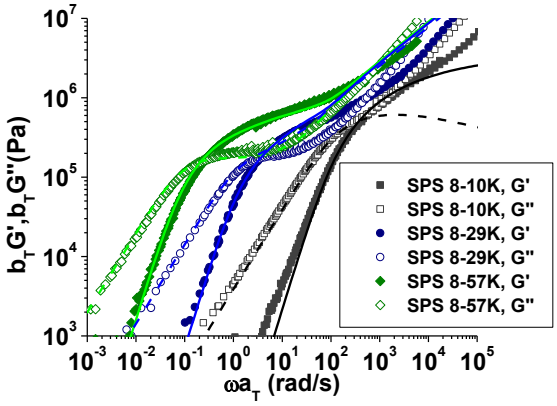

Figure II.6: Storage and loss modulus master curves for 8 arm stars. Closed symbols for experimental data of storage modulus; open symbols for experimental data of loss modulus. Grey squares (SPS8-10K); blue circles (SPS8-29K); green diamonds (SPS8-57K). Dashed curves correspond to MM fits for the loss modulus; solid curves correspond to MM fits for the storage modulus. Colors of fits correspond to the respective experimental data. Reference temperature is $T=T_g+50°C$.

For linear chain polymers, the critical molecular weight M_c denotes the onset of the effects of entanglements on the viscosity, so it might be interesting to examine the extent to which these parameters play a role toward determining the dynamics of star polymers, particularly for high *f*. To this end we probed the viscoelastic relaxations of stars where $M_a \sim M_c$. The data in Figure 7 shows the mechanical relaxations for SPS molecules of $8<f<64$ where $M_a \sim M_c$. It is evident that for this molecular weight M_c the core region begins to influence the dynamics of the star center-of-mass when $f \geq 16$ (7a&b); these deviations become larger as *f* is increased and are largest when $f \geq 64$.

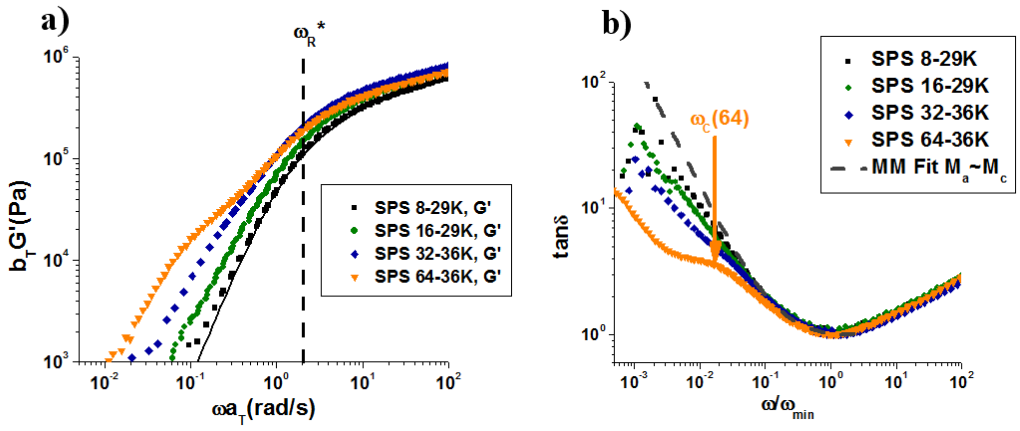

Figure II.7: a) Storage modulus master curves for stars with an arm length of $M_a \sim M_c$. Closed symbols for experimental data of storage modulus. Black squares (SPS8-29K); green circles (SPS16-29K); blue diamonds (SPS32-52K); orange triangles (SPS64-52K). Solid curve corresponds to MM fit for the storage modulus of SPS 8-29K. Reference temperature is T=145°C. **b)** Normalized *tan δ* with respect to normalized frequency. Dashed line is MM fit at M_c. MM fit parameters for all stars: $G_n=4.5e5\ Pa$, $\tau_e=0.05s$, $M_e=13.3\ kg/mol$.

When $f=64$, and the arms are short, a large fraction of the star is occupied by the core and intermolecular repulsions between the arms are responsible for the onset of structural order, reported earlier. The dynamics of these molecules is necessarily cooperative with an onset frequency of ω_c. Evidence of the onset of this cooperative process is apparent in Figure 8, where deviations from arm relaxation dominated center-of-mass dynamics are observed for $f \geq 8$ (8b). The frequency ω_c associated with the cooperative rearrangements also occurs at higher values than the longer arm stars at M_c.

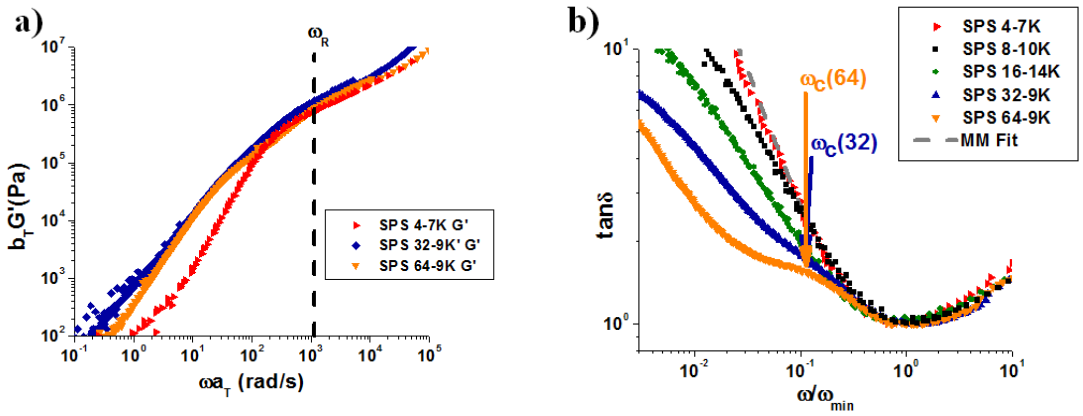

Figure II.8: a) Storage modulus master curves for stars with an arm length of $M_a<M_e$. Red triangles (SPS4-7K); blue diamonds (SPS32-9K); orange triangles (SPS64-9K). Solid curve corresponds to MM fit for the storage modulus of SPS 4-7K. Reference temperature is T=145°C. **b)** Normalized *tanδ* with respect to normalized frequency. Dashed line is MM fit at M_e. MM fit parameters for all stars: G_n*=4.5e5 Pa,* τ_e*=0.05s,* M_e*=13.3 kg/mol.*

The behavior described in the foregoing is summarized in Figure 9a, where *f* is plotted as a function of M_a*;* three regions are evident: a region where the arm retraction mechanism dominates, a region where cooperative dynamics are dominant, and a transitional region. The open symbols at low *f* represent star-shaped polymers undergoing arm relaxation dynamics, well described by the Milner-McLeish model, whereas the filled symbols identify stars that undergo purely cooperative dynamics. In the transition regime, represented by the half-filled symbols, the dynamics do not exhibit linear viscoelastic behavior -in the low ω regime, the storage modulus exhibits a weaker power law dependence on ω, $G'(\omega) \propto \omega^a$ (a <2), and tan δ deviates from the ω^{-1}. This behavior, as illustrated above in Figures 3 and 6, is indicative of contributions from the cooperative mechanism to the overall dynamics. However, when the core becomes comparable to the size of the molecule $r_c \sim R_g$, the dynamics are purely cooperative, similar to the behavior of soft colloids. Under these conditions tan δ *exhibits a shoulder (see Figs. 3b 7b and 8b).*

The boundaries between these regimes are largely determined by the size of the core relative to the overall size of the molecule –r_c/R_g. Based on equations 5 and 8, as well as the relationship between the radius of gyration and molecular weight for polystyrene in cyclohexane ($R_g = 2.79 \times 10^{-2} M^{1/2}$) [64], a relationship between f, M_a and r_c/R_g may be determined.

$$\frac{r_C}{R_g}\sqrt{M_a} \sim \frac{l_p}{0.0279}\sqrt{\frac{f^2}{3f-2}} \tag{9}$$

Equation 9 was used to plot f as a function of M_a (Fig. 9b) illustrating that as the core fraction decreases, f exhibits a weaker dependence on M_a. This would correspond to an increasing contribution of cooperativity to the overall dynamics of the molecule. The line in Figure 9a, dividing the region where the dynamics are purely cooperative and the transition region, was calculated using equation 9, and a core fraction of r_c/R_g=0.7. The boundary between the transition region and the arm-retraction region was calculated using equation 9, with r_c/R_g =0.23.

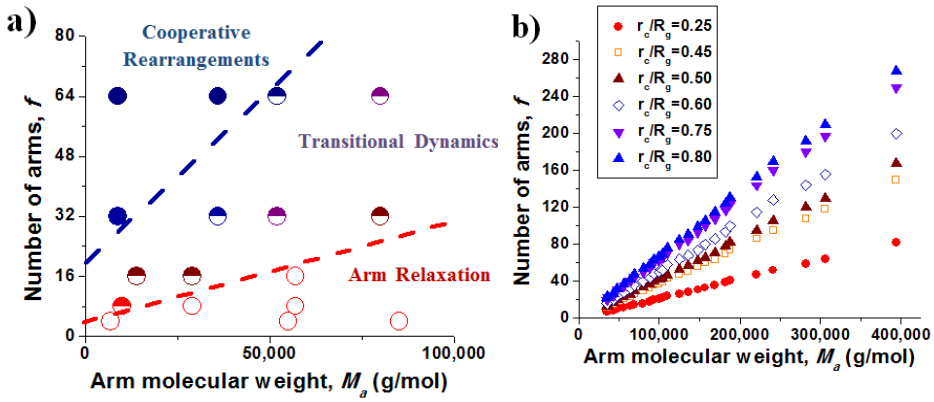

Figure II.9: a) Phase diagram of star dynamic behavior as a function of number of arms and number of entanglements per arm. Open symbols represent polymeric behavior (arm retraction), closed symbols represent soft colloidal behavior and the region enclosed by the lines -half filled symbols -represent the transition between the two mechanisms of dynamics. **b)** Graphic description of how core volume fraction is represented for various f and M_a.

It is evident that for low functionalities the arm retraction mechanism is entirely responsible for translational dynamics of the molecule. At higher functionalities, and over a range of shorter chain lengths, the stars exhibits a high degree of structural order and the translational dynamics appear to be due largely to the cooperative process, reminiscent of the behavior of colloidal-particles.

II.4. Conclusion:

We showed that when the functionality of the star molecules is low the polymers exhibit linear viscoelastic behavior, and the dynamics are characterized by an arm retraction mechanism, as described by the model of Milner and McLeish. For high functionalities and short, unentangled arms, the cores of the molecules occupy a substantial fraction of the molecule and intermolecular entropic repulsions between the stars influence the structural organization and hence the dynamics. For the largest functionalities and the shortest, unentangled, arms, the dynamics are highly cooperative. There is a transitional regime, characterized by intermediate values of f and M_a, where the arm retraction process begins to be strongly influenced by the increasing size of the impenetrable cores; this is manifested in the emergence of the cooperative rearrangements associated with soft-colloid behavior. The influence of the core region on the arm retraction mechanism is clear from the viscoelastic spectrum, where there is evidence of

increased elasticity. The dependence of the glass transition on molecular weight and functionality also manifest the changes in structure, with f and M_a.

References:

(1) Archer, A. J.; Likos, C. N.; Evans, R. Binary Star-Polymer Solutions: Bulk and Interfacial Properties. *J. Phys.-Condens. Matter* 2002, *14* (46), 12031–12050

(2) Qian, Z.; Minnikanti, V. S.; Sauer, B. B.; Dee, G. T.; Archer, L. A. Surface Tension of Symmetric Star Polymer Melts. *Macromolecules* 2008, *41* (13), 5007–5013

(3) Irvine, D. J.; Mayes, A. M.; GriffithCima, L. Self-Consistent Field Analysis of Grafted Star Polymers. *Macromolecules* 1996, *29* (18), 6037–6043

(4) Walton, D. G.; Mayes, A. M. Entropically Driven Segregation in Blends of Branched and Linear Polymers. *Phys. Rev. E* 1996, *54* (3), 2811–2815

(5) Roovers, J.; Toporows.pm. Glass-Transition Temperature of Star-Shaped Polystyrenes. *J. Appl. Polym. Sci.* 1974, *18* (6), 1685–1691 DOI:

(6) Glynos, E.; Frieberg, B.; Oh, H.; Liu, M.; Gidley, D. W.; Green, P. F. Role of Molecular Architecture on the Vitrification of Polymer Thin Films. *Phys. Rev. Lett.* 2011, *106* (12), 128301

(7) Green, P. F.; Glynos, E.; Frieberg, B. Polymer Films of Nanoscale Thickness: Linear Chain and Star-Shaped Macromolecular Architectures. *Mrs Commun.* 2015, *5* (3), 423–434

(8) Glynos, E.; Chremos, A.; Frieberg, B.; Sakellariou, G.; Green, P. F. Wetting of Macromolecules: From Linear Chain to Soft Colloid-Like Behavior. *Macromolecules* 2014, *47* (3), 1137–1143 (9) Glynos, E.; Frieberg, B.; Green, P. F. Wetting of a Multiarm Star-Shaped Molecule. *Phys. Rev. Lett.* 2011, *107* (11), 118303

(10) Frieberg, B.; Glynos, E.; Sakellariou, G.; Green, P. F. Physical Aging of Star-Shaped Macromolecules. *Acs Macro Lett.* 2012, *1* (5), 636–640

(11) Frieberg, B.; Glynos, E.; Green, P. F. Structural Relaxations of Thin Polymer Films. *Phys. Rev. Lett.* 2012, *108* (26), 268304

(12) Glynos, E.; Frieberg, B.; Chremos, A.; Sakellariou, G.; Gidley, D. W.; Green, P. F. Vitrification of Thin Polymer Films: From Linear Chain to Soft Colloid-like Behavior. *Macromolecules* 2015, *48* (7), 2305–2312

(13) Kisliuk, A.; Ding, Y.; Hwang, J.; Lee, J. S.; Annis, B. K.; Foster, M. D.; Sokolov, A. P. Influence of Molecular Architecture on Fast and Segmental Dynamics and the Glass Transition in Polybutadiene. *J. Polym. Sci. Part B-Polym. Phys.* 2002, *40* (21), 2431–2439

(14) Wang, S.; Yang, S.; Lee, J.; Akgun, B.; Wu, D. T.; Foster, M. D. Anomalous Surface Relaxations of Branched-Polymer Melts. *Phys. Rev. Lett.* 2013, *111* (6), 068303

(15) Liu, B.; Narayanan, S.; Wu, D. T.; Foster, M. D. Polymer Film Surface Fluctuation Dynamics in the Limit of Very Dense Branching. *Macromolecules* 2013, *46* (8), 3190–3197 (16) Watanabe, H.; Matsumiya, Y.; Inoue, T. Dielectric and Viscoelastic Relaxation of Highly Entangled Star Polyisoprene: Quantitative Test of Tube Dilation Model. *Macromolecules* 2002, *35* (6), 2339–2357

(17) Matsumiya, Y.; Watanabe, H. Further Test of the Tube Dilation Process in Star-Branched Cis-Polyisoprene: Role of Branching-Point Fluctuation. *Macromolecules* 2001, *34* (16), 5702–5710

(18) Watanabe, H.; Matsumiya, Y.; Osaki, K. Tube Dilation Process in Star-Branched Cis-Polyisoprenes. *J. Polym. Sci. Part B-Polym. Phys.* 2000, *38* (8), 1024–1036

(19) Matsumiya, Y.; Masubuchi, Y.; Inoue, T.; Urakawa, O.; Liu, C.-Y.; van Ruymbeke, E.; Watanabe, H. Dielectric and Viscoelastic Behavior of Star-Branched Polyisoprene: Two Coarse-Grained Length Scales in Dynamic Tube Dilation. *Macromolecules* 2014, *47* (21), 7637–7652

(20) Vlassopoulos, D.; Fytas, G.; Pakula, T.; Roovers, J. Multiarm Star Polymers Dynamics. *J. Phys.-Condens. Matter* 2001, *13* (41), R855–R876
(21) Pakula, T.; Vlassopoulos, D.; Fytas, G.; Roovers, J. Structure and Dynamics of Melts of Multiarm Polymer Stars. *Macromolecules* 1998, *31* (25), 8931–8940
(22) Vlassopoulos, D.; Pakula, T.; Fytas, G.; Roovers, J.; Karatasos, K.; Hadjichristidis, N. Ordering and Viscoelastic Relaxation in Multiarm Star Polymer Melts. *Europhys. Lett.* 1997, *39* (6), 617–622
(23) Chremos, A.; Douglas, J. F. Communication: When Does a Branched Polymer Become a Particle? *J. Chem. Phys.* 2015, *143* (11), 111104
(24) Fitzgerald, B. W.; Lentzakis, H.; Sakellariou, G.; Vlassopoulos, D.; Briels, W. J. A Computational and Experimental Study of the Linear and Nonlinear Response of a Star Polymer Melt with a Moderate Number of Unentangled Arms. *J. Chem. Phys.* 2014, *141* (11), 114907
(25) Polgar, L. M.; Lentzakis, H.; Collias, D.; Snijkers, F.; Lee, S.; Chang, T.; Sakellariou, G.; Wever, D. A. Z.; Toncelli, C.; Broekhuis, A. A.; Picchioni, F.; Gotsis, A. D.; Vlassopoulos, D. Synthesis and Linear Viscoelasticity of Polystyrene Stars with a Polyketone Core. *Macromolecules* 2015, *48* (18), 6662–6671
(26) Snijkers, F.; Cho, H. Y.; Nese, A.; Matyjaszewski, K.; Pyckhout-Hintzen, W.; Vlassopoulos, D. Effects of Core Microstructure on Structure and Dynamics of Star Polymer Melts: From Polymeric to Colloidal Response. *Macromolecules* 2014, *47* (15), 5347–5356
(27) Hadjichristidis, N.; Iatrou, H.; Pitsikalis, M.; Mays, J. Macromolecular Architectures by Living and Controlled/Living Polymerizations. *Prog. Polym. Sci.* 2006, *31* (12), 1068–1132
(28) Lee, J. S.; Quirk, R. P.; Foster, M. D. Synthesis and Characterization of Well-Defined, Regularly Branched Polystyrenes Utilizing Multifunctional Initiators. *Macromolecules* 2005, *38* (13), 5381–5392
(29) Daoud, M.; Cotton, J. Star Shaped Polymers - a Model for the Conformation and Its Concentration-Dependence. *J. Phys.* 1982, *43* (3), 531–538
(30) Grest, G. S.; Fetters, L. J.; Huang, J. S.; Richter, D. Star Polymers: Experiment, Theory, and Simulation. *Adv. Chem. Phys. Vol Xciv* 1996, *94*, 67–163 DOI: 10.1002/9780470141533.ch2.
(31) Yu, H.-Y.; Koch, D. L. Structure of Solvent-Free Nanoparticle−Organic Hybrid Materials. *Langmuir* 2010, *26* (22), 16801–16811
(32) Pakula, T. Static and Dynamic Properties of Computer Simulated Melts of Multiarm Polymer Stars. *Comput. Theor. Polym. Sci.* 1998, *8* (1–2), 21–30
(33) Chremos, A.; Glynos, E.; Green, P. F. Structure and Dynamical Intra-Molecular Heterogeneity of Star Polymer Melts above Glass Transition Temperature. *J. Chem. Phys.* 2015, *142* (4), 044901
(34) Willner, L.; Jucknischke, O.; Richter, D.; Roovers, J.; Zhou, L.; Toporowski, P.; Fetters, L.; Huang, J.; Lin, M.; Hadjichristidis, N. Structural Investigation of Star Polymers in Solution by Small-Angle Neutron-Scattering. *Macromolecules* 1994, *27* (14), 3821–3829
(35) Rubinstein, M.; Colby, R. *Polymer Physics*, 1 edition.; Oxford University Press: Oxford ; New York, 2003.
(36) Likos, C. N.; Lowen, H.; Watzlawek, M.; Abbas, B.; Jucknischke, O.; Allgaier, J.; Richter, D. Star Polymers Viewed as Ultrasoft Colloidal Particles. *Phys. Rev. Lett.* 1998, *80* (20), 4450–4453
(37) Rouse, P. A Theory of the Linear Viscoelastic Properties of Dilute Solutions of Coiling Polymers. *J. Chem. Phys.* 1953, *21* (7), 1272–1280
(38) Rouse, P.; Sittel, K. Viscoelastic Properties of Dilute Polymer Solutions. *J. Appl. Phys.* 1953, *24* (6), 690–696
(39) Gennes, P.-G. *Scaling Concepts in Polymer Physics*; Cornell University Press: Ithaca, NY, 1979.
(40) Gennes, P. G. de. Reptation of a Polymer Chain in the Presence of Fixed Obstacles. *J. Chem. Phys.* 1971, *55* (2), 572–579
(41) Doi, M.; Edwards, S. F. *The Theory of Polymer Dynamics*; Clarendon Press: Oxford, 1988.
(42) Fetters, L.; Kiss, A.; Pearson, D.; Quack, G.; Vitus, F. Rheological Behavior of Star-Shaped Polymers. *Macromolecules* 1993, *26* (4), 647–654

(43) Ball, R.; Mcleish, T. Dynamic Dilution and the Viscosity of Star Polymer Melts. *Macromolecules* 1989, *22* (4), 1911–1913
(44) Pearson, D.; Helfand, E. Viscoelastic Properties of Star-Shaped Polymers. *Macromolecules* 1984, *17* (4), 888–895 DOI: 10.1021/ma00134a060.
(45) Doi, M.; Kuzuu, N. Rheology of Star Polymers in Concentrated-Solutions and Melts. *J. Polym. Sci. Part C-Polym. Lett.* 1980, *18* (12), 775–780
(46) Adams, C. H.; Brereton, M. G.; Hutchings, L. R.; Klein, P. G.; McLeish, T. C. B.; Richards, R. W.; Ries, M. E. A Deuterium NMR Study of Selectively Labeled Polybutadiene Star Polymers. *Macromolecules* 2000, *33* (19), 7101–7106
(47) Adams, C. H.; Hutchings, L. R.; Klein, P. G.; McLeish, T. C. B.; Richards, R. W. Synthesis and Dynamic Rheological Behavior of Polybutadiene Star Polymers. *Macromolecules* 1996, *29* (17), 5717–5722
(48) Milner, S. T.; McLeish, T. C. B. Arm-Length Dependence of Stress Relaxation in Star Polymer Melts. *Macromolecules* 1998, *31* (21), 7479–7482
(49) Milner, S. T.; McLeish, T. C. B. Parameter-Free Theory for Stress Relaxation in Star Polymer Melts. *Macromolecules* 1997, *30* (7), 2159–2166
(50) Semenov, A. N.; Vlassopoulos, D.; Fytas, G.; Vlachos, G.; Fleischer, G.; Roovers, J. Dynamic Structure of Interacting Spherical Polymer Brushes. *Langmuir* 1999, *15* (2), 358–368
(51) Kapnistos, M.; Semenov, A. N.; Vlassopoulos, D.; Roovers, J. Viscoelastic Response of Hyperstar Polymers in the Linear Regime. *J. Chem. Phys.* 1999, *111* (4), 1753–1759
(52) Roovers, J.; Zhou, L.; Toporowski, P.; Vanderzwan, M.; Iatrou, H.; Hadjichristidis, N. Regular Star Polymers with 64 and 128 Arms - Models for Polymeric Micelles. *Macromolecules* 1993, *26* (16), 4324–4331
(53) Vlassopoulos, D.; Fytas, G.; Roovers, J.; Pakula, T.; Fleischer, G. Ordering and Dynamics of Soft Spheres in Melt and Solution. *Faraday Discuss.* 1999, *112*, 225–235.
(54) Hadjichristidis, N.; Iatrou, H.; Pispas, S.; Pitsikalis, M. Anionic Polymerization: High Vacuum Techniques. *J. Polym. Sci. Part -Polym. Chem.* 2000, *38* (18), 3211–3234
(55) Uhrig, D.; Mays, J. W. Experimental Techniques in High-Vacuum Anionic Polymerization. *J. Polym. Sci. Part -Polym. Chem.* 2005, *43* (24), 6179–6222
(56) Dealy, J.; Larson, R. *Structure and Rheology of Molten Polymers*; Hanser Publications: Munich : Cincinnati, 2006.
(57) Likos, C. N. Effective Interactions in Soft Condensed Matter Physics. *Phys. Rep.-Rev. Sect. Phys. Lett.* 2001, *348* (4–5), 267–439
(58) Timothy Lodge; Hiemenz, P. C. *Polymer Chemistry, Second Edition*, 2 edition.; CRC Press: Boca Raton, 2007.
(59) Larson, R. G. Combinatorial Rheology of Branched Polymer Melts. *Macromolecules* 2001, *34* (13), 4556–4571
(60) Wang, Z.; Chen, X.; Larson, R. G. Comparing Tube Models for Predicting the Linear Rheology of Branched Polymer Melts. *J. Rheol.* 2010, *54* (2), 223–260
(61) Park, S. J.; Shanbhag, S.; Larson, R. G. A Hierarchical Algorithm for Predicting the Linear Viscoelastic Properties of Polymer Melts with Long-Chain Branching. *Rheol. Acta* 2005, *44* (3), 319–330
(62) Ferry, J. D. *Viscoelastic Properties of Polymers*; Wiley, 1961.
(63) Jr, T. G. F.; Flory, P. J. Second-Order Transition Temperatures and Related Properties of Polystyrene. I. Influence of Molecular Weight. *J. Appl. Phys.* 1950, *21* (6), 581–591
(64) Fetters, L.; Hadjichristidis, N.; Lindner, J.; Mays, J. Molecular-Weight Dependence of Hydrodynamic and Thermodynamic Properties for Well-Defined Linear-Polymers in Solution. *J. Phys. Chem. Ref. Data* 1994, *23* (4), 619–640.

Chapter III

Confinement Effects on Dynamics in Polymer Nanocomposite Films

III.1. Introduction:

The incorporation of nanoparticles (NPs) within a polymer host to form polymer nanocomposites (PNCs) typically has the effect introducing and changing many physical properties of the polymer[1], including chain dynamics,[2–5] mechanical,[6,7] thermal[8,9] and electronic properties,[7,10–12] thereby rendering the material useful for diverse applications, such as energy conversion, lighting, and a variety of functional environmental and biomedical purposes.[1,11,13,14] The properties of PNCs are largely determined by the functionalities of the polymer and of the NPs and their spatial distribution, together with the nano, meso, and macroscale morphologies. Local, microscopic and macroscopic aggregation of NPs can greatly minimize the behavior that may be achieved.[15–17] One strategy commonly employed to achieve NP dispersion throughout a PNC is to graft polymer chains onto the NP surfaces.[18–25] A number of parameters contribute to the overall morphology of the PNCs: the surface chemistry of the NPs, grafted chains and polymer host chains, the degree of polymerization of grafted and host chains, the NP surface grafting densities σ, the thermodynamic interactions between the grafted and host chains,[26] as well as the size and shape of the nanoparticles . Intermixing between the grafted and free host

chains may be controlled through changes in key molecular parameters. For the simplest case chains of degree of polymerization N grafted on a flat surface, mixed with free chains of identical chemistry, but of degree of polymerization P, can exhibit different behavior – intermixing may be quite significant (the "wet-brush" condition) of it may be minimal (the "dry-brush" condition) provided the following condition is met:[22]

$$\sigma\sqrt{N} = (N/P)^2 \quad (1)$$

With regard to the miscibility of grafted NPs of radius R in a polymer host of free chains, dispersion of the NPs is favored when R is comparable to, or smaller than, the radii of gyration R_g of the chains.[18,27] Additionally, the condition $N > P$ further favors dispersion of the nanoparticles.[28–31]

For bulk PNCs with low NP concentrations, the dynamics of the NPs are strongly impacted by their size with respect to the host polymer chains and by interactions between the grafted polymer chains and host polymer chains. In cases where the particle radius is much larger than the equilibrium polymer coil size or the characteristic entanglement mesh, the dynamics of the particles have been shown to be dictated by the classical Stokes-Einstein (SE) equation.[32–38] When the particle size is less than the characteristic entanglement mesh, faster particle dynamics than predicted by the SE prediction have been observed both experimentally and computationally.[33–35,39] With regard to the dynamics of the host chains of a PNC, the situation depends on whether the host chains are entangled or unentangled. For the simplest case, where $\chi = 0$ and the grafted particles are dispersed throughout an unentangled host, the translational dynamics of the host chains are fast compared to the neat polymer host, whereas the dynamics

decrease compared to the neat host when the grafted chain lengths are long compared to the entanglement molecular weight. [40,41]

When PNCs are confined to a thickness of nanoscale (nanometers to tens of nanometers) dimensions, the morphology can differ appreciably from the bulk. The NPs preferentially segregate to interfaces for various reasons: increased configurational freedom is gained by the host chains; the grafted chains suffer lower entropic losses in comparison to host chains at a free surface; the nanoparticles are attracted to the substrate due to van der Waals interactions.[18,42,43] This tendency towards interfacial segregation renders PNCs thermodynamically less stable than their bulk analogs.[15,44–46] On the other hand, dispersion of the nanoparticles, and increased thermodynamic stability, is achieved when the nanoparticles are small compared to the R_gs of the chains, and the host and grafted chains satisfy a "wet" brush condition.[15,18]

Virtually all the research on dynamics of PNCs has focused on bulk systems; in thin films research has primarily been focused on pure homopolymers where the effects of confinement and polymer chain/external interface (substrate or free surface) interactions on chain dynamics have been widely reported. While the structure and morphology of PNC thin films has been well-explored, the overall dynamics of these systems have remained largely unexplored.[47,48] Of particular interest here is to understand the effect of decreasing the thickness of the PNC to nanoscale dimensions on the viscosity/chain dynamics. While this is understood for pure homopolymer films, this question has been difficult to adequately address in nanoscale thick films. To accomplish this, we used x-ray photon correlation spectroscopy (XPCS) and X-ray standing wave based resonance enhanced XPCS to probe the dynamics of host chains and nanoparticles, respectively, in PNCs composed of short unentangled poly (2-vinyl pyridine) (N=96) chains grafted onto NPs and unentangled poly (2-vinyl pyridine) (P=44) hosts. Samples

that met the wet-brush condition were designed and prepared in order to understand this phenomenon. A key finding is that the film thickness *h* together with the average separation l_D between the NPs and the relative mobilities of the NPs are shown to strongly influence the viscosity/dynamics of the system under conditions of nanoscale confinement.

III.2. Experimental Methods:

Gold (Au) nanoparticles with average size $d = 2.7 \pm 1.08\, nm$ were densely grafted ($\Sigma \sim 1.9\ chains/nm^2$) with thiol-terminated linear P2VP chains ($M_w = 10{,}000\ g/mol$, PDI = 1.1) using a one-step synthesis method.[49] The resulting product was subjected to a rigorous centrifugation process which was repeated several times to remove unbound thiols and salts. The size of the core gold particle was determined with a JEOL 2010F transmission electron microscope at an accelerating voltage of 200 kV in scanning mode (STEM) using a high-angle annular dark-field (HAADF) detector.[15,44] Thermogravimetric analysis was used to determine the weight fractions of gold and polymer ligands; measurements were taken under air environments on a TA2960 instrument at a heating rate of 5˚C/min. The grafting density was determined from the weight fraction of gold and grafted P2VP chains, the densities of the species, and the average volume and surface area per gold particle. The brush layer height was estimated to be $h_{brush} = 4.86 \pm 2.09\, nm$ by calculating the nearest neighbors distance between particles for ~300 pairs of particles. From this information, the effective particle diameter d_{eff} was determined to be $d_{eff} = d + 2h_{brush} = 11.07\, nm$.

These particles were mixed in an unentangled P2VP host ($M_w = 4{,}500\ g/mol$, PDI = 1.08) at a weight fraction of 2 wt% using tetrahydrofuran (THF) as a cosolvent. The mixture was evaporated under vacuum and resuspended in butanol. Films were prepared from this solution by

spin-coating onto precleaned silicon substrates with a native oxide layer of approximately 1.5 nm and annealed for 24 hours at 150˚C. Neat films were prepared through the same process in the absence of nanoparticles. The samples were verified to be smooth and contiguous by optical microscopy and atomic force microscopy. The interparticle spacing was determined using the equation:

$$\frac{l_D}{d} \approx \left(\frac{\varphi_m}{\varphi}\right)^{\frac{1}{3}} - 1 \qquad (2)$$

where $\varphi_m = 0.638$ the maximum random packing volume fraction and φ is the volume fraction of particles in the film.[2] The interparticle spacing l_D between core gold nanoparticles was further verified through an estimation of the nearest neighbor distance between ~300 pairs of particles in the PNC film as determined from STEM images and were found to be in good agreement.

The glass transition temperature T_g of the films were first determined by monitoring the thickness of each film as it was cooled from a temperature T= 150˚C at 1˚C using a M-2000 (J.A. Woollam Co.) variable angle spectrometric ellipsometer (VASE). Measurements were performed at a fixed angle of 70˚. The thickness *h(T)* and refractive index *n(T)* were determined by fitting the ellipsometric angles to a Cauchy/SiO_x/Si model over the spectral range λ=400-1700 nm. Measurements were kept under an inert environment by purging the sample stage using purified nitrogen. The T_g was identified as the intersection of extrapolated linear fits through the glassy and rubbery regions of the thickness vs temperature plot. The characteristics of these films are summarized in table 1:

Table III.1: Nanocomposite film properties

Sample	h (nm)	T_g (℃)	l_D (nm)
Au(3)P2VP96 0.5 wt% 50nm	**51**	**75.3**	**103.7**
Au(3)P2VP96 2wt% 50nm	**55**	**78.1**	**61.9**
Au(3)P2VP96 2 wt% 200nm	**196**	**76.3**	**61.9**
P2VP 50nm	**51**	**74.6**	**neat**

P2VP 200nm	**208**	**76.2**	**neat**

The viscosity and glass transition temperature of the bulk homopolymer were determined using rheometry and differential scanning calorimetry (DSC) respectively. The viscosity measurements were measured using an ARES 2K FRTN1 strain controlled rheometer with parallel plates 8 mm in diameter with a temperature controlled air/nitrogen convection oven in an inert environment. The bulk glass transition temperature measured using modulated DSC was determined to be T_g=75.1˚C.

XPCS experiments were performed at beamline 8-ID-I at the Advanced Photon Source (APS) Argonne National Laboratory. The high electron density of gold by comparison to the surrounding polymer host allows them to be used as markers for dynamics of the polymer film.[50,51] The beam dimension used was $20 \times 20\ \mu m^2$ which is less than the x-ray coherence length and the x-ray energy was 7.35 keV. XPCS probes dynamics at length scales of 10-10^3 nm and time scales of 1-10^3 seconds. The off-specular diffuse scattering from the neat homopolymer and nanocomposite films was measured with a direct illumination charge-coupled device (CCD) camera. Two illuminated modes were used in this study: (i) at an incident angle of $0.16°$, just below the critical angle for total external reflection $\theta_c = 0.175°$ of P2VP (ii) and at an incident angle of $0.18°$, just above θ_c at the "first resonance mode" where resonance enhancement of the electric field intensity (EFI) and resonance enhanced x-rays near the center of the film are intensified.[51] The first measurement probes scattering from the thermal capillary waves at the polymer film free surface, while the second measurement eliminates scattering from free surface which improves the resolution of resonance enhanced x-rays. This enhancement in resolution allows for the gold nanoparticles to act as a tracer to probe dynamics in the film interior. This allows the use of the nanoparticles as a probe of dynamics at both the free surface and in the

interior of the film, and has been used previously to show the presence of both a free-surface and adsorbed layer in PNC films.[50,51]

III.3. Results & Discussion:

We begin by describing the spatial distribution of the P2VP grafted Au nanoparticles within the thin polymer film hosts. Scanning transmission electron microscopy (STEM) was used to image the distribution of nanoparticles throughout the films. The STEM images in Figure 1of the distribution of gold nanoparticles suggest that the nanoparticles are well dispersed. The average interparticle spacing of these nanoparticles, at 2 wt% Au, was calculated to be $l_D \approx 61.9\ nm$. The determination of the interparticle spacing assumed a relatively uniform distribution of NPs in three-dimensions; a description of how this was determined is included in the experimental section.[2,52] We anticipate surface segregation to be minor based on the fact that the molecular parameters of the system were chosen to meet the wet-brush condition.[15]

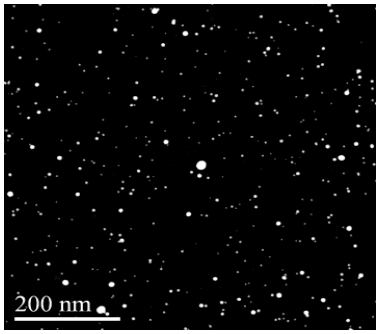

Figure III.1: STEM image of polymer nanocomposite film with 2 wt% added nanoparticles of thickness *h=50 nm*. The relative particle contrast is associated with the relative depth below the surface; the brightest particles are closest to the free surface.

X-ray photon correlation spectroscopy (XPCS) was used to investigate the dynamics of the homogenous P2VPpolymer and polymer nanocomposite films; the data were analyzed using the hydrodynamic continuum theory (HCT). HCT, which assumes a no-slip condition at the polymer/substrate interface and a uniform viscosity throughout the film, enables the viscosity of a molten polymer film to be calculated from the XPCS data.

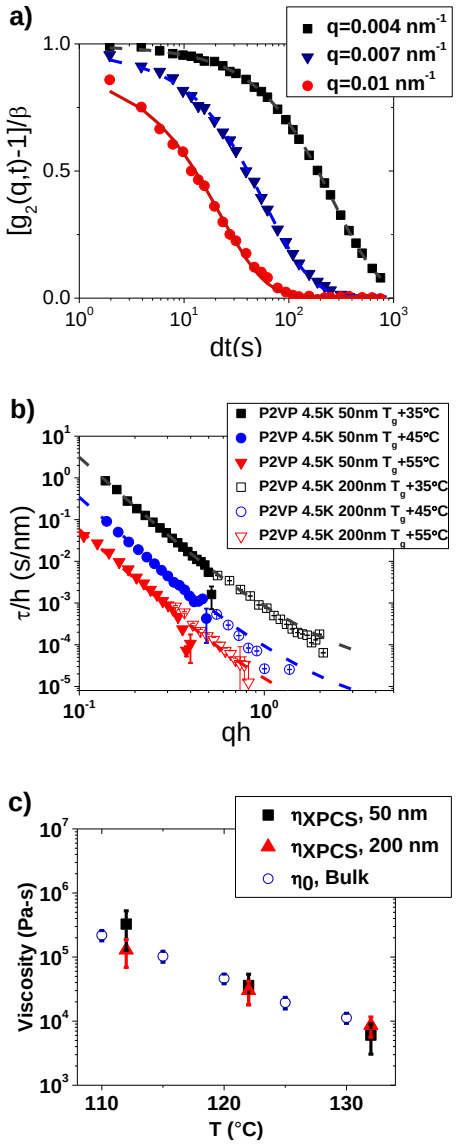

Figure III.2: a) Characteristic intensity-intensity auto correlation function of 50 nm thick neat P2VP film at T=112˚C at a few wave vectors. **b)** Comparison of relaxation time/film thickness vs wave vector ∗ film thickness ($\frac{\tau}{h}$ **vs** qh) in neat polymer films of both *h=50 nm* and *h=200 nm* at T_g*+35-55.* Dashed lines are fits to the HCT model using the bulk homopolymer viscosity. **c)** Viscosity as a function of temperature calculated from the relaxation time vs wave vector fit for each neat film using the HCT model for both *h=50 nm* and *h=200 nm* by comparison to the bulk viscosity.

The XPCS relaxation time of the surface height fluctuations of the polymer film were determined from the normalized intensity-intensity autocorrelation function of the coherent surface scattering $g_2(q_\parallel, t)$ is given by:

$$g_2(q_\parallel, dt) = \frac{\langle I\left(q_\parallel, t^{'}\right) I(q_\parallel, t^{'} + dt)\rangle}{\langle I(q_\parallel, t^{'})\rangle^2} \tag{3}$$

where $I(q_\parallel, t')$ is the scattering of the in-plane wave vector at instantaneous time *t'* and *dt* is the delay time. For viscous polymers, the capillary wave dynamics are overdamped so $g_2(q_\parallel, t)$ may be described by a stretched exponential decay fit:

$$g_2(q_\parallel, t) = 1 + \beta \exp[-(\frac{2t}{\tau})^{\alpha}] \tag{4}$$

where β is the speckle contrast, $\alpha(0 < \alpha \leq 1)$ is a stretching exponent and $\tau = \tau(q_\parallel)$ is the relaxation time of the surface height fluctuations. For a simple exponential relaxation, as observed in the homopolymer films where $T \gg T_g$ the exponent $\alpha = 1$. The deviation of α from unity corresponds to the existence of a distribution of fluctuation time scales in the system contributing within the measurement window. A typical $g_2(q_\parallel, t)$ for a neat 50 nm P2VP film is

shown in figure 2a over a range of wave vectors. The relaxation times exhibited by all P2VP films were each characterized by single exponential behavior, regardless of film thickness. Hydrodynamic continuum theory describes the relaxation time to be dependent on the ratio of the viscosity η and surface tension γ:[49–52]

$$\tau(q_{\parallel}) = \frac{2\eta_{XPCS}[cosh^2(q_{\parallel}h)+q_{\parallel}{}^2h^2]}{\gamma q_{\parallel}[sinh(q_{\parallel}h)\cosh(q_{\parallel}h)-q_{\parallel}h]} \quad (5)$$

The viscosities of polystyrene (PS) films, calculated using this equation, has been shown to be independent of film thickness and equal to the bulk viscosity when $h > 4R_g$.[56] The viscosities of our P2VP system were also found to be independent of film thickness (Fig. 2b) and equal to the bulk viscosity of the polymer (see Fig. 2c), as measured using rheology (see Supplemental Figure S1). The fact that the magnitudes of the viscosities of the films and the bulk are equal is not unexpected and was shown to be true for PS.[53,54] This is reasonable largely because the film thicknesses are larger than the average radii of gyration R_g of the chains and the experimental temperatures are sufficiently higher than T_g ($T_g + 35\,℃ < T < T_g + 55\,℃$). It should be noted that when the polymer chains are confined to thickness $h \leq 4R_g$, the viscosity is no longer thickness independent and manifests the effects of heterogeneous interactions associated with that degree of confinement.

The relaxations measured from the surface height fluctuations and measured by XPCS manifest a range of relaxations, from segmental relaxations of the chains to the center of mass translational relaxations. In the case of the neat homopolymer films used in this study, we believe it is safe to assume that the relaxations at these temperatures are largely probing the

center of mass translational dynamics of the polymer chains. This is also corroborated by the fact that the stretching exponent is unity; it would otherwise be less than unity as described earlier.

In order to begin our discussion of the polymer nanocomposite film, we performed XPCS measurements on h=200 nm PNC films. These measurements reveal that the relaxations in the polymer nanocomposite are similar in behavior to those of the homopolymer film (both are well described by the HCT model). Note that the viscosity of the P2VP film is determined by the translational dynamics (center-of-mass motions) of the host chains; the translational dynamics of the chains in the PNCs are slower than that of the neat polymer due to the presence of spatially dispersed NPs. This is consistent with the notion that the host chains pervade the volume of the longer grafted chains that relax more slowly because they are longer and they are tethered to the NPs. This is evident from the data in Figs. 3a and 3b, for measurements at temperatures of T= T_g+35˚C and T=T_g+45˚*C*. The relaxations were also well described by single exponential fits, which is to be expected if only the translational dynamics (one dynamic process) are being probed..

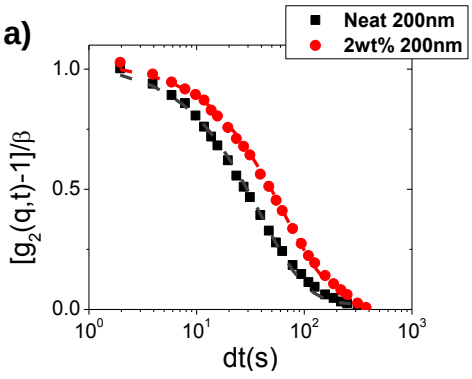

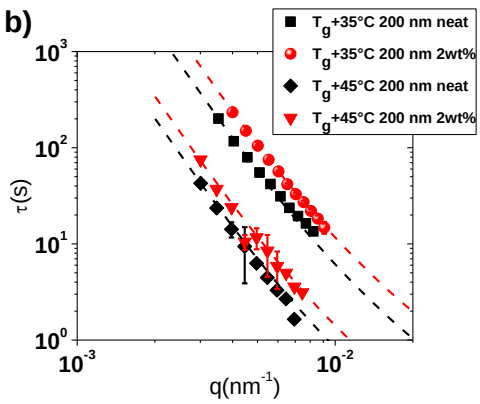

Figure III.3: a) Comparison of the intensity-intensity autocorrelation function for 2 wt% PNC and neat homopolymer films at T=112˚C and $\boldsymbol{q_{\parallel} \approx 0.004\, nm^{-1}}$ when *h=200nm*. **b)** Relaxation time as a function of wave vector determined for neat homopolymer and 2 wt% PNC films at T_g*+35*℃ and T_g*+45*℃. Dashed lines are HCT fit for the respective film.

To further explore the influence of the grafted layer on the dynamics of the host polymer, the dynamics of the grafted nanoparticles in the interior of the film are now considered. In order to probe the behavior of the grafted nanoparticles and gain additional insight into the interactions between the particles and the surrounding polymer host, we used resonance enhanced x-rays to probe the dynamics of nanoparticles within the interior of the film. Because the electron density of gold is much higher than the surrounding polymer, this allows us to measure the dynamics of the gold particle exclusively in the interior. We achieve this by increasing the incident angle θ above the critical angle θ_c to the first resonance mode where resonance enhanced x-rays are confined and intensified due to an enhancement of the electric field intensity close to the center of the film. This measurement is further described in the experimental section.

The results of these measurements in Figure 4a reveal that the particle motions are hindered at length scales larger than the interparticle spacing and begin to transition to diffusive

behavior at length scales shorter than the interparticle spacing ($q_{\parallel,l_D} \approx 0.1\, nm^{-1}$). The dynamics observed at long length scales ($q_\parallel \leq q_{\parallel,l_D}$) are evidence of the role that spatial confinement from neighboring nanoparticles has on the relaxation behavior of nanoparticles in the interior, preventing diffusion of the nanoparticles over long distances. The observed relaxation behavior at short length scales ($q_\parallel > q_{\parallel,l_D}$) is characterized by a dependence of the relaxation time on the in-plane wave vector such that $\tau(q_\parallel) \sim \frac{1}{q_\parallel^{1.8\pm0.22}}$, akin to a particle in a viscous medium.[32,57] The dynamics across the entire measurement are well-described by a single exponential relaxation.

Due to the local dynamics of the particle being well-represented by a diffusive relaxation mechanism, we compared the diffusion coefficient of the grafted particle to that of the Stokes-Einstein prediction for a bare particle in a viscous polymer host. The grafted particle diffusion coefficient was taken from the equation:

$$D_{XPCS} = \frac{1}{2\tau q^2} \tag{6}$$

This equation is reliable when the relaxation can be described by a single exponential relaxation process. This diffusion coefficient was compared as a function of temperature to the diffusion coefficient of a bare spherical particle with the radius of the gold core particle ($r = 1.35\, nm$) and a bare spherical particle with the effective grafted particle radius ($r = 5.5\, nm$) in the polymer host. The diffusion coefficient D for these model bare particles is estimated using the classical Stokes-Einstein relation:[3]

$$D_{SE} = \frac{k_B T}{6\pi\eta_{Bulk} r} \tag{7}$$

It is evident from the comparison in Figure 4b, that the diffusion coefficient of the grafted nanoparticles in the polymer host is smaller than that of both bare nanoparticles in the polymer host, over the temperature range of interest. This is expected because the brush layer, mixed with the host chains, would have the effect of decreasing the rate of translation of the grafted nanoparticle. The grafted particle also exhibits a different temperature dependence than a bare nanoparticle. These deviations are due to the relaxations of the brush chains that contribute to the particle diffusion in this local regime. These changes indicate that interactions between the grafted chains and the polymer host have a strong influence on the local dynamics of the host polymer.

We measured the dynamics of PNCs of varying thisknesses in order to understand the effect of confinement. Films with thicknesses comparable to the average interparticle spacing ($h \approx 50\ nm$), while keeping the nanoparticle concentration and interparticle spacing constant, were investigated.

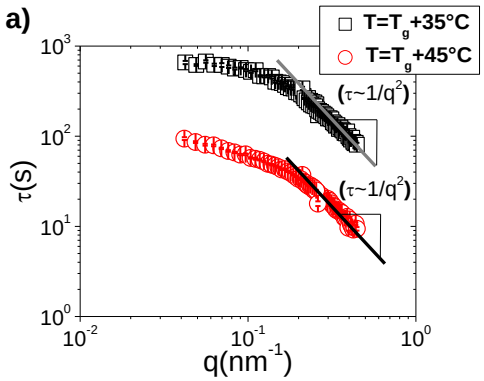

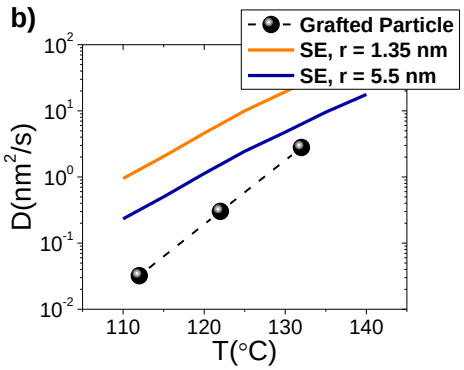

Figure III.4: a) XPCS measurement of the dynamics of nanoparticles in the interior of the film at T_g+*35*℃ and T_g+*45*℃ in 200 nm films. Dashed line represents a slope of -2. **b)** Diffusion coefficient as a function of temperature. Dashed orange and blue lines represent Stokes-Einstein calculation using a solid particle of r = 1.35 nm and r = 5.5 nm respectively, in a film with the bulk homopolymer viscosity. Solid black symbols represent the calculated XPCS diffusion coefficient for the grafted nanoparticles from the resonance-enhanced XPCS measurement. The dashed black line between points is a guide to the eye.

For these $h \approx 50\ nm$ nanocomposite films, the translational dynamics of the host P2VP chains in the PNC films are substantially slowed down in comparison to the neat film (Figure 5a). The intensity-intensity autocorrelation function at T=T_g+35℃ and T=T_g+45℃ are stretched, with a stretching exponent of $\alpha \approx 0.73 \pm 0.08$, suggesting a distribution of relaxation times. At higher temperatures T_g+55℃, the relaxation rates of the PNC and the neat P2VP film are comparable, whereas the relaxations of the PNC become comparatively slower, with decreasing T (see Fig. 5b). The slowing down of the relaxation of the polymer host chains and the appearance of a distribution of relaxations for temperatures, which increases as T approaches to the glass transition temperature of the film, is likely a manifestation of additional contributions of segmental relaxations from both the grafted and free chains, within the XPCS experimental window.

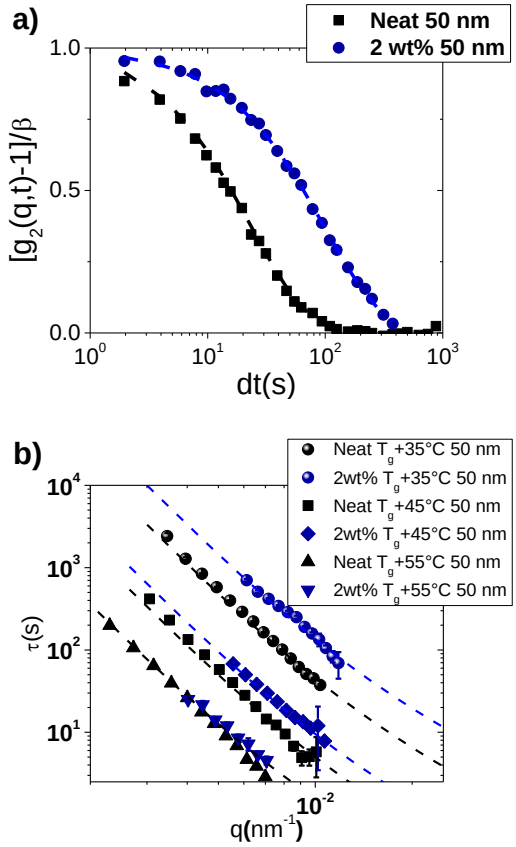

Figure III.5: a) Comparison of the intensity-intensity autocorrelation function for 2 wt% PNC and neat homopolymer films at T=112˚C and $q_{\parallel} \approx 0.004\ nm^{-1}$ when *h=50nm.* **b)** Relaxation time as a function of wave vector determined for neat homopolymer and 2 wt% PNC films at T=T_g*+35-55*℃. Dashed lines are HCT fit for the respective film.

In order to determine how larger degrees of confinement to thinner films would influence the dynamics of the nanoparticles, we performed additional resonance enhanced x-ray measurements on h=50 nm thick films. We learned that the relaxation times in such films were temperature and wave vector independent and outside the window of our measurement. This observation suggests that in contrast to the thicker h=200 nm film the dynamics of the NPs in these 50 nm films, are suppressed substantially –virtually immobile.

We subsequently performed XPCS measurements of films containing a much smaller concentration of particles, 0.5 wt%, and hence larger interparticle spacings, l_D~103.7 nm. The

relaxations from the surface height fluctuations are faster than the 2 wt% nanocomposite, but slower than that of the neat film, as shown in Figure 6a. Moreover, the autocorrelation function is characterized by a single exponential - not stretched, as it was for the 2 wt% film. The data in Figure 6b show the viscosities calculated using the HCT model for each of the films in this study. Notably, the viscosity and temperature dependence of the 2 wt%, $h \approx 200$ nm film, and the 0.5 wt% $h \approx 50$ nm film, are virtually identical, whereas the 2 wt% $h \approx 50$ nm film exhibited the most substantial increases –over an order of magnitude -in viscosity. This result confirms the notion that the combined effect of thickness and spatial nanoparticle confinement is responsible for the decreasing the host chain dynamics - larger deviation from bulk behavior than either thickness confinement or NP confinement alone.

Recent work performed by Composto and co-workers on the influence of nanoparticle confinement on the dynamics of host chains in the bulk, shows that control of spatial confinement through the interparticle spacing and the size of the host chains can lead to substantial changes to the dynamics of the host chain in entangled polymer systems.[52,58,59] They quantified this effect using a so-called confinement parameter $ID_{eff}=(l_D-2h_{brush})/2R_g$, where h_{brush} is the brush layer thickness of the nanoparticle and R_g is the radius of gyration of the free host chains. They demonstrated that the interparticle spacing between the nanoparticles would influence the translational diffusion for conditions such that $ID_{eff}<10$. For $ID_{eff}<2$, the host chains would be entropically restricted and this would lead to a significant decrease of the translational diffusion coefficient, in in turn the viscosity.

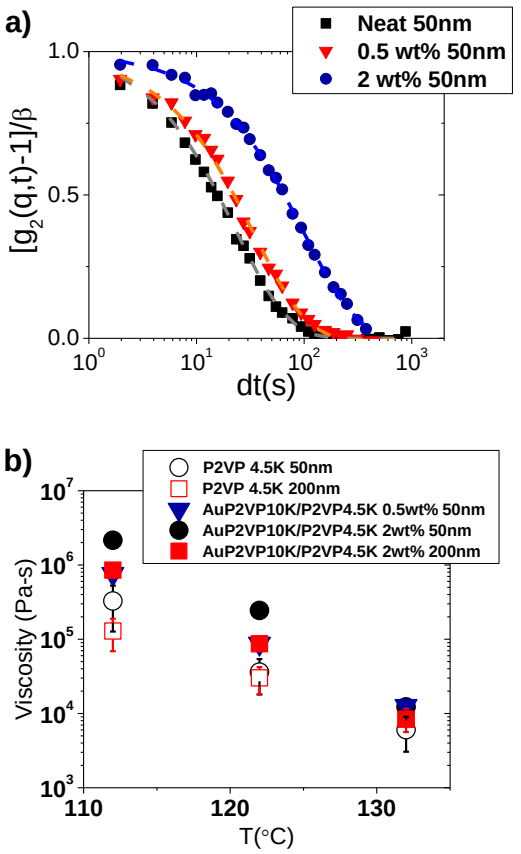

Figure III.6: a) Comparison of the autocorrelation function for neat, 0.5 wt% and 2 wt% PNC homopolymer films of thickness $h = 50nm$ at T=112˚C and $\boldsymbol{q_{\parallel} \approx 0.004\ nm^{-1}}$. **b)** Viscosity as a function of temperature calculated from the relaxation time vs wave vector fit for each nanocomposite and homopolymer film measured in this study using the HCT model.

We determined that the confinement factor for our system to be 10, suggesting that this is evidently not the reason for the suppression of our dynamics –increase of the viscosity. The substantial increase of our viscosity for inter NP separations of l_D=50 nm within the h=50 nm thickness confinement is associated with an immobilization of NPs; the NPs are mobile in the thicker films. Moreover the NP brush layers would be stretched significantly beyond $h_{brush}=4.86 \pm 2.09\ nm$, due to the intermixing with the shorter host chains. This may be the reason the NP motions are restricted. Under these conditions, the dynamics of the host chains

would be largely suppressed because they would be mostly intermixed with the significantly slower relaxing tethered chains that constitute the brush layer. This entropic restriction would be the reason the host chain dynamics would be much slower. When the inter NP distances are increased the viscosity of the film approaches the bulk value.

III.4. Conclusion:

The morphologies of PNCs containing polymer brush-coated nanoparticles, where the chemistry of the tethered chains is identical to that of the free host chains, are dictated by the NP size and by the relative lengths of the tethered and free chains. In the bulk, under wet brush conditions, the host chains pervade the volume of the tethered chains to a significant degree. Under these conditions, the tethered nanoparticles are spatially dispersed and the dynamics of the free host chains are slowed down, largely because the relaxation times of the tethered chains are longer than those of the free chains. This behavior persists to the regime of nanoscale thickness confinement where, as we have shown, a new mechanism ensues. When the film thickness becomes comparable to the average spacing between the NPs, the NPs motions are suppressed and the free chains experience an entropic restriction, leading to an increase in the activation barriers that facilitate their translational motions. This behavior is associated with an appreciable increase in the viscosity –an order of magnitude. An increase of the film thickness or an increase of the nanoparticle separation was sufficient alleviate this “entropic crowding,” leading a decrease of the viscosity. These results suggest new ways to tailor the viscosities of nanoscale thick PNCs, without changing molecular parameters like the chain lengths and nanoparticle core sizes.

References:

(1) Paul, D. R.; Robeson, L. M. Polymer Nanotechnology: Nanocomposites. *Polymer* 2008, *49*, 3187–3204.
(2) Oh, H.; Green, P. F. Polymer Chain Dynamics and Glass Transition in Athermal Polymer/Nanoparticle Mixtures. *Nat. Mater.* 2009, *8*, 139–143.
(3) Mangal, R.; Srivastava, S.; Narayanan, S.; Archer, L. A. Size-Dependent Particle Dynamics in Entangled Polymer Nanocomposites. *Langmuir* 2016, *32*, 596–603.
(4) Srivastava, S.; Agarwal, P.; Mangal, R.; Koch, D. L.; Narayanan, S.; Archer, L. A. Hyperdiffusive Dynamics in Newtonian Nanoparticle Fluids. *ACS Macro Lett.* 2015, *4*, 1149–1153.
(5) Mangal, R.; Srivastava, S.; Archer, L. A. Phase Stability and Dynamics of Entangled Polymer-Nanoparticle Composites. *Nat. Commun.* 2015, *6*, 7198.
(6) Giannelis, E. P. Polymer Layered Silicate Nanocomposites. *Adv. Mater.* 1996, *8*, 29-.
(7) Kim, H.; Abdala, A. A.; Macosko, C. W. Graphene/Polymer Nanocomposites. *Macromolecules* 2010, *43*, 6515–6530.
(8) Gilman, J. W. Flammability and Thermal Stability Studies of Polymer Layered-Silicate (Clay) Nanocomposites. *Appl. Clay Sci.* 1999, *15*, 31–49.
(9) Sunday, D. F.; Green, D. L. Thermal and Rheological Behavior of Polymer Grafted Nanoparticles. *Macromolecules* 2015, *48*, 8651–8659.
(10) Holder, E.; Tessler, N.; Rogach, A. L. Hybrid Nanocomposite Materials with Organic and Inorganic Components for Opto-Electronic Devices. *J. Mater. Chem.* 2008, *18*, 1064–1078.
(11) Godovsky, D. Y. Device Applications of Polymer-Nanocomposites. In *Biopolymers/Pva Hydrogels/Anionic Polymerisation Nanocomposites*; Abe, A., Ed.; Springer-Verlag Berlin: Berlin, 2000; Vol. 153, pp. 163–205.
(12) Gangopadhyay, R.; De, A. Conducting Polymer Nanocomposites: A Brief Overview. *Chem. Mater.* 2000, *12*, 608–622.
(13) Hussain, F.; Hojjati, M.; Okamoto, M.; Gorga, R. E. Review Article: Polymer-Matrix Nanocomposites, Processing, Manufacturing, and Application: An Overview. *J. Compos. Mater.* 2006, *40*, 1511–1575.
(14) Beecroft, L. L.; Ober, C. K. Nanocomposite Materials for Optical Applications. *Chem. Mater.* 1997, *9*, 1302–1317.
(15) Meli, L.; Arceo, A.; Green, P. F. Control of the Entropic Interactions and Phase Behavior of Athermal Nanoparticle/Homopolymer Thin Film Mixtures. *Soft Matter* 2009, *5*, 533–537.
(16) Srivastava, S.; Agarwal, P.; Archer, L. A. Tethered Nanoparticle-Polymer Composites: Phase Stability and Curvature. *Langmuir* 2012, *28*, 6276–6281.
(17) Mackay, M. E.; Tuteja, A.; Duxbury, P. M.; Hawker, C. J.; Van Horn, B.; Guan, Z. B.; Chen, G. H.; Krishnan, R. S. General Strategies for Nanoparticle Dispersion. *Science* 2006, *311*, 1740–1743.
(18) Green, P. F. The Structure of Chain End-Grafted Nanoparticle/Homopolymer Nanocomposites. *Soft Matter* 2011, *7*, 7914–7926.
(19) Akcora, P.; Liu, H.; Kumar, S. K.; Moll, J.; Li, Y.; Benicewicz, B. C.; Schadler, L. S.; Acehan, D.; Panagiotopoulos, A. Z.; Pryamitsyn, V.; *et al.* Anisotropic Self-Assembly of Spherical Polymer-Grafted Nanoparticles. *Nat. Mater.* 2009, *8*, 354-U121.
(20) Kango, S.; Kalia, S.; Celli, A.; Njuguna, J.; Habibi, Y.; Kumar, R. Surface Modification of Inorganic Nanoparticles for Development of Organic-Inorganic Nanocomposites-A Review. *Prog. Polym. Sci.* 2013, *38*, 1232–1261.
(21) Hasegawa, R.; Aoki, Y.; Doi, M. Optimum Graft Density for Dispersing Particles in Polymer Melts. *Macromolecules* 1996, *29*, 6656–6662.

(22) Ferreira, P. G.; Ajdari, A.; Leibler, L. Scaling Law for Entropic Effects at Interfaces between Grafted Layers and Polymer Melts. *Macromolecules* 1998, *31*, 3994–4003.
(23) Gast, A.; Leibler, L. Interactions of Sterically Stabilized Particles Suspended in a Polymer-Solution. *Macromolecules* 1986, *19*, 686–691.
(24) Gast, A.; Leibler, L. Effect of Polymer-Solutions on Sterically Stabilized Suspensions. *J. Phys. Chem.* 1985, *89*, 3947–3949.
(25) Wijmans, C.; Zhulina, E.; Fleer, G. Effect of Free Polymer on the Structure of a Polymer Brush and Interaction Between 2 Polymer Brushes. *Macromolecules* 1994, *27*, 3238–3248.
(26) Matsen, M. W.; Gardiner, J. M. Autophobic Dewetting of Homopolymer on a Brush and Entropic Attraction between Opposing Brushes in a Homopolymer Matrix. *J. Chem. Phys.* 2001, *115*, 2794–2804.
(27) Pryamtisyn, V.; Ganesan, V.; Panagiotopoulos, A. Z.; Liu, H.; Kumar, S. K. Modeling the Anisotropic Self-Assembly of Spherical Polymer-Grafted Nanoparticles. *J. Chem. Phys.* 2009, *131*, 221102.
(28) Binder, K.; Milchev, A. Polymer Brushes on Flat and Curved Surfaces: How Computer Simulations Can Help to Test Theories and to Interpret Experiments. *J. Polym. Sci. Part B-Polym. Phys.* 2012, *50*, 1515–1555.
(29) Semenov, A. N.; Vlassopoulos, D.; Fytas, G.; Vlachos, G.; Fleischer, G.; Roovers, J. Dynamic Structure of Interacting Spherical Polymer Brushes. *Langmuir* 1999, *15*, 358–368.
(30) Lo Verso, F.; Egorov, S. A.; Milchev, A.; Binder, K. Spherical Polymer Brushes under Good Solvent Conditions: Molecular Dynamics Results Compared to Density Functional Theory. *J. Chem. Phys.* 2010, *133*, 184901.
(31) Akgun, B.; Ugur, G.; Jiang, Z.; Narayanan, S.; Song, S.; Lee, H.; Brittain, W. J.; Kim, H.; Sinha, S. K.; Foster, M. D. Surface Dynamics of "Dry" Homopolymer Brushes. *Macromolecules* 2009, *42*, 737–741.
(32) Kalathi, J. T.; Yamamoto, U.; Schweizer, K. S.; Grest, G. S.; Kumar, S. K. Nanoparticle Diffusion in Polymer Nanocomposites. *Phys. Rev. Lett.* 2014, *112*, 108301.
(33) Tuteja, A.; Mackay, M. E.; Narayanan, S.; Asokan, S.; Wong, M. S. Breakdown of the Continuum Stokes-Einstein Relation for Nanoparticle Diffusion. *Nano Lett.* 2007, *7*, 1276–1281.
(34) Cai, L.-H.; Panyukov, S.; Rubinstein, M. Mobility of Nonsticky Nanoparticles in Polymer Liquids. *Macromolecules* 2011, *44*, 7853–7863.
(35) Yamamoto, U.; Schweizer, K. S. Microscopic Theory of the Long-Time Diffusivity and Intermediate-Time Anomalous Transport of a Nanoparticle in Polymer Melts. *Macromolecules* 2015, *48*, 152–163.
(36) Guo, H.; Bourret, G.; Corbierre, M. K.; Rucareanu, S.; Lennox, R. B.; Laaziri, K.; Piche, L.; Sutton, M.; Harden, J. L.; Leheny, R. L. Nanoparticle Motion within Glassy Polymer Melts. *Phys. Rev. Lett.* 2009, *102*, 075702.
(37) Ganesan, V.; Pryamitsyn, V.; Surve, M.; Narayanan, B. Noncontinuum Effects in Nanoparticle Dynamics in Polymers. *J. Chem. Phys.* 2006, *124*, 221102.
(38) Jang, W.-S.; Koo, P.; Bryson, K.; Narayanan, S.; Sandy, A.; Russell, T. P.; Mochrie, S. G. Dynamics of Cadmium Sulfide Nanoparticles within Polystyrene Melts. *Macromolecules* 2014, *47*, 6483–6490.
(39) Grabowski, C. A.; Mukhopadhyay, A. Size Effect of Nanoparticle Diffusion in a Polymer Melt. *Macromolecules* 2014, *47*, 7238–7242.
(40) Yamamoto, U.; Schweizer, K. S. Theory of Nanoparticle Diffusion in Unentangled and Entangled Polymer Melts. *J. Chem. Phys.* 2011, *135*, 224902.
(41) Egorov, S. A. Anomalous Nanoparticle Diffusion in Polymer Solutions and Melts: A Mode-Coupling Theory Study. *J. Chem. Phys.* 2011, *134*, 084903.
(42) Lee, J. Y.; Shou, Z.; Balazs, A. C. Predicting the Morphologies of Confined Copolymer/Nanoparticle Mixtures. *Macromolecules* 2003, *36*, 7730–7739.

(43) McGarrity, E. S.; Frischknecht, A. L.; Mackay, M. E. Phase Behavior of Polymer/Nanoparticle Blends near a Substrate. *J. Chem. Phys.* 2008, *128*, 154904.
(44) Meli, L.; Green, P. F. Aggregation and Coarsening of Ligand-Stabilized Gold Nanoparticles in Poly(methyl Methacrylate) Thin Films. *Acs Nano* 2008, *2*, 1305–1312.
(45) Chen, X. C.; Green, P. F. Control of Morphology and Its Effects on the Optical Properties of Polymer Nanocomposites. *Langmuir* 2010, *26*, 3659–3665.
(46) Kim, J.; Yang, H.; Green, P. F. Tailoring the Refractive Indices of Thin Film Polymer Metallic Nanoparticle Nanocomposites. *Langmuir* 2012, *28*, 9735–9741.
(47) Narayanan, S.; Lee, D. R.; Hagman, A.; Li, X.; Wang, J. Particle Dynamics in Polymer-Metal Nanocomposite Thin Films on Nanometer-Length Scales. *Phys. Rev. Lett.* 2007, *98*, 185506.
(48) Narayanan, S.; Lee, D. R.; Guico, R. S.; Sinha, S. K.; Wang, J. Real-Time Evolution of the Distribution of Nanoparticles in an Ultrathin-Polymer-Film-Based Waveguide. *Phys. Rev. Lett.* 2005, *94*, 145504.
(49) Yee, C. K.; Jordan, R.; Ulman, A.; White, H.; King, A.; Rafailovich, M.; Sokolov, J. Novel One-Phase Synthesis of Thiol-Fuctionalized Gold, Palladium, and Iridium Nanoparticles Using Superhydride. *Langmuir* 1999, *15*, 3486–3491.
(50) Koga, T.; Li, C.; Endoh, M. K.; Koo, J.; Rafailovich, M.; Narayanan, S.; Lee, D. R.; Lurio, L. B.; Sinha, S. K. Reduced Viscosity of the Free Surface in Entangled Polymer Melt Films. *Phys. Rev. Lett.* 2010, *104*, 066101.
(51) Koga, T.; Jiang, N.; Gin, P.; Endoh, M. K.; Narayanan, S.; Lurio, L. B.; Sinha, S. K. Impact of an Irreversibly Adsorbed Layer on Local Viscosity of Nanoconfined Polymer Melts. *Phys. Rev. Lett.* 2011, *107*, 225901.
(52) Choi, J.; Hore, M. J. A.; Meth, J. S.; Clarke, N.; Winey, K. I.; Composto, R. J. Universal Scaling of Polymer Diffusion in Nanocomposites. *Acs Macro Lett.* 2013, *2*, 485–490.
(53) Kim, H.; Ruhm, A.; Lurio, L. B.; Basu, J. K.; Lal, J.; Lumma, D.; Mochrie, S. G. J.; Sinha, S. K. Surface Dynamics of Polymer Films. *Phys. Rev. Lett.* 2003, *90*, 068302.
(54) Li, C. H.; Koga, T.; Jiang, J.; Sharma, S.; Narayanan, S.; Lurio, L. B.; Hu, Y.; Jiao, X.; Sinha, S. K.; Billet, S.; *et al.* Viscosity Measurements of Very Thin Polymer Films. *Macromolecules* 2005, *38*, 5144–5151.
(55) Jiang, Z.; Kim, H.; Lee, H.; Lee, Y. J.; Jiao, X.; Li, C.; Lurio, L. B.; Hu, X.; Lal, J.; Narayanan, S.; *et al.* Structure and Dynamics of Thin Polymer Films Using Synchrotron X-Ray Scattering. *J. Appl. Crystallogr.* 2007, *40*, S18–S22.
(56) Jiang, Z.; Mukhopadhyay, M. K.; Song, S.; Narayanan, S.; Lurio, L. B.; Kim, H.; Sinha, S. K. Entanglement Effects in Capillary Waves on Liquid Polymer Films. *Phys. Rev. Lett.* 2008, *101*, 246104.
(57) Agrawal, A.; Wenning, B. M.; Choudhury, S.; Archer, L. A. Interactions, Structure, and Dynamics of Polymer-Tethered Nanoparticle Blends. *Langmuir* 2016, *32*, 8698–8708.
(58) Griffin, P. J.; Bocharova, V.; Middleton, L. R.; Composto, R. J.; Clarke, N.; Schweizer, K. S.; Winey, K. I. Influence of the Bound Polymer Layer on Nanoparticle Diffusion in Polymer Melts. *Acs Macro Lett.* 2016, *5*, 1141–1145.
(59) Lin, C.-C.; Parrish, E.; Composto, R. J. Macromolecule and Particle Dynamics in Confined Media. *Macromolecules* 2016, *49*, 5755–5772.

Chapter IV

Free Surface Dynamics in Polymer Nanocomposite Films

IV.1. Introduction:

The dynamic behavior of polymers in thin films has been a subject of research interests for several decades and has highlighted the importance of interfaces towards influencing the morphology and properties polymers in thin films. Interfacial interactions have been shown to substantially influence a number of polymer properties in both thin supported and unsupported films, including the host polymer glass transition temperature, local density, wetting and aging behavior.[1–5] Dynamic behavior of polymers in thin films has been shown to change substantially due to geometric restrictions and interfacial interactions.[2,6–9] Control of these interactions opens the door for new application and understanding of polymeric materials.

The influence of interfacial interactions and confinement effects on the dynamics in polymer thin films is especially important when discussing polymer nanocomposite films. The addition of nanoscale particles to a polymer host has been shown to dramatically alter host chain dynamics depending on particle shape, size and host polymer properties.[10–14] The influence of

these nanoparticles on the polymer host has a strong dependence upon their miscibility and dispersion throughout the system, and a common method of controlling this is through the grafting of a polymer brush layer to the surface of the nanoparticle. Several parameters contribute to the morphology of these PNCs: the degree of polymerization and chemistry of the grafted and host chains, the surface chemistry and grafting density on the surface of the nanoparticles and particle size.[11,15,16] The intermixing of grafted and host chains can be controlled through these parameters and allow for tunable dispersion of the nanoparticles in the polymer host.[17–19] In the simple case where chains of degree of polymerization N grafted onto a flat surface are mixed with host chains of degree of polymerization P and identical chemistry (Flory-Huggins interaction parameter $\boldsymbol{X = 0}$), mixing of the grafted and host chains can be controlled by the condition:[15]

$$\boldsymbol{\sigma\sqrt{N} = (N/P)^2} \quad (1)$$

The influence of the brush layer on the host chain dynamics in the bulk has been previously studied, with the relaxations of the host chains being strongly dependent upon the intermixing of the grafted and host chains or "wetting" of the grafted brush layer by the polymer host.[20,21] The dynamics of particle grafted chains have also been studied to determine the influence of grafting density, grafted chain and host chain length on their behavior. These studies revealed that at low particle concentrations, the segmental dynamics of the polymer host chains were decreased upon the addition of particles with a grafted brush layer that satisfied the "dry brush" condition ($\boldsymbol{\sigma\sqrt{N} > (N/P)^2}$). Conversely, the segmental dynamics of the host were increased upon the addition of particles with a grafted brush layer that intermixed with the

polymer host chains. The effects of tuning the brush layer behavior were shown to be mitigated when particle concentrations were substantially increased due to increased particle aggregation.

Upon confinement to a thin film geometry, the morphology of these polymer nanocomposite films changes substantially. When weak intermixing between the grafted and host chains is observed, the nanoparticles have a tendency to aggregate due to thermodynamic interactions which minimize surface energy.[11,12,22] In thin film polymer nanocomposites, these particles have been shown to exhibit strong evidence of nanoparticle segregation to both the vacuum/polymer and polymer/substrate interfaces. While some surface segregation is observed in most polymer nanocomposite systems, it is particularly prevalent when the grafted brush layer satisfies the "dry brush" condition.

In this study, we look to gain an understanding of how weakly intermixing, "dry brush" nanoparticles alter the properties of the host chains when confined to a thin film using x-ray photon correlation spectroscopy (XPCS) and broadband dielectric spectroscopy (BDS). The system used in this study involves an entangled poly (2-vinyl pyridine) (P2VP) host ($\boldsymbol{P = 288}$) mixed with gold nanoparticles grafted with short unentangled ($\boldsymbol{N = 12.5}$) P2VP chains at a high grafting density. We hope to provide insight into how changes to nanocomposite morphology, due to interfacial segregation of nanoparticles upon confinement to a thin film, alter the dynamics of the host chain behavior.

IV.2. Experimental Section:

Gold (Au) nanoparticles with average size $\boldsymbol{d = 2.9 \pm 1.08\ nm}$ were densely grafted ($\boldsymbol{\Sigma \sim 1.79\ chains/nm^2}$) with thiol-terminated linear P2VP chains ($\boldsymbol{M_w = 1,300\ g/mol}$, PDI

= 1.04) using a one-step synthesis method.[23] The resulting product was subjected to a rigorous centrifugation process which was repeated several times to remove unbound thiols and salts. The size of the core gold particle was determined with a JEOL 2010F transmission electron microscope at an accelerating voltage of 200 kV in scanning mode (STEM) using a high-angle annular dark-field (HAADF) detector.[11,12] Thermogravimetric analysis was used to determine the weight fractions of gold and polymer ligands; measurements were taken under air environments on a TA2960 instrument at a heating rate of 5˚C/min. The grafting density was determined from the weight fraction of gold and grafted P2VP chains, the densities of the species, and the average volume and surface area per gold particle. The brush layer height was estimated to be $\boldsymbol{h_{brush} = 1.43 \pm 0.67 nm}$ by calculating the nearest neighbors distance between particles for ~300 pairs of particles. From this information, the effective particle size $\boldsymbol{d_{eff}}$was determined to be $\boldsymbol{d_{eff} = d + 2h_{brush} \approx 5.7\ nm}$.

These particles were mixed in an entangled P2VP host ($\boldsymbol{M_w = 30,000\ g/mol}$, PDI = 1.12) at weight fractions of 1 and 2 wt% using tetrahydrofuran (THF) as a cosolvent. The mixture was evaporated under vacuum and resuspended in butanol. Films were prepared from this solution by spin-coating onto precleaned silicon substrates with a native oxide layer of approximately 1.5 nm and annealed for 48 hours at 150˚C. Neat films were prepared through the same process in the absence of nanoparticles. The samples were verified to be smooth and contiguous by optical microscopy and atomic force microscopy.

The glass transition temperature T_g of the films were first determined by monitoring the thickness of each film as it was cooled from a temperature T= 150˚C at 1˚C using a M-2000 (J.A. Woollam Co.) variable angle spectrometric ellipsometer (VASE). Measurements were performed at a fixed angle of 70˚. The thickness *h(T)* and refractive index *n(T)* were determined

by fitting the ellipsometric angles to a Cauchy/SiO_x/Si model over the spectral range λ=400-1700 nm. Measurements were kept under an inert environment by purging the sample stage using purified nitrogen.

For thin film broadband dielectric spectroscopy (BDS) measurements, the films were prepared between two aluminum (Al) electrodes using a thin film sample preparation technique where aluminum electrodes 0.5-0.8 mm in width and ~100 nm thick are evaporate onto glass substrates (1 cm × 1 cm × 1 mm). The substrates are thoroughly cleansed using glass detergent, piranha solution, and acetone in the ultrasonic cleaner. Frequency sweeps were taken over a range of $\omega = 10^7 - 10^{-1}s^{-1}$. This experimental procedure has been previously used to explore the dynamic properties of a number of thin film polymer and polymer blend systems.[24,25]

XPCS experiments were performed at beamline 8-ID-I at the Advanced Photon Source (APS) Argonne National Laboratory. The high electron density of gold by comparison to the surrounding polymer host allows them to be used as markers for dynamics of the polymer film.[8,26] The beam dimension used was $\mathbf{20 \times 20\ \mu m^2}$ which is less than the x-ray coherence length and the x-ray energy was 7.35 keV. XPCS probes dynamics at length scales of 10-10^3 nm and time scales of 1-10^3 seconds. The off-specular diffuse scattering from the neat homopolymer and nanocomposite films was measured with a direct illumination charge-coupled device (CCD) camera. Two illuminated modes were used in this study: (i) at an incident angle of $\mathbf{0.16°}$, just below the critical angle for total external reflection $\boldsymbol{\theta_c = 0.175°}$ of P2VP (ii) and at an incident angle of $\mathbf{0.18°}$, just above $\boldsymbol{\theta_c}$ at the "first resonance mode" where resonance enhancement of the electric field intensity (EFI) and resonance enhanced x-rays near the center of the film are intensified.[26] The first measurement probes scattering from the thermal capillary waves at the polymer film free surface, while the second measurement eliminates scattering from free surface

which improves the resolution of resonance enhanced x-rays. This enhancement in resolution allows for the gold nanoparticles to act as a tracer to probe dynamics in the film interior. This allows the use of the nanoparticles as a probe of dynamics at both the free surface and in the interior of the film, and has been used previously to show the presence of both a free-surface and adsorbed layer in PNC films.[8,26]

IV.3. Results & Discussion:

X-ray photon correlation spectroscopy (XPCS) was used to investigate the dynamics of the homogenous polymer and polymer nanocomposite films; the data were analyzed in terms of hydrodynamic continuum theory. Specifically, hydrodynamic continuum theory (HCT), which assumes a no-slippage condition at the polymer/substrate interface and a uniform viscosity throughout the film, enables the viscosity of a molten polymer film to be calculated from the XPCS data.[6,7,9] The XPCS relaxation time of the surface height fluctuations of the polymer film were determined from the normalized intensity-intensity autocorrelation function of the coherent surface scattering $\boldsymbol{g_2(q_\parallel, t)}$ is given by:

$$\boldsymbol{g_2(q_\parallel, dt) = \frac{\langle I(q_\parallel, t') I(q_\parallel, t'+dt)\rangle}{\langle I(q_\parallel, t')\rangle^2}} \qquad (2)$$

where $\boldsymbol{I(q_\parallel, t')}$ is the scattering of the in-plane wave vector at instantaneous time *t'* and *dt* is the delay time. For viscous polymers, the capillary wave dynamics are overdamped so $\boldsymbol{g_2(q_\parallel, t)}$ may be described by a stretched exponential decay fit:

$$g_2(q_{\parallel}, t) = 1 + \beta \exp[-(\frac{2t}{\tau})^{\alpha}] \quad (3)$$

where β is the speckle contrast, $\alpha(0 < \alpha \leq 1)$ is a stretching exponent and $\tau = \tau(q_{\parallel})$ is the relaxation time of the surface height fluctuations. For a simple exponential relaxation, as observed in the homopolymer films where $T \gg T_g$ the exponent $\alpha = 1$. The deviation of α from unity corresponds to the existence of a distribution of fluctuation time scales in the system contributing within the measurement window.

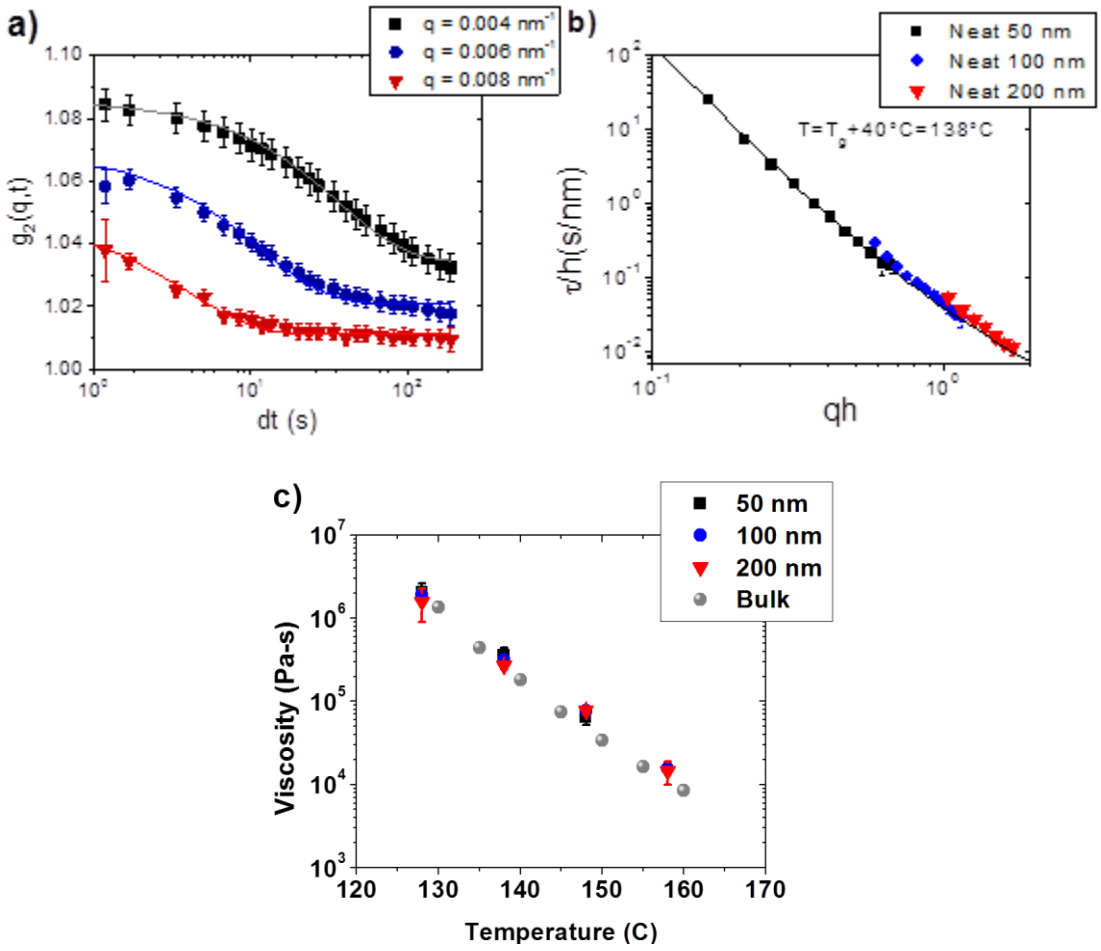

Figure IV.1: a) Characteristic intensity-intensity auto correlation function of 100 nm thick neat P2VP film at T=138˚C at a few wave vectors. Solid lines are single exponential fits to the measured data. **b)** Comparison of relaxation time/film thickness vs wave vector ∗ film thickness ($\frac{\tau}{h} vs\ qh$) in neat polymer films of *h=50, 100* and *200 nm* at T_g*+40*℃. Solid line is a fit to the HCT model. **c)** Viscosity as calculated from the relaxation time vs wave vector fit for each film using the HCT model for *h=50, 100* and *200 nm* neat P2VP films by comparison to the bulk viscosity.

A typical $\boldsymbol{g_2(q_\parallel, t)}$ for a neat 100 nm P2VP film is shown in figure 1a over a range of wave vectors. The relaxation times exhibited by all P2VP films were each characterized by single exponential behavior, regardless of film thickness. Hydrodynamic continuum theory describes the relaxation time to be dependent on the ratio of the viscosity $\boldsymbol{\eta}$ and surface tension $\boldsymbol{\gamma}$:[6,7,9,27]

$$\boldsymbol{\tau(q_\parallel) = \frac{2\eta_{XPCS}[cosh^2(q_\parallel h)+q_\parallel{}^2h^2]}{\gamma q_\parallel[sinh(q_\parallel h)\cosh(q_\parallel h)-q_\parallel h]}} \quad (4)$$

The viscosity of polystyrene (PS) films, calculated using this equation, has been shown to be independent of film thickness and equal to the bulk viscosity when $\boldsymbol{h > 4R_g}$.[27] The viscosity in our P2VP system are also found to be independent of film thickness (Fig. 1b) and equal to the bulk viscosity of the polymer as measured using rheology.

The relaxations measured from the surface height fluctuations and measured by XPCS manifest a range of relaxations, from segmental relaxations of the chains to the center of mass translational relaxations. In the case of the films used in this study, we believe it is safe to assume that the relaxations at these temperatures are largely probing the center of mass translational dynamics of the polymer chains. This is also corroborated by the fact that the stretching exponent is unity; otherwise it would be less than unity as described earlier.

We now look to explore the influence of dry brush nanoparticles on the dynamics of an entangled host polymer. For this measurement, we conducted measurements in poly (2-vinyl pyridine) (P2VP) using XPCS. We measured the surface height fluctuations of these films with different concentrations of nanoparticles in order to determine the influence of the nanoparticle on the dynamics of the polymer film. Figure 2 shows that as nanoparticle concentration is increased, we observe an increase in the relaxation time of the homopolymer by up to a factor of three for nanocomposites with 2 wt% gold particles.

In order to gain further insight into why the dynamics of the free host polymer differ from the behavior observed in similar bulk nanocomposite systems, we performed resonance enhanced XPCS measurements in order to probe the behavior of the nanoparticle as a tracer within the polymer host.[26] Performing this measurement allow us to effectively probe the dynamics of the host polymer within the "bulk-like" interior. The relaxation of the nanoparticles within the host polymer is shown in figure 3. The relaxation time follows the behavior $\boldsymbol{\tau \sim {}^{1}/_{q_{\parallel}{}^{2}}}$ which can be represented by Stokes-Einstein diffusion of a particle in a viscous medium. [28,29]The nanoparticles diffusion through the polymer host in the films interior indicates that the relaxation of the host chains in the film interior are not substantially influenced by the presence of the nanoparticles. At lower particle concentrations (1 wt%), no relaxation was observed from the nanoparticles which may indicate that there were no nanoparticles present in the interior for these films.

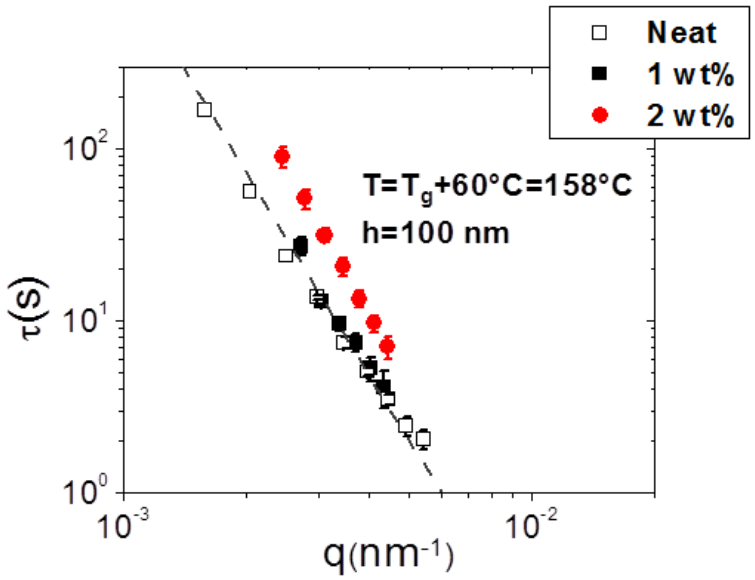

Figure IV.2: Relaxation time as a function of wave vector determined for neat homopolymer, 1 wt% and 2 wt% PNC films at T_g+*60*℃. Dashed line is a HCT fit for the neat homopolymer film.

In order to further explore the influence of the nanoparticles on other host polymer relaxations, we performed broadband dielectric spectroscopy measurements on thin capped films of polymer nanocomposites at a thickness of h = 100 nm over a range of concentrations. In figure 4, we show that the segmental relaxations of the polymer host are unaffected by the addition of the nanoparticles up to 2 wt%. This is further indication that the nanoparticles themselves are providing a relatively minor influence on the dynamics of the host chains when considering the dynamics in the film interior – in the absence of interactions with the interfaces.

The difference in behavior observed between the measurement of the surface height fluctuations and the interior measurements of the nanoparticles as tracers as well as broadband dielectric segmental relaxations suggest that the nanoparticles have a substantially different

influence on the host chain dynamics at the free interface as opposed to the interior. Because this nanocomposite system satisfies the dry brush condition, we may expect that the interfacial segregation of nanoparticles to the substrate and the free surface are responsible for the difference in behavior we observe.

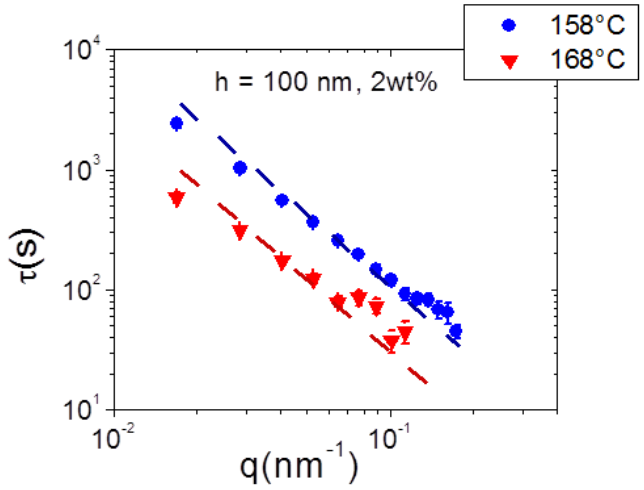

Figure IV.3: XPCS measurement of the dynamics of nanoparticles in the interior of a 2 wt% *h = 100 nm* film at T_g*+60* & T_g *+70*℃. Dashed line represents a slope of -2.

To further explore this hypothesis, we performed reflectivity measurements to determine whether the surface segregation is observed in these systems and how it evolves as a function of film thickness. X-ray reflectivity (XR) measurements provided the reflectivity as a function of the scattering angle. With this information, the density of particles was extracted as a function of depth throughout the film. The XR measurements may be understood on the basis of Fresnel's law of reflection for x-rays, concerned only with the specular part of the signal, where the incident angle θ_i and the exit angle θ_f are equal.[30–32] For XR measurements, the x-rays are either

transmitted or reflected through the material and the signal intensity, of course, is dictated by the electron density contrast *n* of the materials

$$n = 1 - \delta - i\beta \tag{5}$$

with

$$\delta = \frac{\lambda^2}{2\pi} r_e \rho_e \tag{6}$$

and

$$\beta = \frac{\lambda}{4\pi} \mu_x \tag{7}$$

where λ is the wavelength of the x-rays (determined from the energy of the incident x-rays), $r_e = 2.818 \times 10^{-15} m$ is the Thomson's classical electron radius, ρ_e is the electron density of the material and $\mu_x$is the absorption cross-section density. The transmission β is usually much smaller than the dispersion δ for dielectric materials and can thus be ignored. We can determine the electron density contrast from δ using equation 6, below, where θ_c is the critical angle.

$$\cos\theta_c = n = 1 - \delta \tag{8}$$

$$\theta_c{}^2 \approx 2\delta \tag{9}$$

From Snell's law, it is readily known that total external reflection occurs for angles $\theta_i < \theta_c$. The reflected intensity is the square of the complex reflection co-efficient such that:

$$R(\theta) = \left| \frac{\theta - \sqrt{\theta^2 - \theta_c{}^2 - 2i\beta}}{\theta + \sqrt{\theta^2 - \theta_c{}^2 - 2i\beta}} \right|^2 \tag{10}$$

The data in Figure 5a shows the reflectivity plotted as a function of scattering angle for the 50 nm film, which contains 2wt% grafted nanoparticles. The solid line drawn through the reflected intensity does an excellent job of describing the behavior of the reflectivity of the film. This fit to the data was performed for each sample and was used to determine the electron density, using equations 6, 9 and 10. The results for the 2wt% nanocomposite films over a range of thicknesses are shown in Fig. 5b with the electron density plotted as a function of depth into the film from the free surface. In figure 5b, we observe a region of high electron density near the film free surface that takes up an increasing proportion of the film as thickness is decreased. We also observe a very high electron density region near the substrate, which is consistent with nanoparticle segregation to a solid interface. The strong nanoparticle segregation to the interfaces may explain why little influence of the nanoparticles on the segmental dynamics was observed in the dielectric measurement; with two solid interfaces from the aluminum electrodes, most of the nanoparticles segregated to the electrodes and didn't interact with the host chains or influence their dynamic behavior.

Figure 5c shows that by comparison to the neat 50 nm P2VP film, the nanocomposite film shows noticeable segregation to both the substrate and free surface – as expected from previous work with polymer nanocomposite films where grafted dry brush particles of this size were incorporated. When we compare this behavior to nanocomposites where the poly (2-vinyl pyridine) grafted and host chains are replaced by polystyrene,[11,22] we observe segregation of the nanoparticles to both interfaces so we may expect to find a similar result here.

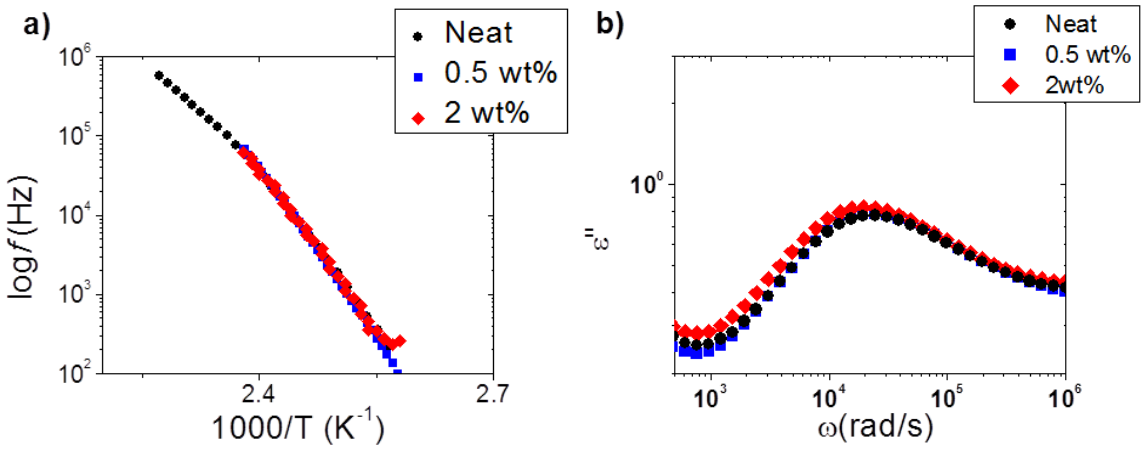

Figure IV.4: a) VFT plot of the frequency associated with the dielectric segmental relaxation peak plotted as a function of temperature for neat 0.5 and 2 wt% polymer nanocomposite films of thickness h = 100nm. **b)** Comparison of dielectric segmental relaxation peak for neat, 0.5 and 2 wt% polymer nanocomposite films of thickness h = 100 nm at T = 136˚C.

In order to probe the extent to which this surface segregation influences the dynamics of the host chains in the film, we probed the surface height fluctuations of nanocomposite films with 2 wt% particles at different thicknesses. The surface dynamics exhibit a substantial increase in the relaxation of the polymer host as thickness is decreased (Figure 6a), with increases over the relaxation times of the neat polymer film by a factor of four observed for a film thickness h = 50 nm. This change in the relaxation time from the neat behavior indicates a different thickness dependence from the neat films where the dynamics of the film can be represented by a homogenous polymer film when $T \gg T_g$.

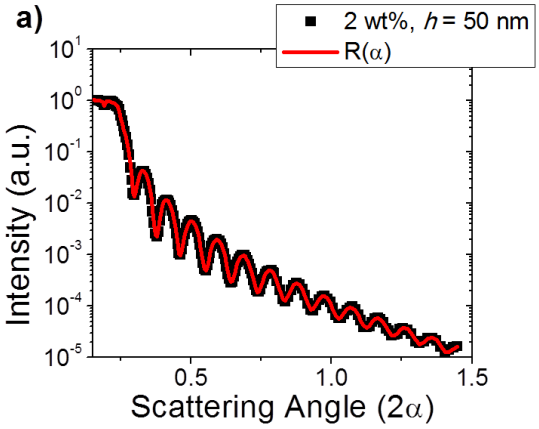
a)
2 wt%, h = 50 nm
R(α)
Intensity (a.u.)
Scattering Angle (2α)

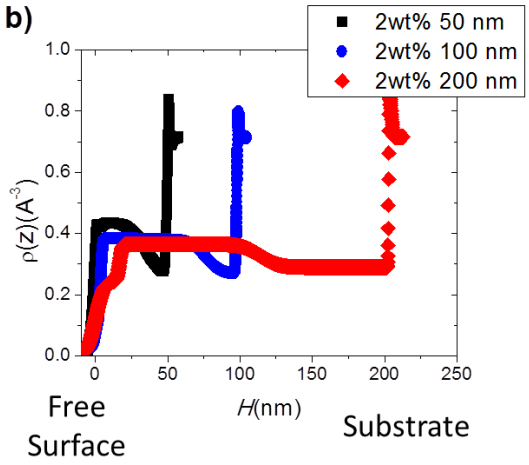
b)
2wt% 50 nm
2wt% 100 nm
2wt% 200 nm
ρ(z)(A-3)
H(nm)
Free Surface
Substrate

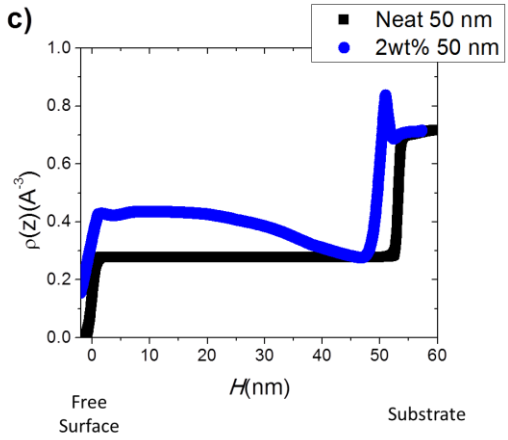
c)
Neat 50 nm
2wt% 50 nm
ρ(z)(A-3)
H(nm)
Free Surface
Substrate

Figure IV.5: a) Reflectivity measurement of 2 wt% gold nanocomposite h = 50 nm film. **b)** Electron density depth profiles of 2 wt% nanocomposite h =50, 100 and 200 nm films. **c)** Electron density depth profile of h = 50 nm neat and 2 wt% nanocomposite films.

The change in thickness dependence upon the addition of nanoparticles indicates that for these nanocomposite films, the polymer film can no longer be described using the HCT model. When the relaxation time as a function of wave vector is normalized by film thickness for the 2 wt% nanocomposite film (Figure 6b), we find that the relaxations of the PNC film are not well-described by the model of Sinha for a homogenous film with a single viscosity. This observed change in behavior holds for multiple temperatures above the glass transition. The normalized nanocomposite film data indicates that while the deviations away from the neat behavior we observed indicate a slowing of the host chain dynamics, the data also appear to collapse to a single curve with different characteristics from that of a homogenous polymer film.

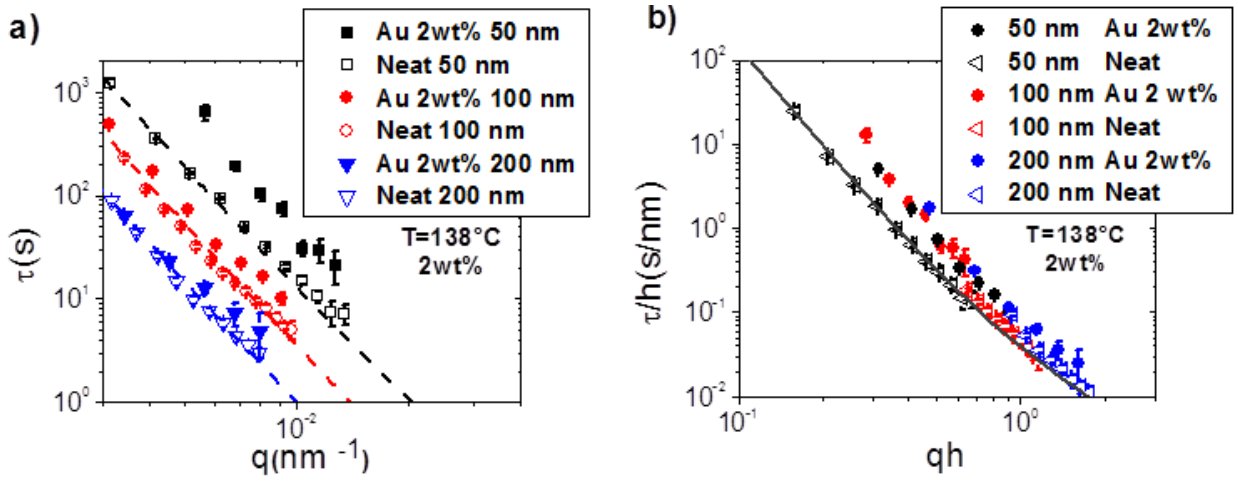

Figure IV.6: a) Relaxation time as a function of wave vector determined for 2 wt% PNC films at T_g*+40*℃ over a range of thicknesses (*h = 50-200 nm*). Dashed lines are HCT fit for the neat homopolymer films. **b)** Comparison of relaxation time/film thickness vs wave vector ∗ film thickness ($\frac{\tau}{h} vs\ qh$) measurements in neat polymer and 2 wt% PNC films of *h=50, 100* and *200 nm* at T_g*+40*℃. Solid line is a fit to the HCT model.

This thickness dependence is consistent with the results of the x-ray reflectivity measurement, such that the dynamic influence of nanoparticle interfacial segregation has an increased influence as thickness is decreased. The nanocomposite film behavior when normalized is reminiscent of work by Sinha and coworkers where they looked to expand their model to the behavior of bilayer films. [33] Based upon the information from systems with similar brush layer conditions in polystyrene, we may anticipate that the segregation of nanoparticles to the free surface leads to a region of increased viscosity at this interface. As thickness is decreased, the higher viscosity of the region near the free surface has an increased influence on the average behavior of the film. We should note that because of the limitations of the x-ray reflectivity measurement, we cannot comment on the exact size of this region. Because of this refrain from making a quantitative analysis of the surface layer viscosity or size for some of these films. Nevertheless, the behavior observed in the nanocomposite films exhibits signatures of a polymer film with a high viscosity surface layer.

This result indicates that this film can no longer be described as homogenous and interfacial segregation must be accounted for when discussing nanocomposites that are not well-dispersed. The nanoparticles segregated to the free surface of the polymer film play a substantial role on the dynamic behavior of the host chains in the polymer nanocomposite film, and the

interfacial changes lead to local changes in polymer host chain behavior which have a dramatic effect.

IV.4. Conclusion:

In summary, we characterized the dynamic relaxations in polymer nanocomposite thin films consisting of chain-end grafted gold nanoparticles in an athermal mixture with an entangled polymer host using x-ray photon correlation spectroscopy, x-ray reflectivity, and broadband dielectric spectroscopy. We observed that while the behavior in the interior of the film exhibited dynamics consistent with the behavior of similar systems in the bulk, surface height fluctuations of these films reveal slower dynamics of the polymer host upon the addition of nanoparticles. These slower dynamics are shown to be due to the segregation of these nanoparticles to the free surface of the film. This region near the free surface is shown to have an increased influence on the behavior of the host chains in the film as thickness is decreased. This study of the dynamic behavior in these nanocomposite films emphasizes that while the entropic interactions between grafted nanoparticles and the host polymer chains in the interior film largely resembles the behavior observed in the bulk; interfacial segregation of the nanoparticles produces a profoundly different effect on the host chain dynamics.

References:

(1) Frieberg, B.; Glynos, E.; Green, P. F. Structural Relaxations of Thin Polymer Films. *Phys. Rev. Lett.* 2012, *108* (26), 268304.
(2) de Gennes, P. G. Glass Transitions in Thin Polymer Films. *Eur. Phys. J. E* 2000, *2* (3), 201–203.
(3) Forrest, J. A.; Dalnoki-Veress, K. The Glass Transition in Thin Polymer Films. *Adv. Colloid Interface Sci.* 2001, *94* (1–3), 167–196.

(4) Kim, J. H.; Jang, J.; Zin, W. C. Estimation of the Thickness Dependence of the Glass Transition Temperature in Various Thin Polymer Films. *Langmuir* 2000, *16* (9), 4064–4067.
(5) Kim, J. H.; Jang, J.; Zin, W. C. Thickness Dependence of the Glass Transition Temperature in Thin Polymer Films. *Langmuir* 2001, *17* (9), 2703–2710.
(6) Jiang, Z.; Kim, H.; Lee, H.; Lee, Y. J.; Jiao, X.; Li, C.; Lurio, L. B.; Hu, X.; Lal, J.; Narayanan, S.; et al. Structure and Dynamics of Thin Polymer Films Using Synchrotron X-Ray Scattering. *J. Appl. Crystallogr.* 2007, *40*, S18–S22.
(7) Kim, H.; Ruhm, A.; Lurio, L. B.; Basu, J. K.; Lal, J.; Lumma, D.; Mochrie, S. G. J.; Sinha, S. K. Surface Dynamics of Polymer Films. *Phys. Rev. Lett.* 2003, *90* (6), 068302.
(8) Koga, T.; Li, C.; Endoh, M. K.; Koo, J.; Rafailovich, M.; Narayanan, S.; Lee, D. R.; Lurio, L. B.; Sinha, S. K. Reduced Viscosity of the Free Surface in Entangled Polymer Melt Films. *Phys. Rev. Lett.* 2010, *104* (6), 066101.
(9) Li, C. H.; Koga, T.; Jiang, J.; Sharma, S.; Narayanan, S.; Lurio, L. B.; Hu, Y.; Jiao, X.; Sinha, S. K.; Billet, S.; et al. Viscosity Measurements of Very Thin Polymer Films. *Macromolecules* 2005, *38* (12), 5144–5151.
(10) Narayanan, S.; Lee, D. R.; Hagman, A.; Li, X.; Wang, J. Particle Dynamics in Polymer-Metal Nanocomposite Thin Films on Nanometer-Length Scales. *Phys. Rev. Lett.* 2007, *98* (18), 185506.
(11) Meli, L.; Arceo, A.; Green, P. F. Control of the Entropic Interactions and Phase Behavior of Athermal Nanoparticle/Homopolymer Thin Film Mixtures. *Soft Matter* 2009, *5* (3), 533–537.
(12) Meli, L.; Green, P. F. Aggregation and Coarsening of Ligand-Stabilized Gold Nanoparticles in Poly(methyl Methacrylate) Thin Films. *Acs Nano* 2008, *2* (6), 1305–1312.
(13) Chao, H.; Riggleman, R. A. Effect of Particle Size and Grafting Density on the Mechanical Properties of Polymer Nanocomposites. *Polymer* 2013, *54* (19), 5222–5229.
(14) Riggleman, R. A.; Toepperwein, G. N.; Papakonstantopoulos, G. J.; de Pablo, J. J. Dynamics of a Glassy Polymer Nanocomposite during Active Deformation. *Macromolecules* 2009, *42* (10), 3632–3640.
(15) Green, P. F. The Structure of Chain End-Grafted Nanoparticle/Homopolymer Nanocomposites. *Soft Matter* 2011, *7* (18), 7914–7926.
(16) Mackay, M. E.; Tuteja, A.; Duxbury, P. M.; Hawker, C. J.; Van Horn, B.; Guan, Z. B.; Chen, G. H.; Krishnan, R. S. General Strategies for Nanoparticle Dispersion. *Science* 2006, *311* (5768), 1740–1743.
(17) Kumar, S. K.; Jouault, N.; Benicewicz, B.; Neely, T. Nanocomposites with Polymer Grafted Nanoparticles. *Macromolecules* 2013, *46* (9), 3199–3214.
(18) Jancar, J.; Douglas, J. F.; Starr, F. W.; Kumar, S. K.; Cassagnau, P.; Lesser, A. J.; Sternstein, S. S.; Buehler, M. J. Current Issues in Research on Structure-Property Relationships in Polymer Nanocomposites. *Polymer* 2010, *51* (15), 3321–3343.
(19) Chung, H.-J.; Kim, J.; Ohno, K.; Composto, R. J. Controlling the Location of Nanoparticles in Polymer Blends by Tuning the Length and End Group of Polymer Brushes. *Acs Macro Lett.* 2012, *1* (1), 252–256.
(20) Oh, H.; Green, P. F. Polymer Chain Dynamics and Glass Transition in Athermal Polymer/Nanoparticle Mixtures. *Nat. Mater.* 2009, *8* (2), 139–143.
(21) Green, P. F.; Oh, H.; Akcora, P.; Kumar, S. K. *Structure and Dynamics of Polymer Nanocomposites Involving Chain-Grafted Spherical Nanoparticles*; GarciaSakai, V., AlbaSimionesco, C., Chen, S. H., Eds.; Springer: New York, 2012.
(22) Arceo, A.; Meli, L.; Green, P. F. Glass Transition of Polymer-Nanocrystal Thin Film Mixtures: Role of Entropically Directed Forces on Nanocrystal Distribution. *Nano Lett.* 2008, *8* (8), 2271–2276.
(23) Yee, C. K.; Jordan, R.; Ulman, A.; White, H.; King, A.; Rafailovich, M.; Sokolov, J. Novel One-Phase Synthesis of Thiol-Fuctionalized Gold, Palladium, and Iridium Nanoparticles Using Superhydride. *Langmuir* 1999, *15* (10), 3486–3491.
(24) Serghei, A.; Tress, M.; Kremer, F. Confinement Effects on the Relaxation Time Distribution of the Dynamic Glass Transition in Ultrathin Polymer Films. *Macromolecules* 2006, *39* (26), 9385–9387.

(25) Tress, M.; Erber, M.; Mapesa, E. U.; Huth, H.; Mueller, J.; Serghei, A.; Schick, C.; Eichhorn, K.-J.; Volt, B.; Kremer, F. Glassy Dynamics and Glass Transition in Nanometric Thin Layers of Polystyrene. *Macromolecules* 2010, *43* (23), 9937–9944.
(26) Koga, T.; Jiang, N.; Gin, P.; Endoh, M. K.; Narayanan, S.; Lurio, L. B.; Sinha, S. K. Impact of an Irreversibly Adsorbed Layer on Local Viscosity of Nanoconfined Polymer Melts. *Phys. Rev. Lett.* 2011, *107* (22), 225901.
(27) Jiang, Z.; Mukhopadhyay, M. K.; Song, S.; Narayanan, S.; Lurio, L. B.; Kim, H.; Sinha, S. K. Entanglement Effects in Capillary Waves on Liquid Polymer Films. *Phys. Rev. Lett.* 2008, *101* (24), 246104.
(28) Gam, S.; Meth, J. S.; Zane, S. G.; Chi, C.; Wood, B. A.; Winey, K. I.; Clarke, N.; Composto, R. J. Polymer Diffusion in a Polymer Nanocomposite: Effect of Nanoparticle Size and Polydispersity. *Soft Matter* 2012, *8* (24), 6512–6520.
(29) Kim, D.; Srivastava, S.; Narayanan, S.; Archer, L. A. Polymer Nanocomposites: Polymer and Particle Dynamics. *Soft Matter* 2012, *8* (42), 10813–10818.
(30) Chandran, S.; Begam, N.; Padmanabhan, V.; Basu, J. K. Confinement Enhances Dispersion in Nanoparticle-Polymer Blend Films. *Nat. Commun.* 2014, *5*, 3697.
(31) Chandran, S.; Basu, J. K.; Mukhopadhyay, M. K. Variation in Glass Transition Temperature of Polymer Nanocomposite Films Driven by Morphological Transitions. *J. Chem. Phys.* 2013, *138* (1), 014902.
(32) Wallace, W. E.; Tan, N. C. B.; Wu, W. L.; Satija, S. Mass Density of Polystyrene Thin Films Measured by Twin Neutron Reflectivity. *J. Chem. Phys.* 1998, *108* (9), 3798–3804.
(33) Jiang, Z.; Kim, H.; Mochrie, S. G. J.; Lurio, L. B.; Sinha, S. K. Surface and Interfacial Dynamics of Polymeric Bilayer Films. *Phys. Rev. E* 2006, *74* (1), 011603.

Chapter V
Conclusions and Future Work

V.1. Summary

Dynamic behavior of complex polymer systems in the melt state was studied in this thesis. The role of both macromolecular architecture and nanoparticle additives were explored as options for altering polymer properties without changing polymer chemistry. The bulk dynamics of star-shaped polystyrene was explored in order to gain insight into the transitional behavior observed in the physical properties of these polymers as their molecular parameters are manipulated. The influence of nanoparticle additives on the behavior of a polymer host was also explored in thin film geometries where morphology changes are known to occur in polymer nanocomposites as polymer-particle interactions are tailored. In this thesis, the influences of both interfacial interactions and confinement on host chain dynamics in polymer nanocomposites were explored. The study of these materials provided insight into new options for controlling polymer properties for applications both in thin films and in the bulk.

In chapter 2, we showed that when the functionality of the star molecules is low the polymers exhibit linear viscoelastic behavior, and the dynamics are characterized by an arm retraction mechanism, as described by the model of Milner and McLeish. For the largest functionalities and the shortest, unentangled, arms, the dynamics are highly cooperative and the

Milner-McLeish model fails. We showed that, for high functionalities and short, unentangled arms, the cores of the molecules occupy a substantial fraction of the molecule and intermolecular entropic repulsions between the stars influence the structural organization and hence the dynamics. We show evidence of a transitional regime, characterized by intermediate values of f and M_a, where the arm retraction process begins to be strongly influenced by the increasing size of the impenetrable cores; this is manifested in the emergence of the cooperative rearrangements associated with soft-colloid behavior. The influence of the core region on the arm retraction mechanism is clear from the viscoelastic spectrum, where there is evidence of increased elasticity. The dependence of the glass transition on molecular weight and functionality also manifest the changes in structure, with f and M_a.

In chapter 3, the influences of both spatial nanoparticle confinement and thickness confinement on the dynamics of host polymer chains were studied using X-ray photon correlation spectroscopy. We show that for thick films, the tethered nanoparticles are spatially dispersed and the dynamics of the free host chains are slowed down, largely because the relaxation times of the tethered chains are longer than those of the free chains. This behavior persists to the regime of nanoscale thickness confinement where, as we have shown, a new mechanism ensues. When the film thickness becomes comparable to the average spacing between the NPs, we show that the NPs motions are suppressed and the free chains experience an entropic restriction, leading to an increase in the activation barriers that facilitate their translational motions. This behavior is associated with an order of magnitude increase in the polymer viscosity. An increase of the film thickness or an increase of the nanoparticle separation was shown to alleviate this "entropic crowding," leading a decrease of the viscosity. These results suggest new ways to tailor the viscosities of nanoscale thick PNCs, without changing

molecular parameters like the chain lengths and nanoparticle core sizes.

In chapter 4, we characterized the dynamic relaxations in polymer nanocomposite thin films consisting of chain-end grafted gold nanoparticles in an athermal mixture with an entangled polymer host using x-ray photon correlation spectroscopy, x-ray reflectivity, and broadband dielectric spectroscopy. We observed that while the behavior in the interior of the film exhibited dynamics consistent with the behavior of similar systems in the bulk, surface height fluctuations of these films reveal slower dynamics of the polymer host upon the addition of nanoparticles. These slower dynamics are shown to be due to the segregation of these nanoparticles to the free surface of the film. This region near the free surface is shown to have an increased influence on the behavior of the host chains in the film as thickness is decreased. This study of the dynamic behavior in these nanocomposite films emphasizes that while the entropic interactions between grafted nanoparticles and the host polymer chains in the interior film largely resembles the behavior observed in the bulk; interfacial segregation of the nanoparticles produces a profoundly different effect on the host chain dynamics.

This thesis work has focused on altering polymer dynamics through the use of polymer architecture and the addition of inorganic nanoparticle fillers. These two methods of manipulating polymer dynamics offer alternatives to changing polymer chemistry or blending different polymers. The dynamics of these polymers have been shown to be strongly dependent on local behavior and interactions, and the research presented here contributes improved understanding in the field which will hopefully open the door for further research interest and discovery.

V.2. Future Work- *Proof of Concept:* Dynamics in star-shaped polymer films

In this section, the concept of studying dynamics in star-shaped polymer films is introduced. This topic was pursued in collaboration with researches at the Foundation of Research and Technology-Hellas and extends from the work on star-shaped polymers discussed in this thesis.

Polymer thin films, with applications ranging from lubrication and adhesion to energy conversion and actuation, continue to receive significant scientific attention. Despite the enormous scientific progress that has been made toward understanding their physical properties many important challenges remain. One area of current interest involves understanding implications of a free surface on physical properties, such as depth dependent glass transition temperatures T_gs and depth dependent segmental dynamics, occurring over distances of tens of nanometers, and physical aging.[1-4] It is well understood that for linear chain polymers, the enhanced configurational freedom of chain segments at the free interface is associated with lower free surface T_gs, and enhanced segmental dynamics. Below the bulk T_g, experiments reveal the existence of a liquid-like layer of a few nanometers in thickness, at the free surface of linear chain polymer films. In the glassy state ($T < T_g$) the thickness of this surface layer increases with decreasing temperature.[5,6] Ediger and coworkers have suggested that for temperatures not far above T_g, $T > T_g + 10$ K -in the melt state -the surface and bulk dynamics of linear-chain polymer films become comparable.[7,8]

Independent X-ray photon correlation spectroscopy (XPCS) measurements of the surface capillary waves emanating from linear chain polymer films at temperatures in the melt state, $T > T_g$, show that the viscosities of thin films supported by non-wetting surfaces are equal to their bulk viscosities. These results are based on the notion that hydrodynamic continuum theory

(HCT) may reliably be used to extract the viscosities of liquid films from XPCS data. The HCT assumes non-slip boundary conditions at the liquid/substrate interface and that the film possesses a uniform viscosity η. It predicts that the relaxation time is proportional to η/γ, where γ is the surface tension of the film.[9] Measurements of the viscosities of supported molten entangled polystyrene (PS) films (molecular weight M_w = 123 kg/mol., the molecular weight between entanglements M_e for linear PS is 14 kg/mol[10]) are in excellent agreement with the bulk zero-shear viscosities η_0, measured using oscillatory shear rheology.[11] That the surface and bulk dynamics are equal is consistent with the notion that the surface dynamics are not fast compared to the bulk.[8] As a cautionary note, it should be emphasized that for temperatures sufficiently above T_g, the translational dynamics are generally captured within the window of the XPCS experiments (time scales of 1-10^3 sec and associated length scales of 10-10^3 nm). Since the translational dynamics dictate the viscosity, then the XPCS measurements would yield viscosities that are equal to the bulk zero shear viscosities. However, at lower temperatures closer to T_g, where the translational dynamics are orders of magnitude slower, the faster segmental dynamics are generally captured within the XPCS experimental window; hence the experimental data would manifest the dynamics of a much faster process, and likely a broader distribution of relaxation times.[12]

Foster and collaborators recently investigated the effect of macromolecular architecture on the surface dynamics of thin polymer films by XPCS.[13-15] In contrast to unentangled linear and cyclic chains[13], branching (they considered 6-arm star-shaped, 6-pom, 6-end branched stars, and bottle brushes) may have significant effect of the surface fluctuation dynamics.[14,15] The values of η_{XPCS} were reported to be larger than the values measured using bulk rheology η_0.[14] The HCT provided a good description of the all their data. However, a rationale for this slow

surface dynamics is yet to be identified. A natural question therefore arises regarding a universal explanation for this phenomenon exhibited by these branched systems.

Recently, we showed that the local glass transition temperature at the free surface (T_g^{surf}) of 8-arm star polymer films with a molecular weight per arm of M_w^{arm} = 10 kg / mol. was higher than the bulk T_g^{bulk}, $T_g^{surf} > T_g^{bulk}$.[5,16,17] However T_g^{surf} became gradually lower than T_g^{bulk} as M_w^{arm} increased, consistent with the behavior of linear chain polymers.[5,16,17] Molecular dynamics simulations revealed that $T_g^{surf} > T_g^{bulk}$ for 8-arms with M_w^{arm} = 10 kg / mol is might be due to strong positional correlations and spatial ordering of the star-shaped molecular at the free surface.[17] In this letter we investigate, with the use of XPCS, rheology, and dielectric spectroscopy, the surface and bulk relaxations of a series of star polystyrene thin films, composed of molecules with f = 8-arms and varying arm lengths, from unentangled (M_w^{arm} = 10 and 25 kg/mol) to entangled arms (M_w^{arm} = 57 kg/mol). We show that when the arm lengths are sufficiently long, the dynamics measured using XPCS are comparable to those determined using bulk rheology, whereas for short (unentangled) arms the surface relaxation were slower than the bulk. An initially surprising observation was that when M_w^{arm} was sufficiently short, the HCT failed to describe the XPCS data. Subsequent molecular dynamics simulations revealed that there was a significant difference structurally between the free surface region and the interior/bulk for this 8-arm molecule. The stars exhibited evidence of spatial ordering at the free surface; such a positional autocorrelation was not evident within the film interior.

Measurements of the relaxations supported PS films, with thickness of approximately h = 200 nm, were performed using XPCS. The surface fluctuation dynamics were characterized by the normalized intensity-intensity autocorrelation function of the coherent surface scattering $g_2(q,t)$ given by $g_2(q_\parallel,t) = \langle I(q_\parallel,t')I(q_\parallel,t'+t)\rangle / \langle I(q_\parallel,t')\rangle^2$, where $I(q_\parallel,t')$ is the scattering

intensity for the in-plane vector at time t', and t is the delay time. For highly viscous polymers, the capillary waves are over damped so $g_2(q,t)$ may be described by an exponential decay: $g_2(q,t) = 1 + \beta\exp[-(2t/\tau)^{\alpha}]$, where β is the speckle contrast, α ($0 < \alpha < 1$) is a stretching exponent, and $\tau = \tau(q_{\parallel})$ is the average relaxation time; where $\alpha = 1$ corresponds to a simple exponential decay. For the LPS-13K, the g_2 data were described well by a simple exponential decay (in accordance with the data reported by Kim *et al.*[11]), whereas for SPS-8-57K, g_2 followed a stretched exponential decay.

The XPCS data suggest surprising differences between relaxation processes that occur in films composed of linear chains and of SPS molecules of different arm lengths. First, our studies confirm that the viscosities η_{XPCS} of linear chain PS are in excellent agreement with values of the zero shear viscosities, measured using bulk oscillatory shear rheology ($\eta_{XPCS} \approx \eta_0$, Figure 1a & 2a). This result also indicates that the time-scales measured by the XPCS experiments encompass those of the center of mass translational dynamics of the chains in the temperature range of our experiments, $T > T_g^{bulk} + 30$ K.[11,12] With regard to measurements of the 8-arms SPS films (SPS-8-25K and SPS-8-57K), the HCT describes the τ versus $q_{\parallel}$ dependence quite well, as shown in Figure 1b.

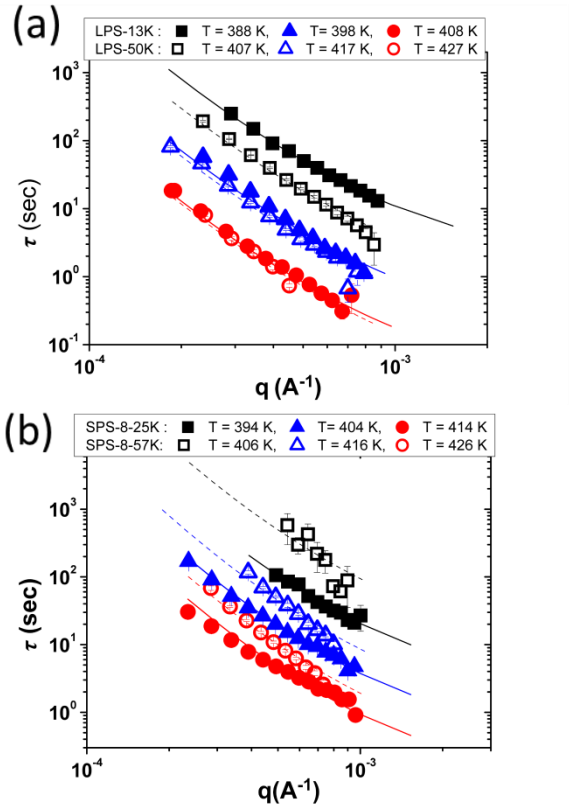

Figure V.1: Relaxation times as a function of wave function for various PS films at different temperatures, *T*, for: (a) LPS-13K (solid symbols) and LPS 50K (open symbols); (b) SPS-8-25K (solid symbols) SPS-8-57K (open symbols). The curves represent the least-squared fits of data to the HCT.

However the effect of architecture is manifested in the corresponding magnitudes of η_{XPCS}, and associated implications for the fact that $\eta_{XPCS} \neq \eta_o$, for different temperature ranges. The data in Figure 2b show the differences between η_{XPCS} and η_o, (see supplementary information and also Ref[18]), for these molecules -SPS-8-25K and SPS-8-57K samples. In order to extract the viscosities of the SPS molecules, their surface tensions were estimated using the work of Archer and co-workers.[19,20] For the slightly entangled SPS-8-57K, η_{XPCS} is slightly

lower than η_0 whereas for SPS-8-25K, η_{XPCS} , at the lowest temperature, is smaller than η_0 by an order of magnitude. The value of η_{XPCS} becomes comparable to η_0 for the highest temperature $T \approx T_g$ + 50 K. With regard to SPS-8-10K, the HCT model completely fails to describe the τ – vs- $q_{\|}$ data throughout the entire temperature ranges. This is shown in Figure 3, where the solid symbols represent the XPCS data and the solid lines were computed with the HCT model (using the values of bulk zero-shear viscosities).

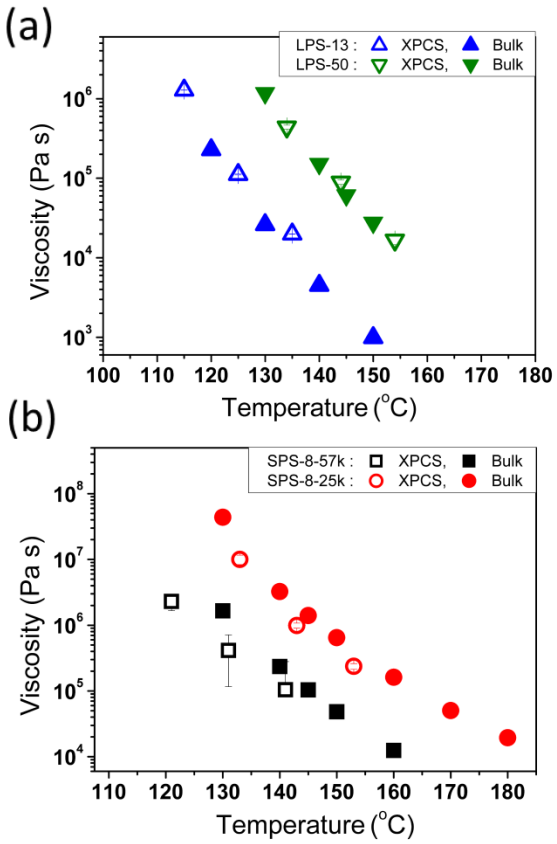

Figure V.2: A comparison of viscosities of films determined using XPCS data (filled symbols) and bulk viscosities measured by rheometry (open symbols) as a function of ΔT_g for (a) LPS-13K (blue symbols) and LSP-50K (green symbols) and (b) SPS-8-25K (black symbols) and SPS-8-57K (red symbols).

The q-dependence of the relaxation times of the SPS-8-10 K molecules is instructive with regard to identifying potential differences between the relaxation mechanisms of this polymer and the others. For the temperatures $T \approx T_g + 40$ K and $T \approx T_g + 50$K the relaxation times scale as $\tau \sim 1/q$. Additionally, the relaxation times are significantly longer than the relaxation times in the bulk. These combined observations would suggest that the dynamics of the molecules at the free surface are "caged." [21,22] We will return to this point later in the manuscript, after the molecular dynamic simulations of supported films are described.

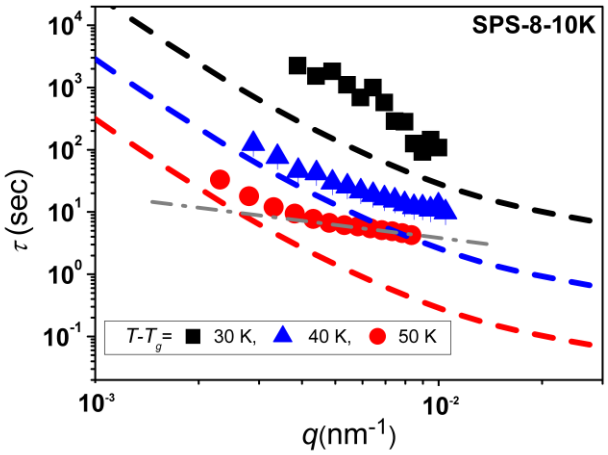

Figure V.3: XPCS surface relaxation time for the SPS-8-10K measured at different temperatures. The solid curves represent the estimated surface relaxation times based on HCT using the zero-shear viscosity. The dashed line indicates the $\tau \sim q^{-1}$.

In the meantime it is worth examining the distribution of relaxation times in this system in order to gain further insight into the behavior of the molecules. The stretching exponents (α_{XPCS}) of the intermediate scattering functions, obtained from the XPCS measurements, shown in Figure 4. For the linear chain PS samples, $\alpha_{XPCS} = 1$ as expected for the experimental window which captures only translational relaxations.[12] For star-shaped PS samples, α_{XPCS} is not only

dependent on M_w^{arm} but it is also T dependent, increasing with T. A stretched exponent of α_{XPCS} < 1 suggests that more than one, or a distribution, relaxation process occurs at a given temperature. For the highest temperature $T = T_g + 50$ K, $\alpha_{XPCS} = 1$ for the SPS-8-25K and SPS-8-10K, suggesting that the same dynamics processes are captured by the XPCS experiment. However, for the SPS-8-57K molecules the values of α_{XPCS} are much smaller, throughout the entire temperature range, suggesting these dynamics are characterized by a broader distribution of relaxation times.[23] With the use of molecular dynamics simulations, we recently showed that due to their architecture and associated monomer packing frustrations, the dynamics of star-shaped polymers would be characterized by broader distributions of relaxation times than their linear chain analogs. This is because the relaxation rates at the arm ends are most rapid and decrease as the distance to the branch points decreases, along each arm.[24] The smaller magnitude of the stretching exponent for the SPS-8-57K than the shorter arm stars would be consistent with this notion.

In order to get additional insight into the relaxation dynamics of these molecules, broadband dielectric spectroscopy (BDS) measurements (the BDS data and the analysis are in the Supplementary Information) were performed to extract the stretching exponent β_{KWW} (from Kohlrausch-Williams-Watts (KWW) of the equation $\varepsilon_{KWW}(t) = \Delta\varepsilon \exp\{-(t/\tau_{KWW})^{\beta_{KWW}}\}$. The magnitudes of β_{KWW} are plotted in Figure 4b. While it would not be wise to compare the magnitudes of the stretching exponents obtained from the BDS and XPCS experiments, a comparison of the trends is instructive. Whereas the values of α_{XPCS} increase with increasing arm length, the opposite is true for the values of β_{KWW}, which indicate that the distribution of relaxation times increases with decreasing arm length. Based on simulations,[24] this result indicates that the broadening of the surface dynamics of the SPS-8-57K, measured using XPCS,

is not due to intermolecular heterogeneities in the segmental dynamics; instead it is due to the presence of more than one relaxation mode within the time and space domain captured by XPCS at the specific temperatures.

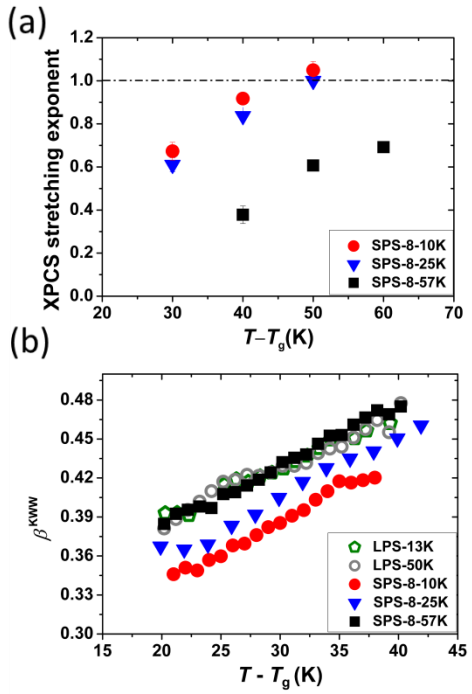

Figure V.4: (a) XPCS stretching exponents as a function of ΔT_g for 8-arm films with M_w^{arm} = 10 kg / mol (solid red symbols), 25 kg / mol (solid blue triangle), and 57 kg / mol (solid black squares); (b) stretching parameter β_{KWW} from BDS measurements for LPS-13K (open green square) and LSP-50K, and 8-arm star films with M_w^{arm} = 10 kg / mol (red solid circles blue), 25 kg / mol (solid blue triangle), and 57 kg / mol (solid black squares).

Further insight into these results -the failure of the HCT to describe the τ-$q_{\parallel}$behavior of the SPS-8-10K molecule and the trend in the α_{XPCS} exponent with arm length – would be learned from molecular dynamics (MD) simulations. MD simulations based on a coarse-grained bead-spring model, were performed. Each star-shaped polymer was represented by a bead (core) onto

which 8 chains, each with M segments of a diameter σ, were attached to its surface. The core particle had a diameter of 0/75 σ. Films of thickness H were "constructed" such that one interface was exposed to a vacuum and the other was in contact with a solid substrate. Simulations of stars where M = 10, 20, and 40 segments per arm were performed. Details of the simulation method are described elsewere.[17,25] The monomer concentration profile of the core particle (the middle particle that all the arms are tethered to) in the z-direction (perpendicular to the substrate) was constructed and plotted in Figure 5a. Three regions are evident: one at the free surface (z/H = 1), a second at the substrate (z/H = 0), and in the interior of the film ($0 < z/H < 1$) that is assumed to behave like the bulk. There is a strong spatial correlation between short 8-arm star polymers at the free interface; this correlation decreases as the arm length increases. Such a positional correlation is not evident within the interior of the film, highlighting the notion that there are significant structural differences between the free surface region and the interior/bulk for 8-arm with short arms; this effect is not observed for linear chain films. To further understand the structural characteristics of the star-shaped polymer at the free surface, the radial distribution function, $g_{cc}(r)$ at the free surface, between the core particles of linear chain polymers and 8-arm stars molecules (with M = 10) were computed (Figure 5b). Strikingly, a peak is observed for the case of 8-arm star revealing evidence of a degree of spatial ordering; which is absent in the linear chain system. In light of this result, it is worth noting that we have shown that molecules for which $f>>8$, and $M_{arm}<M_e$, organize in films to form structures with long-range order. These simulations reveal the ordering is initiated at the external interfaces for molecules with smaller values of f. [1]

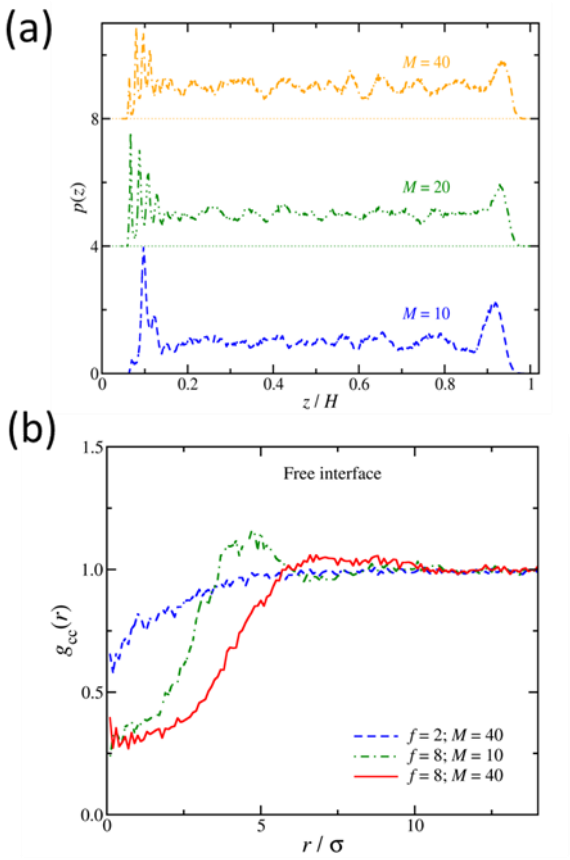

Figure V.5: (a) Concentration profiles of star polymer films with a functionality f =8 and at different molecular weights per arm, M (from bottom to top the M increases from 10 to 40). (b) The radial distribution functions of the core particles for different star polymers at the free interface (2-dimenions) are shown.

Based on the foregoing it is evident that the large values of the viscosity determined using XPCS compared to the bulk viscosity, not exhibited by linear chain polymers, are associated with the ordering of the macromolecules at the free surface. The additional findings that for the SPS-8-10K system $\tau \sim q^{-1}$ and that the relaxation rates are slow would be consistent with this observation. Since the $\tau \sim q^{-1}$ suggest evidence that the dynamics of the molecules are caged,[23] then it is reasonable to conclude that the dynamics of the molecules at the free surface would occur via a slower cooperative process.

In conclusion, we have shown that for temperatures far above T_g, the surface dynamics of thin film SPS molecules with $M_{arm}<M_e$ are slow compared to the bulk. This is in contrast to linear chain polymer films where the surface and bulk dynamics are comparable in the melt state. The surface relaxations occur via a slow cooperative process. MD simulations of supported films indicate that the slow surface relaxation processes stem from the notion that star-shaped molecules exhibit an additional spatial ordering at the free surface, not present in the bulk. Recent oscillatory shear experiments reveal that for bulk systems, the molecules with $f \geq 8$ and $M_{arm}<M_e$ undergo flow via a cooperative mechanism, unlike the conventional arm retraction mechanism characteristic of the long-range dynamics of long armed ($M_{arm}>>M_e$) star shaped macromolecules.[18] This new phenomenon –slow surface dynamics–should be a general phenomenon provided the molecules are branched and their motions are "caged" due to a tendency toward aggregation or spatial ordering at the free surface. These findings have important implications with the regard to the use of polymers for applications that include, lubrication, tribology and adhesion.

References

(1) Green, P. F.; Glynos, E.; Frieberg, B. *MRS Communications* 2015, *5*, 423.
(2) Napolitano, S.; Capponi, S.; Vanroy, B. *Eur. Phys. J. E* 2013, *36*, 37.
(3) DeFelice, J., Milner, S. T. & Lipson, J. E. G. *Macromolecules* 49, 1822–1833 (2016)
(4) Mirigian, S. &, Schweizer. K. *J. Chem. Phys.* 143, 244705 (2015)
(5) Frieberg, B.; Glynos, E.; Green, P. F. *Phys. Rev. Lett.* 2012, *108*.
(6) Ediger, M. D.; Forrest, J. A. *Macromolecules* 2014, *47*, 471.
(7) Paeng, K.; Swallen, S. F.; Ediger, M. D. *Journal of the American Chemical Society* 2011, *133*, 8444.
(8) Paeng, K.; Richert, R.; Ediger, M. D. *Soft Matter* 2012, *8*, 819.
(9) Sinha, S. K.; Jiang, Z.; Lurio, L. B. *Adv. Mater.* 2014, *26*, 7764.
(10) Dealy, J.; Larson, R. *Structure and Rheology of Molten Polymers*; Hanser Publications: Munich, 2006.
(11) Kim, H.; Ruhm, A.; Lurio, L. B.; Basu, J. K.; Lal, J.; Lumma, D.; Mochrie, S. G. J.; Sinha, S. K. *Phys. Rev. Lett.* 2003, *90*, 4.
(12) Jiang, Z.; Mukhopadhyay, M. K.; Song, S.; Narayanan, S.; Lurio, L. B.; Kim, H.; Sinha, S. K. *Phys. Rev. Lett.* 2008, *101*, 4.

(13) Wang, S. F.; Jiang, Z.; Narayanan, S.; Foster, M. D. *Macromolecules* 2012, *45*, 6210.
(14) Wang, S. F.; Yang, S.; Lee, J.; Akgun, B.; Wu, D. T.; Foster, M. D. *Phys. Rev. Lett.* 2013, *111*.
(15) Liu, B. X.; Narayanan, S.; Wu, D. T.; Foster, M. D. *Macromolecules* 2013, *46*, 3190.
(16) Glynos, E.; Frieberg, B.; Oh, H.; Liu, M.; Gidley, D. W.; Green, P. F. *Phys. Rev. Lett.* 2011, *106*.
(17) Glynos, E.; Frieberg, B.; Chremos, A.; Sakellariou, G.; Gidley, D. W.; Green, P. F. *Macromolecules* 2015, *48*, 2305.
(18) Johnson, K. J.; Glynos, E.; Sakellariou, G.; Green, P. *Macromolecules* 2016, *49*, 5669.
(19) Minnikanti, V. S.; Archer, L. A. *Macromolecules* 2006, *39*, 7718.
(20) Qian, Z. Y.; Minnikanti, V. S.; Sauer, B. B.; Dee, G. T.; Archer, L. A. *Macromolecules* 2008, *41*, 5007.
(21) Srivastava, S.; Agarwal, P.; Mangal, R.; Koch, D. L.; Narayanan, S.; Archer, L. A. *ACS Macro Lett.* 2015, *4*, 1149.
(22) Caronna, C.; Chushkin, Y.; Madsen, A.; Cupane, A. *Phys. Rev. Lett.* 2008, *100*, 4.
(23) Ruegg, M. L.; Patel, A. J.; Narayanan, S.; Sandy, A. R.; Mochrie, S. G. J.; Watanabe, H.; Balsara, N. P. *Macromolecules* 2006, *39*, 8822.
(24) Chremos, A.; Glynos, E.; Green, P. F. *J. Chem. Phys.* 2015, *142*, 9.
(25) Glynos, E.; Chremos, A.; Frieberg, B.; Sakellariou, G.; Green, P. F. *Macromolecules* 2014, *47*, 1137.
(26) Pakula, T.; Vlassopoulos, D.; Fytas, G.; Roovers, J. *Macromolecules* 1998, *31*, 8931.
(27) Vlassopoulos, D.; Fytas, G.; Pakula, T.; Roovers, J. *J. Phys.-Condes. Matter* 2001, *13*, R855.
(28) Vlassopoulos, D.; Fytas, G. In *High Solid Dispersions*; Cloitre, M., Ed. 2010; Vol. 236, p 1.

Appendices

Appendix A: Nanoparticle synthesis method

1) Dissolve anhydrous hydrogen tetrachloroaureate (III) trihydrate ($HAuCl_4$) in methanol (MeOH)
2) Dissolve thiol-terminated poly (2-vinyl pyridine) (P2VP) in MeOH
3) Mix solutions from steps 1) and 2)
4) Stir vigorously for 30 min
5) Dissolve sodium borohydrate ($NaBH_4$) in MeOH and add solution dropwise.

   The mixture immediately turns a pale/dark grey and transition to a dark red-brown color as the dropwise addition is continued. The reducing agent should be added until the color saturates and no gas evolution can be observed. [1]

Nanoparticle size can be tailored through control of the molar ratios of the reagents, particularly the ratio of gold to the thiol-terminated P2VP ligands. STEM images in Figure A show the size and distribution of particles synthesized using different ligand lengths.

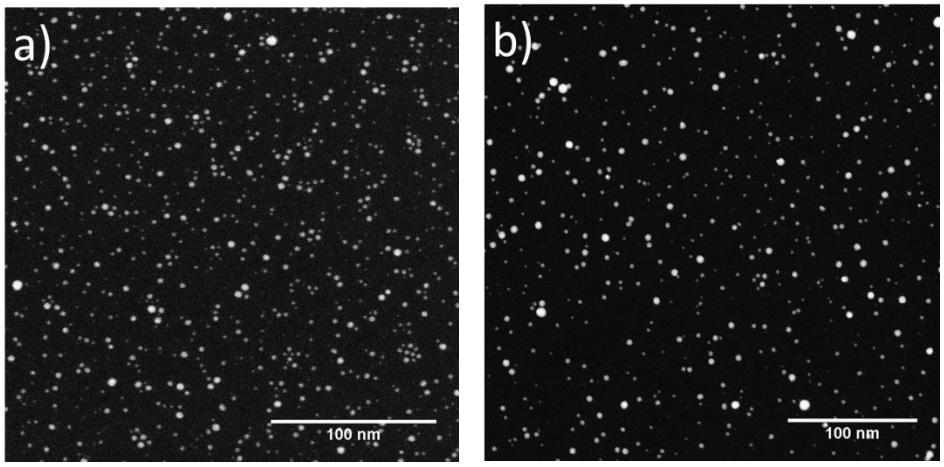

Figure A: STEM images of poly (2-vinyl pyridine) grafted gold nanoparticles post synthesis and purification. Grafted ligand molecular weights of **a)** 1 kg/mol and **b)** 10 kg/mol.

Appendix B: X-ray photon correlation spectroscopy (XPCS)

X-ray photon correlation spectroscopy (XPCS) is a surface sensitive grazing incidence x-ray scattering technique which uses the specular diffuse scattering of x-rays to measure dynamics in polymer and inorganic systems. The x-ray beam used in XPCS is collimated through an aperture which limits the size of the beam to a length-scale comparable to the coherence length of the incident x-ray beam. This generates a partially coherent x-ray beam which, upon interaction with a disordered material, gives rise to a "speckle pattern" or "speckled" scattering signal. This signal provides information about the dynamics of the disordered material. Examples of this speckle pattern for the surface and interior measurements of the films used in this study are shown in figure B.[2,3]

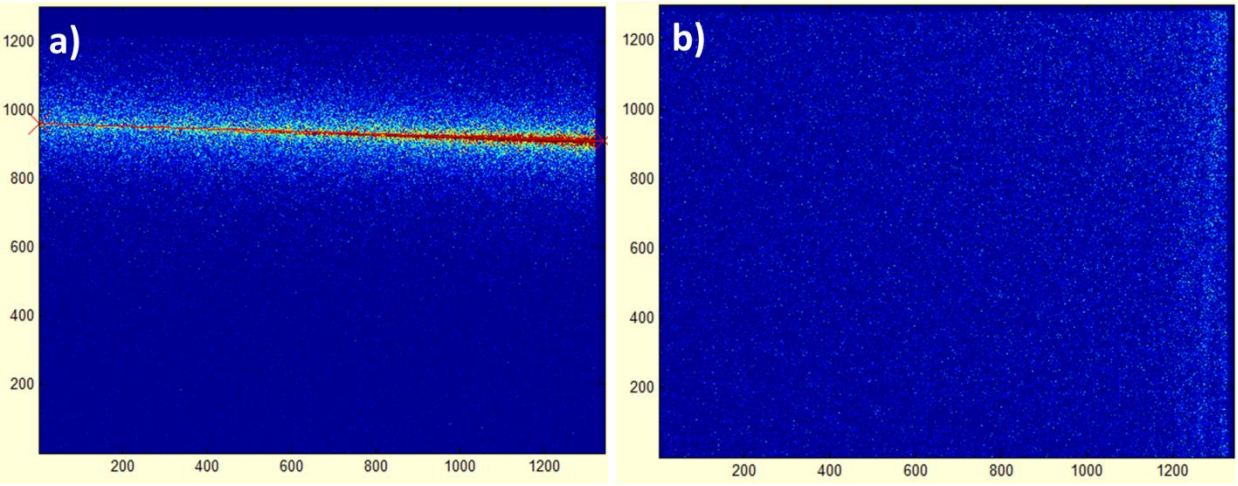

Figure B: Examples of speckle patterns for the XPCS measurements. The different incidence angles have a substantial impact on strength of signal **a)** Surface measurement **b)** Resonance enhanced x-ray measurement.

When applied to a thin film, XPCS becomes particularly useful. By limiting the incident angle of the x-ray beam, the penetration depth of the x-rays can be limited to ~10 nm. When the partially coherent x-ray beam is reflected from the surface of the film, the temporal evolution of the scattering signal provides information about the dynamics of the thermal surface height fluctuations of the film. Monitoring the evolution of the speckle scattering intensity yields a time-scale dictated by the surface fluctuations which can be determined using an intensity-intensity autocorrelation function.

References:

(1) Yee, C. K.; Jordan, R.; Ulman, A.; White, H.; King, A.; Rafailovich, M.; Sokolov, J. Novel One-Phase Synthesis of Thiol-Fuctionalized Gold, Palladium, and Iridium Nanoparticles Using Superhydride. *Langmuir* 1999, *15*, 3486–3491.
(2) Leheny, R. L. XPCS: Nanoscale Motion and Rheology. *Curr. Opin. Colloid Interface Sci.* 2012, *17*, 3–12.
(3) Kim, H.; Ruhm, A.; Lurio, L. B.; Basu, J. K.; Lal, J.; Lumma, D.; Mochrie, S. G. J.; Sinha, S. K. Surface Dynamics of Polymer Films. *Phys. Rev. Lett.* 2003, *90*, 068302.